UNIVERSITY OF SOUTHAMPTON

FACULTY OF MATHEMATICAL STUDIES

NUMERICAL MODELLING OF NATURAL CONVECTION IN CRYOGENIC LIQUIDS

BY

AGANADEN THANCANAMOOTOO

This thesis is submitted for the degree of Master of Philosophy at the University of Southampton

1986

TABLE OF CONTENTS

UNIVERSITY OF SOUTHAMPTON

ABSTRACT

FACULTY OF MATHEMATICAL STUDIES

Master of Philosophy

NUMERICAL MODELLING OF NATURAL CONVECTION IN CRYOGENIC LIQUIDS

by Aganaden Thancanamootoo

In this thesis, we look at the numerical modelling of natural convection in a cryogenic liquid contained in a storage vessel, when the motion is caused by heat leakages through the vessel's sides and bottom. The problem of natural convection, in general, involves the solution of the full Navier Stokes equations coupled with the energy equation and the equation of continuity. Here, the pressure terms in the momentum equation are eliminated and the resulting equation is written in stream function vorticity type, the stream function being connected to the vorticity through a Poisson equation. A numerical solution, based on finite difference methods, is obtained, using non-uniform grid which leads to better resolution of the boundary layers. The transport equations are solved by the Alternating Direct Implicit method. This method requires the transport equations to be converted into parabolic partial differential equations, by the inclusion of the time dependent terms, thereby enabling us to march forward in time to the steady state solution. Solution of the Poisson equation by the cyclic reduction method yields the stream function. The governing equations are solved in both Cartesian and cylindrical polar coordinates, but similar numerical procedures are adopted in each case. Various ways of enhancing the rate of convergence to the steady state are examined. Numerical results are obtained for a variety of Grashof numbers for various boundary conditions and aspect ratios and, for the Cartesian case, the numerical method is stable for Grashof numbers up to 10^{12}. The derived results show good agreement with available experimental data.

ACKNOWLEDGEMENTS

I would like to express my gratitude to my supervisor, Dr. R. E. Craine for his guidance, encouragement and support during the course of this research and for his valuable advice during the writing of this thesis. I would like to thank Dr. D. G. Drake and Professor R. G. Scurlock for many useful comments and suggestions.

I am also grateful to the University of Southampton for having offered me a research studentship.

Finally, my special thanks to Mrs. K. Drust for the careful typing of this thesis.

CHAPTER 1
INTRODUCTION

Cryogenics - a brief outlook

Cryogenic engineering deals with the practical application of very low temperature processes and techniques and is generally concerned with temperatures below $-150^{\circ}C$. In general, there is ample reason for treating cryogenics as a special field. However, although certain physical properties of materials at very low temperatures differ greatly from those commonly encountered at room temperatures cryogenic fluids are, like most ordinary fluids, Newtonian. The cryogenic fluids that are most widely encountered are Liquid Natural Gas (LNG), Liquid Air, Liquid Oxygen, Liquid Nitrogen and Liquid Helium. They find wide application, for instance in medicine, space exploration and in gas separation. LNG is, in particular, a very useful source of energy, and is widely used for domestic purposes. One of the major problems encountered in cryogenics is the storage of cryogenic fluids. Only a few decades ago evaporation was a major threat due to the poor design of storage tanks and the poor quality of insulation. Over the years design and insulation techniques have improved enormously and nowadays, fluid loss due to evaporation has been considerably reduced. However, cryogenic fluids being very expensive, engineers are constantly aiming at ways of minimising fluid losses.

Convective heat transfer

When there is transfer of heat by mass movement of fluid, the resulting thermal-energy exchange process is called convection heat transfer. There are two kinds of convection processes: natural and forced convection. In the first type, the driving force arises from the density difference in the fluid, which gives rise to buoyant forces.

Forced convection, on the other hand, occurs when an external driving force moves a fluid past a surface at a higher or lower temperature than the fluid. Natural convection occurs in cryogenic storage tanks and in many other engineering applications, e.g. petroleum storage vessels on hot days, the thermal response of a building to a change in environment temperature, and the storage of hot fluids for solar power plants. In all these cases the way by which heat enters the enclosure is of great importance and the flow structure depends critically on the applied heating conditions and the geometry of the containers.

Literature review

Theoretical

In the last few decades there has been considerable research interest in natural convection of fluids in cavities. Most of this theoretical and experimental research has been concerned with the natural convection of a Newtonian fluid in two-dimensional rectangular enclosures. Excellent reviews of the area are given in the paper by EcKert and Carlson (1961) and in the articles by Ostrach (1972; 1982) and Catton (1978). Before describing the most important contributions to the literature it is useful to note that all work involves the solution of the Navier Stokes equation coupled with the energy equation. In obtaining numerical solutions the system of equations is normally written in stream function-vorticity form (in which the stream function and vorticity are connected through a Poisson equation) or in primitive variable form (where the dependent variables are the velocity and pressure).

The first successful attempt at a numerical solution of a natural convection problem in a two-dimensional rectangular cavity was performed by Hellums and Churchill (1961). These authors analysed the problem of convection in a rectangular enclosure with differentially heated end walls and adiabatic top and bottom surfaces. They developed an explicit finite difference method for solving the model equations and steady state solutions were obtained. Unfortunately, stability considerations placed severe restrictions on the time step in their explicit method. Wilkes and Churchill (1966) extended the method of solution developed by Hellums and Churchill (1961) to analyse the same problem. They manipulated the momentum equations to eliminate the pressure gradients, preferring to work with vorticity. The vorticity and energy equations were then solved by the alternating direction implicit (ADI) method and the Poisson equation was solved by successive-over-relaxation (SOR) at each time step. Although a theoretical analysis predicted unconditional stability for the numerical scheme, instabilities did occur in practice and the authors were unable to obtain solutions for Grashof numbers greater than 10^5. Torrance (1968) compared several finite difference techniques, both explicit and implicit, that had been developed for the prediction of natural convection flows. In particular, he pointed out that the finite difference form of the equations used by Wilkes and Churchill (1966) did not conserve energy or vorticity. Torrance also discussed, in some detail, the truncation errors of various finite difference representations of the transport equations by introducing false diffusion terms. He concluded that, for buoyancy dominated flows, in order to obtain a stable solution it is necessary to use an upwind or upstream difference representation of the non-linear convective terms.

In 1970 Newell and Schmidt examined the problem of laminar natural convection originally considered by Hellums and Churchill (1961) and investigated a range of parameters sufficient to determine the dependence of Nusselt number on Grashof number and the aspect ratio. Two of the novel features of their numerical investigation were the use of a non-uniform grid spacing and the solution of the governing finite difference equations by a direct matrix inversion. Unfortunately Newell and Schmidt used a non-conservative finite difference scheme and encountered numerical difficulties which prevented them from obtaining solutions for Grashof numbers greater than 10^5.

De Vahl Davis (1968) also studied the steady laminar motion of a fluid in a rectangular cavity with differentially heated end walls. The Navier Stokes equations were written as a fourth order equation in the stream function and the corresponding finite difference equation was solved by direct matrix inversion. An SOR scheme was used to update the temperature. The results were found to be compatible with, and form an extension of, some previous theoretical and experimental results. However, even though it was found that higher Prandtl numbers exert a slight stabilising influence on the numerical solution, instabilities were encountered because of the non-linear terms in the equations and results were found only for Grashof numbers up to 10^5.

In the last ten to fifteen years more complicated numerical schemes have been developed, yet all of the authors concerned have examined the motion of a fluid in a rectangular cavity with differentially heated end walls. A highly efficient method, called cyclic reduction, to solve the Poisson equation was developed by Buzbee et al in 1970. The latter authors examined in detail the additional variants to the method that can be introduced in order to obtain greater numerical stability. Schumann and Sweet (1976) extended the cyclic reduction method to solve the general Poisson equation on a rectangular two-dimensional staggered grid with an arbitrary number of grid points in each direction. However, although any boundary condition could be used in one direction only Neumann boundary conditions were applied in the other. Kublbeck et al (1979) used the ADI scheme to solve the transport equations. The momentum equation was written in stream-function-vorticity type and the Poisson equation was solved by the Cyclic reduction method. Solutions were obtained for Grashof numbers of up to 10^{16}.

The most notable research work in this area in recent years has been carried out by Phillips (1984). He wrote down the momentum equation as a fourth order equation in the stream function and the latter was solved by the Dynamic ADI method. The most important feature of his method, is that it incorporates an automatic step size changer, unfortunately though, at the expense of additional computations. However, Phillips argues that the advantages of having an automatic step size changer which decreases the time step when instabilities occur and attempts to keep it within a region of fast convergence seem to outweigh the extra computation.

Experiments

Even though numerous theoretical investigations of natural convection in rectangular cavities have been reported, detailed experimental results for the temperature and velocity distributions are limited. One major problem in the storage of cryogenic fluids is the increase in pressure. Huntley (1960) carried out experiments with Liquid Nitrogen in a uniformly heated cryogenic container. He confirmed the development of liquid temperature gradients as a contributing factor to the increase in pressure. These gradients became more severe in time. Neff and Chiang (1966) also did experiments in a uniformly heated enclosure to investigate the phenomenon of stratification in cryogenic fluids. Stratification results because the warmer layer has a lower density and the fluid is a poor heat conductor. The authors found that bottom heating of cryogenic containers significantly reduces stratification. Fan, Chu and Scott (1968) did experimental and theoretical work on temperature profiles in pressurised cryogenic vessels subject to a time dependent uniform heat flux. Their theoretical work ignores the axial velocity and yields linear uncoupled equations that can be solved using Duhamel's theory of superposition (Carlslaw, 1959). Unfortunately, they considered a gross oversimplification of the real problem since convection is the main mechanism that creates stratification. Other experiments have dealt with temperature measurements in air enclosed between two vertical plates maintained at different temperatures and results have shown satisfactory agreement with available numerical solutions. Over the years, the experimental techniques have gradually improved - from Mach-Zender interferometer to Schlieren photography and Laser Doppler Velocimeter (LDV) thus enabling highly accurate measurements to be taken.

Experiments studying natural convection in cryogenic fluids have recently been conducted at the Institute of Cryogenics, University of Southampton using modern techniques. In one experiment (Scurlock et al, 1984) LDV and Schlieren Optics were applied to Liquid Nitrogen (LIN) to measure the vertical velocity and temperature profile respectively. Without giving much experimental detail, an inner Dewar flask containing LIN, with a heater coil fixed around it at its mid height, was immersed in a pool of LIN contained in an outer Dewar.

The LIN in the inner Dewar was therefore subjected to a steady lateral heat flux and heat leak at the base was practically zero. A buoyancy-driven flow was set up and measurements using the techniques mentioned above were taken. These measurements were the first ever taken in a Liquid Nitrogen pool. The earlier literature review reveals that analytical results corresponding to Scurlock's experiment have not so far been calculated.

This thesis is concerned with the study of natural convection in a cryogenic fluid in containers of prescribed shape. In particular, the flows of a cryogenic liquid in both rectangular and cylindrical cavities caused by the influx of heat through the sides and base of the cavities are studied. The major physical processes that occur in a real storage situation are shown schematically in Fig. 1.1.

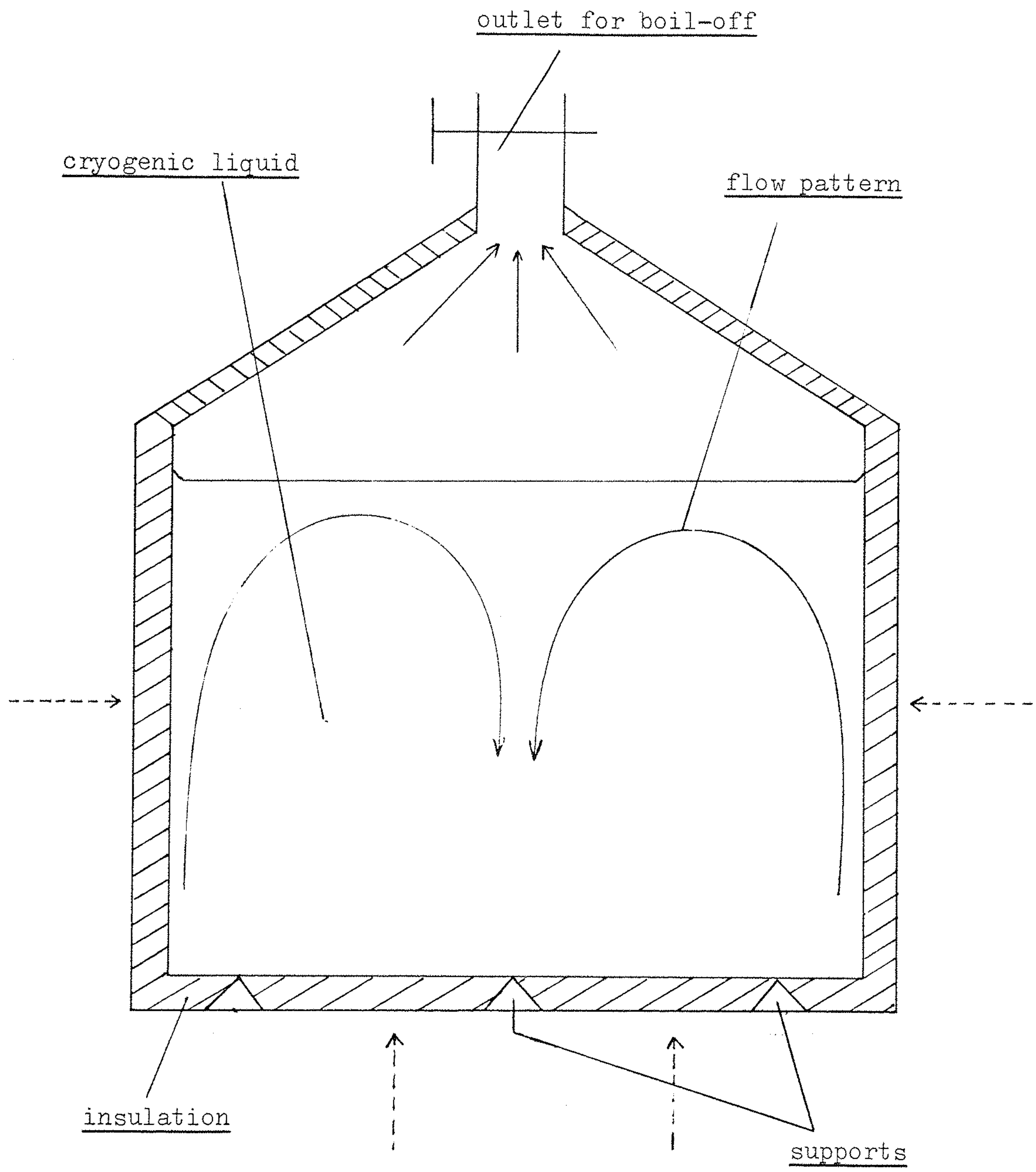

Broken arrows indicate heat flux.

Fig. 1.1 Physical process in an enclosed cavity.

The emphasis in this thesis is placed on developing a simple, but useful, mathematical model. More specifically, the objectives of the research are the following:

1. To develop a mathematical model appropriate to the physical problem using the conservation equations of mass, momentum and the equation of energy transfer.

2. To solve the equations using a reliable numerical method and hence determine the temperature and velocity distributions in the fluid contained in the cavity.

3. To obtain numerical results for different boundary conditions.

4. To compare these numerical results with experimental data (when available) in order to evaluate the usefulness of the model.

5. To suggest possible refinements of the model.

CHAPTER 2
FORMULATION OF THE PROBLEM

§2.1 Choice of coordinate axes

In the previous chapter the problem was set up from a physical point of view. The main aim of this chapter is to construct a mathematical model related to the physical problem. This section provides an introduction and can thus be regarded as a transition from the physical world into the mathematical world.

The problem will in the first instance be investigated in Cartesian coordinates and later on in cylindrical coordinates. Cartesian analogues of engineering problems are, in general, the simplest to work with, although such analogues are strictly valid only for an infinitely long third dimension. Nonetheless, previous theoretical works in the engineering field have shown that Cartesian models provide useful contributions to our understanding of the real world.

In practice heat is likely to enter the container symmetrically and so we adopt this simplifying assumption. As a consequence we assume that the fluid flow in the container is symmetrical about the centre line and hence only one half of the container need be examined which makes the numerical solution much more efficient. The Cartesian set-up is shown in Fig. 2.1.

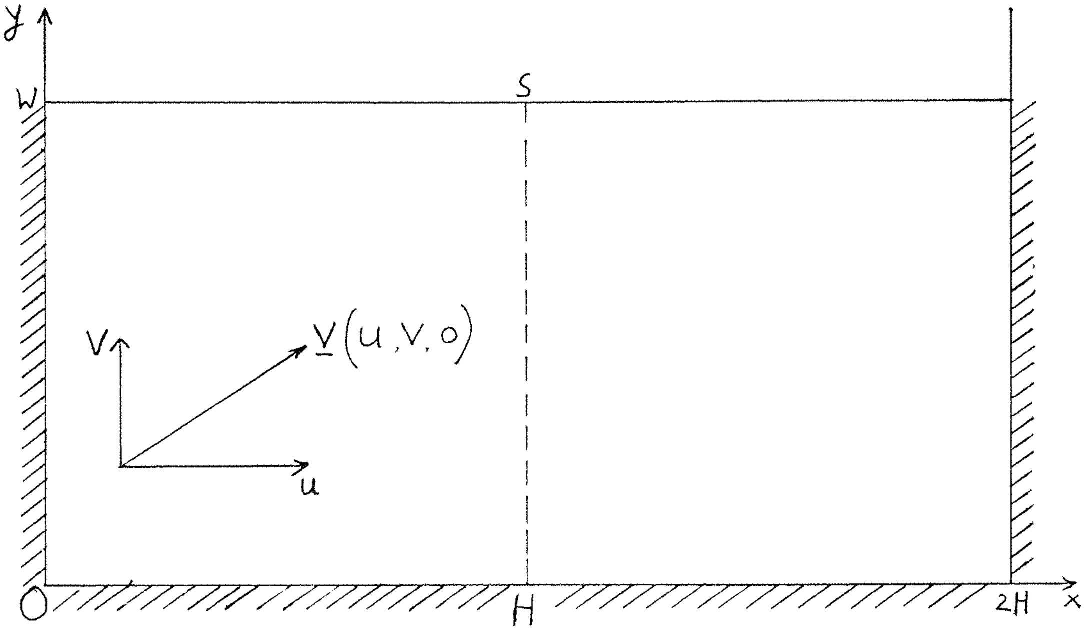

Fig. 2.1 Cartesian representation

In Fig. 2.1 W is the height of the fluid, $2H$ is the width of the container $\underline{V}$ is the fluid velocity with u and v as its components. The base and left wall of the container are represented along axes Ox and Oy respectively. HS is the line of symmetry.

§2.2 Governing equations

Since we are dealing with the motion of a liquid induced by a temperature gradient, the full vector equations governing the motion of the liquid are the Navier-Stokes equations (Milne-Thomson, 1968).

$$\rho\left(\frac{\partial \underline{V}}{\partial t} + (\underline{V}\cdot\nabla)\underline{V}\right) = \mu\left(\nabla^2\underline{V} - \nabla(\nabla\cdot\underline{V})\right) - \nabla p + \underline{b},$$

coupled with the energy equation (Li. Lam, 1966) (2.2.1)

$$\rho C_p \frac{DT}{Dt} = \nabla\cdot k\nabla T + \bar{Q} + \mu \Phi_v$$

and the equation of continuity

$$D\rho/Dt + \rho \operatorname{div} \underline{V} = 0, \qquad (2.2.2)$$

where

$\underline{b}$ is the body force per unit volume,
$\bar{Q}$ represents the internal heat generation,
Φ_v denotes the viscous dissipation,

and $\frac{D}{Dt}$ represents the particle derivative

$$\frac{DT}{Dt} = \frac{\partial T}{\partial t} + (\underline{V}\cdot\nabla)T .$$

In natural convection flows the dominant driving force arises from the temperature variation in the fluid which results in changes in density. The driving force for the flow is then due to the difference between the body force and the force due to the hydrostatic pressure gradient in the ambient medium.

In normal circumstances the body force $\underline{b}$ is given by

$$\underline{b} = \rho \underline{g} \quad , \tag{2.2.3}$$

where $\underline{g}$ is the gravitational force per unit mass of the fluid. If the variation of ρ with temperature were to be neglected, no flow would result.

In the Navier-Stokes equation, the local pressure p may be split into 2 terms, one due to hydrostatic pressure in the ambient medium, p_h and the other due to the motion of the fluid, p_d : viz

$$p = p_h + p_d \ . \tag{2.2.4}$$

From simple hydrostatics it is well known that

$$\nabla p_h = \rho_0 \underline{g} \ , \tag{2.2.5}$$

where ρ_0 is the density of the ambient fluid.

Hence, using equations (2.2.3) - (2.2.5), we may write

$$\underline{b} - \nabla p = (\rho - \rho_0)\underline{g} - \nabla p_d \ . \tag{2.2.6}$$

For vertical buoyant flows,

$$\underline{g} = -g\underline{j} \ , \tag{2.2.7}$$

where $\underline{j}$ is the unit vector in the upward vertical direction and g is the magnitude of $\underline{g}$, and equation (2.2.6) becomes

$$\underline{b} - \nabla p = (\rho_0 - \rho) g \underline{j} - \nabla p_d \, . \qquad (2.2.8)$$

Substituting (2.2.8) into (2.2.1)$_1$ we obtain

$$\rho \frac{D\underline{V}}{Dt} = \mu \left(\nabla^2 \underline{V} - \nabla(\nabla \cdot \underline{V}) \right) + (\rho_0 - \rho) g \underline{j} - \nabla p_d \, . \qquad (2.2.9)$$

In order to make progress with natural convection problems it is usual to introduce the Boussinesq approximation which is now discussed.

If ρ is a function of temperature T and pressure p then the density at a given point in the flow, $\rho(T, p)$ may be written in terms of the density $\rho_0(T_0, p_0)$ in the ambient medium through a double Taylor series expansion about the ambient conditions:

$$\rho = \rho_0 + \left(\partial \rho / \partial T \right)_{p_0} (T - T_0) + \frac{1}{2!} \left(\partial^2 \rho / \partial T^2 \right)_{p_0} (T - T_0)^2 + \cdots$$

$$+ \left(\partial \rho / \partial p \right)_{T_0} (p - p_0) + \frac{1}{2!} \left(\partial^2 \rho / \partial p^2 \right)_{p_0} (p - p_0)^2 + \cdots +$$

$$+ \partial^2 \rho / \partial p \partial T \, (p - p_0)(T - T_0) + \cdots \qquad (2.2.10)$$

$T\,(^{\circ}K)$	p (atm)	ρ (g/cc)
75	0.74992	0.81812
76	0.84901	0.81361
77	0.95784	0.80905
77.36	1.0000	0.80736
78	1.0770	0.80445
79	1.2072	0.79981
80	1.3489	0.79513

Table 1 Liquid Nitrogen along saturation curve

Data for cryogenic fluids (see, for example, Table 1) shows that

$$\left(\partial\rho/\partial p\right)_{T_0} \ll \left(\partial\rho/\partial T\right)_{p_0} , \qquad (2.2.11)$$

an inequality satisfied by most fluids at normal temperatures. Since $(T-T_0)$ and $(p-p_0)$ are in general small quantities it therefore seems reasonable to approximate (2.2.10) by

$$\rho-\rho_0 = -\rho_0\,\beta\,(T-T_0) , \qquad (2.2.12)$$

where we have used the definition of β , the volumetric expansion coefficient, namely

$$\beta = -\frac{1}{\rho_0}\left(\partial\rho/\partial T\right)_{p_0} . \qquad (2.2.13)$$

Equation (2.2.12) indicates that the density difference may be approximated as a pure temperature effect. In the Boussinesq approximation equation (2.2.12) is introduced in the buoyancy term, but in all other places the density is assumed constant.

With the aid of (2.2.12) and assuming that:-

(i) viscous dissipation is negligible;
(ii) there are no internal heat sources;
(iii) the Boussinesq approximation is valid and
(iv) the thermal conductivity of the liquid is independent of temperature

we obtain from equations (2.2.1), (2.2.2) and (2.2.9) the following governing equations:

$$\frac{\partial \underline{V}}{\partial t} + (\underline{V} \cdot \nabla)\underline{V} = \nu \nabla^2 \underline{V} - \frac{1}{\rho_0}\nabla p_d + g\beta(T - T_0)\underline{j}, \quad (2.2.14)$$

$$\frac{\partial T}{\partial t} + (\underline{V} \cdot \nabla) T = K \nabla^2 T, \quad (2.2.15)$$

$$\nabla \cdot \underline{V} = 0, \quad (2.2.16)$$

where
$\nu = \mu/\rho$ – Kinematic viscosity and
$K = k/\rho_0 C_p$ – thermal diffusivity .

The assumption regarding viscous dissipation is reasonable since cryogenic fluids have low viscosity. Data for cryogenic fluids also show that the thermal conductivity does not show any significant variation with temperature. The above equations are time dependent.

For our problem we will impose boundary conditions that are independent of time and will seek the steady-state solution to the above system. This solution can be achieved either by neglecting the time-dependent terms in equations (2.2.14) and (2.2.13) from the outset, or obtaining the solution from the general equations (2.2.14) and (2.2.15) through application of a time-marching numerical method. It is the latter approach that will be adopted in this thesis.

For our two-dimensional situation equation (2.2.16) can be written as

$$\frac{\partial u}{\partial x} + \frac{\partial v}{\partial y} = 0 \; . \tag{2.2.17}$$

This equation implies the existence of $\psi(x,y)$, the stream function, such that

$$u = \frac{\partial \psi}{\partial y} \; , \qquad v = -\frac{\partial \psi}{\partial x} \; . \tag{2.2.18}$$

(Milne-Thompson, 1968)

On substituting equations (2.2.18) into (2.2.17) we find that the latter is identically satisfied.

Equation (2.2.14) is usually referred to as being written in primitive variable form, the primitive variables being p and $\underline{V}$. In our problem we are not interested in the pressure field directly and will place boundary conditions on the velocity and its derivatives. Hence it seems more appropriate to convert equation (2.2.14) to the so-called stream function-vorticity type, with dependent variables the stream function and vorticity. Using familiar vector identities equation (2.2.14) can be written

$$\frac{\partial \underline{V}}{\partial t} + \nabla\left(\frac{1}{2}\underline{V}^2\right) - \underline{V} \times \text{curl}\ \underline{V} =$$

$$= \nu\left(\text{grad}\left(\text{div}\ \underline{V}\right) - \text{curl curl}\ \underline{V}\right) - \frac{1}{\rho}\nabla p_d + g\beta\left(T - T_0\right)\underline{j}\ , \tag{2.2.19}$$

which can be simplified by using (2.2.16). Next the curl operator is applied to both sides of equation (2.2.19). Using the definition of curl and applying some vector identities we obtain

$$\partial \underline{\omega}/\partial t - \text{curl}\left(\underline{V} \times \underline{\omega}\right) = -\nu\ \text{curl curl}\ \underline{\omega} + g\beta\frac{\partial T}{\partial x}\underline{k}\ , \tag{2.2.20}$$

where

$\underline{k}$ is the unit vector in the z -direction

and the vorticity, $\underline{\omega}$ is defined through

$$\underline{\omega} = \text{curl}\ \underline{V}\ . \tag{2.2.21}$$

Substituting (2.2.18) in (2.2.21) and recalling that $\underline{V} = (u, v, 0)$ we obtain

$$\underline{\omega} = (0, 0, Q)\ , \tag{2.2.22}$$

where

$$Q = -\frac{\partial^2 \psi}{\partial x^2} - \frac{\partial^2 \psi}{\partial y^2} = -\nabla^2 \psi\ , \tag{2.2.23}$$

∇^2 denoting the Laplacian operator. Equation (2.2.23) is generally known as the "Poisson Equation for the stream-function." Using the definition of curl, equation (2.2.22) yields

$$\text{Curl}\ \underline{\omega} = \left(\frac{\partial Q}{\partial y}, \ -\frac{\partial Q}{\partial x}, \ 0 \right) \tag{2.2.24}$$

and

$$\text{Curl curl}\ \underline{\omega} = \left(0, \ 0, \ -\nabla^2 Q \right) . \tag{2.2.25}$$

From expressions (2.2.18) and (2.2.22), we find that

$$\left(\underline{V} \times \underline{\omega} \right) = \left(VQ, \ -UQ, \ 0 \right), \tag{2.2.26}$$

from which it follows that

$$\text{curl}\left(\underline{V} \times \underline{\omega} \right) = \left(0, \ 0, \ -\text{div}\left(\underline{V}\, Q \right) \right) . \tag{2.2.27}$$

On substituting (2.2.25) and (2.2.27) into (2.2.20) it is readily observed that the vector equation (2.2.20) reduces to the scalar equation

$$\frac{\partial Q}{\partial t} = -\text{div}\left(\underline{V} Q \right) + \nu \nabla^2 Q + g\beta \frac{\partial T}{\partial x} , \tag{2.2.28}$$

the other two components of the vector equation being identically zero. Using the continuity equation we obtain another expression for $\text{div}\left(\underline{V}\, Q \right)$

$$\text{div}\left(\underline{V}\, Q \right) = Q\ \text{div}\ \underline{V} + \underline{V}\cdot\text{grad}\,Q = U\frac{\partial Q}{\partial x} + V\frac{\partial Q}{\partial y} . \tag{2.2.29}$$

Substituting (2.2.29) into (2.2.28) we finally obtain

$$\frac{\partial Q}{\partial t} + u\frac{\partial Q}{\partial x} + v\frac{\partial Q}{\partial y} = \nu\nabla^2 Q + g\beta\frac{\partial T}{\partial x} \quad . \qquad (2.2.30)$$

§2.3 Governing equations in non-dimensional form

In the previous section it was shown ((2.2.15), (2.2.23), (2.2.30)) that the three governing equations which result from our mathematical model are

$$\frac{\partial Q}{\partial t} + u\frac{\partial Q}{\partial x} + v\frac{\partial Q}{\partial y} = \nu\nabla^2 Q + g\beta\frac{\partial T}{\partial x} , \tag{2.3.1}$$

$$\frac{\partial T}{\partial t} + (\underline{V}\cdot\nabla)T = \kappa\nabla^2 T , \tag{2.3.2}$$

$$\nabla^2\psi = -Q . \tag{2.3.3}$$

We shall now look at the non-dimensionalisation of these governing equations.

Let

α_0 be a characteristic velocity,
H be a characteristic length and
β_0 be a characteristic stream function

From Fourier's law of heat conduction ,

$$Q' = -k\nabla T , \tag{2.3.4}$$

where k is the thermal conductivity
we deduce that a characteristic temperature is

$$Q'H/k_1 . \tag{2.3.5}$$

Put

$$\left.\begin{array}{l} U^* = \dfrac{u}{\alpha_o}, \quad V^* = \dfrac{V}{\alpha_o}, \quad X^* = \dfrac{X}{H}, \\ y^* = y/W, \quad \Psi^* = \Psi/\beta_o, \end{array}\right\} \tag{2.3.6}$$

$$\theta = \frac{T - T_o}{Q'H/k}, \tag{2.3.7}$$

$$\tau = t\alpha_o/H. \tag{2.3.8}$$

In (2.3.7) T_o is the surface temperature of the fluid. In this thesis we assume that the fluid free surface is flat and isothermal. Experiments with cryogenic fluids would suggest that this assumption is quite a reasonable one. It follows from equations (2.2.18) and (2.3.6) that

$$U^* = \left(\beta_o/\alpha_o W\right)\frac{\partial \Psi^*}{\partial y^*}, \quad V^* = \left(-\beta_o/\alpha_o H\right)\frac{\partial \Psi^*}{\partial X^*}. \tag{2.3.9}$$

In order to simplify the above expressions it seems reasonable to assume that

$$\beta_o = \alpha_o H. \tag{2.3.10}$$

Recalling expression (2.2.23) the non-dimensional vorticity component, Q^*, is defined through

$$Q = \frac{\alpha_o}{H} Q^*. \tag{2.3.11}$$

With the aid of equations (2.3.6) - (2.3.9) and (2.3.11), equation (2.3.1) becomes

$$\frac{\partial Q^*}{\partial \tau} + U^*\frac{\partial Q^*}{\partial X^*} + \gamma V^*\frac{\partial Q^*}{\partial y^*} = \frac{\nu}{\alpha_o H}\nabla^{*2}Q^* + \frac{g\beta Q' H^2}{k_1 \alpha_o^2}\frac{\partial \theta}{\partial X^*}, \tag{2.3.12}$$

where $\gamma = \dfrac{H}{W}$, $\nabla^{*2} = \dfrac{\partial^2}{\partial x^{*2}} + \gamma^2 \dfrac{\partial^2}{\partial y^{*2}}$.

Choosing

$$\alpha_0 = \frac{K}{H} , \tag{2.3.13}$$

equation (2.3.12) can be written as

$$\frac{\partial Q^*}{\partial \tau} + U^* \frac{\partial Q^*}{\partial X^*} + \gamma V^* \frac{\partial Q^*}{\partial y^*} =$$

$$= P_r \nabla^{*2} Q^* + G_r P_r^2 \frac{\partial \theta}{\partial X^*} , \tag{2.3.14}$$

where the Prandtl number P_r , Grashof number G_r and Rayleigh number R_a are defined by

$$P_r = \frac{\nu}{K} , \quad G_r = \frac{g \beta Q' H^4}{k \nu^2} , \quad R_a = G_r P_r . \tag{2.3.15}$$

Using the same non-dimensional variables it is easily shown that the non-dimensional forms of the energy equation (2.3.2) and Poisson equation (2.3.3) are

$$\frac{\partial \theta}{\partial \tau} + U^* \frac{\partial \theta}{\partial X^*} + V^* \gamma \frac{\partial \theta}{\partial y^*} = \nabla^{*2} \theta \tag{2.3.16}$$

and

$$\nabla^{*2} \psi^* = - Q^* . \tag{2.3.17}$$

§2.4 Boundary and initial conditions

Before formulating the boundary conditions we introduce a few simplifying assumptions. We assume that

(i) there is no evaporation ;

(ii) there is a constant and uniform heat flux on bottom and sides of the container ;

(iii) there is no shear stress at top surface.

The first two assumptions are not strictly valid; yet if they were disregarded, the model would be very much complicated. Moreover experiments with cryogenic fluids show that evaporation only becomes significant if we are dealing with containers on a laboratory scale. Variations in the influx of heat through the outer surface of the container are more significant at the base than at the walls because of supporting devices at the bottom. With reliable means of insulation existing nowadays, however, the uniformity of the heat flux through the container walls is also a reasonable assumption.

Since the viscosity of the cryogenic vapour is small compared to the liquid viscosity the condition of zero shear stress at the surface is a realistic postulate.

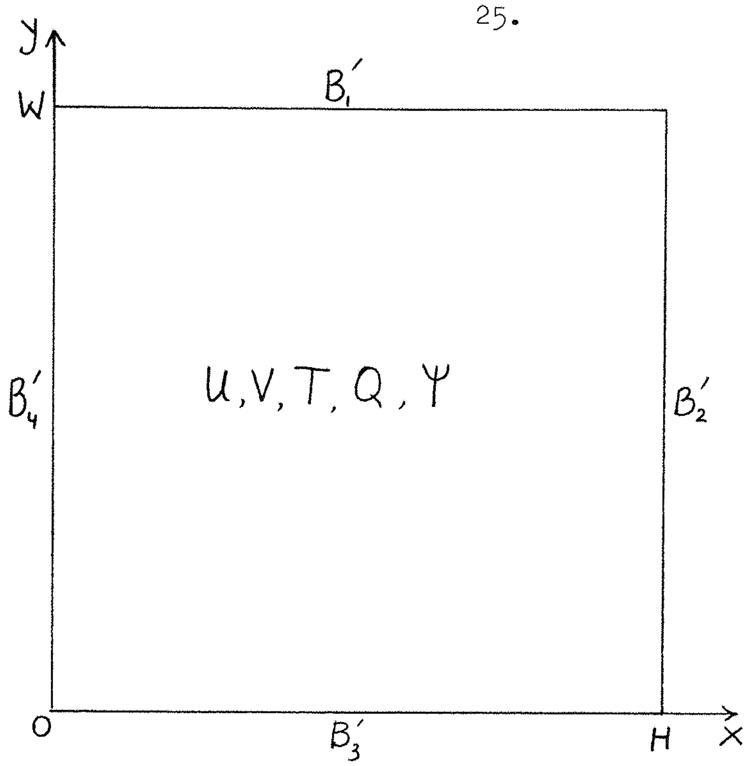

Fig. 2.4.1 Solution domain

We shall now consider the boundary conditions in physical variables. Reference shall be made to Fig. 2.4.1 and each boundary will be separately considered.

1. Consider B_1' : this boundary represents the top surface,

ie $$B_1' = \left\{ (x,y) \middle| \, 0 \leq x \leq H, \; y = W \right\} .$$

It is an isothermal flat surface, so, on B_1' , we require $T = T_0$
Since we are assuming zero evaporation, the fluid molecules are at rest with respect to the y -direction, and we need $v = 0$

This condition implies that
$$\frac{\partial v}{\partial x} = 0 \quad . \tag{2.4.1}$$

The shear stress τ_{xy} is defined by
$$\tau_{xy} = \mu\left(\frac{\partial u}{\partial y} + \frac{\partial v}{\partial x}\right) . \tag{2.4.2}$$

Considering zero shear stress, expressions (2.4.1) and (2.4.2) imply that

$$\frac{\partial u}{\partial y} = 0 \quad . \tag{2.4.3}$$

Equations (2.2.18), (2.2.23), (2.4.1) and (2.4.3) then imply that on B_1'

$$Q = 0 \qquad ; \tag{2.4.4}$$

that is we have zero vorticity on the top surface.

2. Consider next B_2' which represents the mid-line or the line of symmetry:

$$B_2' = \left\{ (x, y) \,\middle|\, 0 < y < W \ , \ x = H \right\} .$$

By symmetry, there is no heat and mass transfer across the mid-line and hence

$$\frac{\partial T}{\partial x} = 0 \ ; \tag{2.4.5}$$

$$u = 0 \quad ; \quad \frac{\partial v}{\partial x} = 0 \quad . \tag{2.4.6}$$

Equations (2.2.18), (2.2.23) and (2.4.6) again imply that on B_2'

$$Q = 0 \quad . \tag{2.4.7}$$

3. The boundary B_3' represents the left-half of the base of the container:

ie $B_3' = \left\{ (x,y) \middle| \; 0 \leq x \leq H, \; y = 0 \right\}$. (2.4.8)

The no-slip condition on this surface implies that the fluid is at rest on B_3' ;

Therefore $$u = 0 \tag{2.4.9}$$

and $$v = 0 \; . \tag{2.4.10}$$

Equations (2.2.18), (2.2.23) and (2.4.9) then reveal that on B_3'

$$Q = -\frac{\partial^2 \psi}{\partial y^2} \; . \tag{2.4.11}$$

Let Q_1 be the value of the external heat flux at the base. Then on B_3'

$$Q_1 = -k \frac{\partial T}{\partial y} \; . \tag{2.4.12}$$

From (2.4.12) we obtain

$$\frac{\partial T}{\partial y} = -\frac{Q_1}{k} \; . \tag{2.4.13}$$

4. Finally, B_4' represents the left wall of the container:

$$B_4' = \left\{ (x,y) \middle| \; 0 < y < W, \; x = 0 \right\} .$$

The no slip condition again implies that on B_4'

$$u = 0 \tag{2.4.14}$$

and $$v = 0 \; . \tag{2.4.15}$$

and (2.2.18), (2.2.23) and (2.4.15) yield

$$Q = -\frac{\partial^2 \psi}{\partial x^2} \quad \text{on} \quad B_4' \ . \tag{2.4.16}$$

Suppose Q_2 is the value of the external heat flux on B_4' , then

$$Q_2 = -k \frac{\partial T}{\partial x} \tag{2.4.17}$$

or

$$\frac{\partial T}{\partial x} = -\frac{Q_2}{k} \quad \text{on} \quad B_4' \ . \tag{2.4.18}$$

Since no fluid crosses the boundaries B_1' , B_2' , B_3' or B_4' all are streamlines. Moreover, since the boundaries intersect, in pairs the stream function has the same constant value on all of the separate boundaries. So on B_1' , B_2' , B_3' and B_4' we take

$$\psi = 0 \ . \tag{2.4.19}$$

Equations (2.2.18), (2.4.10) and (2.4.14) imply that

$$\frac{\partial \psi}{\partial y} = 0 \quad \text{on} \quad B_3' \tag{2.4.20}$$

and

$$\frac{\partial \psi}{\partial x} = 0 \quad \text{on} \quad B_4' \ . \tag{2.4.21}$$

Now we shall put the boundary conditions in non-dimensional variables. Reference is made to § 2.3 and Fig. 2.4.2. Each boundary is separately considered.

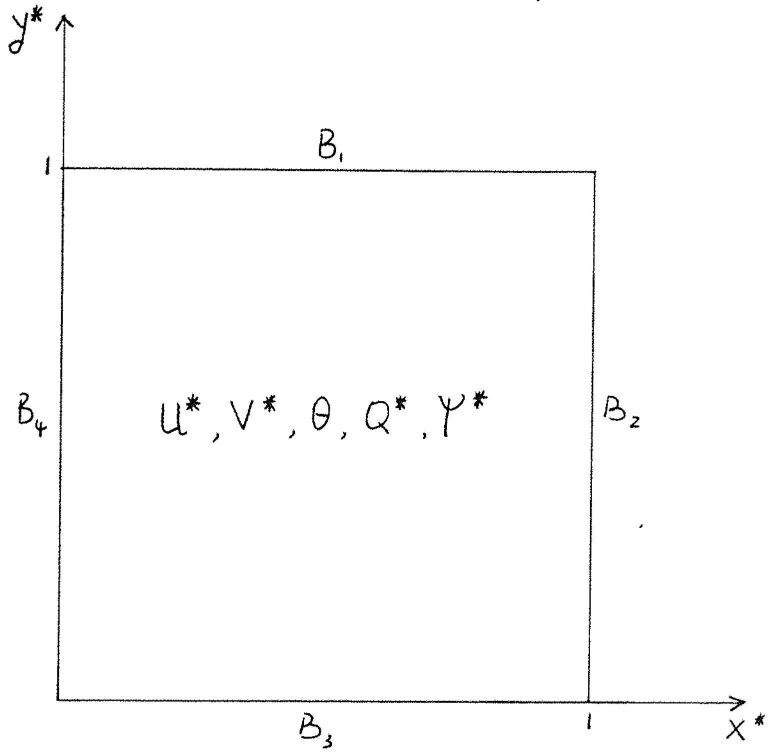

Fig. 2.4.2 Solution domain

Using the definitions for the respective non-dimensional variables in 2.3, the following picture emerges:

1. On $B_1 = \left\{ (x^*, y^*) \mid 0 \le x^* \le 1 \, , \; y^* = 1 \right\}$,

$$\theta = 0 \, , \quad Q^* = 0 \, , \quad \Psi^* = 0 \, . \tag{2.4.22}$$

2. On $B_2 = \left\{ (x^*, y^*) \mid 0 < y^* < 1 \, , \; x^* = 1 \right\}$,

$$\frac{\partial \theta}{\partial x^*} = 0 \, , \tag{2.4.23}$$

$$\Psi^* = 0 \, , \quad Q^* = 0 \, . \tag{2.4.24}$$

3. On $B_3 = \{ (x^*, y^*) \mid 0 \leq x^* \leq 1 , y^* = 0 \}$,

$$\psi^* = 0 , \quad \frac{\partial \psi^*}{\partial y^*} = 0 , \tag{2.4.25}$$

$$Q^* = -\gamma^2 \frac{\partial^2 \psi^*}{\partial y^{*2}} , \tag{2.4.26}$$

$$\frac{\partial \theta}{\partial y^*} = -\frac{1}{\gamma} \frac{Q_1}{Q'} ,$$

where we recall that Q' is a reference heat flux. We shall put Q' equal to Q_1 , in which case

$$\frac{\partial \theta}{\partial y^*} = -\frac{1}{\gamma} . \tag{2.4.27}$$

4. On $B_4 = \{ (x^*, y^*) \mid 0 < y^* < 1 , \quad x^* = 0 \}$,

$$\psi^* = 0 , \quad \frac{\partial \psi^*}{\partial x^*} = 0 , \tag{2.4.28}$$

$$Q^* = -\frac{\partial^2 \psi^*}{\partial x^{*2}} , \tag{2.4.29}$$

$$\frac{\partial \theta}{\partial x^*} = -\frac{Q_2}{Q_1} . \tag{2.4.30}$$

Let us now look at the initial conditions. If our system is sufficiently stable the steady state solution eventually reached with our time-marching method should be independent of the initial conditions. For the present, therefore, it is assumed that

$$\theta = 0 , \quad \psi^* = 0 , Q^* = 0 \quad \text{at} \quad \tau = 0 \tag{2.4.31}$$

throughout the region $0 \leq x^* \leq 1 , \quad 0 \leq y^* \leq 1$.

The choice of initial conditions is discussed further in Chapter 4 of this thesis.

We have now formulated a fairly simple mathematical model. Its usefulness, or otherwise, depends on the sensibility of the numerical results.

Summing up §2.1 – §2.4, we collect together the important equations of our mathematical model.

For convenience the stars on the non-dimensional quantities are now omitted and the governing system of equations plus the boundary and initial conditions are written:

$$\frac{\partial Q}{\partial \tau} + u\frac{\partial Q}{\partial x} + \gamma v\frac{\partial Q}{\partial y} = P_r \nabla^2 Q + G_r P_r^2 \frac{\partial \theta}{\partial x}, \qquad (2.4.32)$$

$$\frac{\partial \theta}{\partial \tau} + u\frac{\partial \theta}{\partial x} + \gamma v\frac{\partial \theta}{\partial y} = \nabla^2 \theta, \qquad (2.4.33)$$

$$\nabla^2 \Psi = -Q, \qquad (2.4.34)$$

where it should be emphasised ∇^2 now denotes

$$\nabla^2 = \frac{\partial^2}{\partial x^2} + \gamma^2 \frac{\partial^2}{\partial y^2}. \qquad (2.4.35)$$

Boundary conditions

1. On $\{ (x,1) \mid 0 \le x \le 1 \}$,

$$\theta = 0, \quad \Psi = 0, \quad Q = 0.$$

2. On $\{(1,y) \mid 0 < y < 1\}$,

$$\frac{\partial\theta}{\partial x} = 0, \quad \Psi = 0, \quad Q = 0.$$

3. On $\{(x,0) \mid 0 \leq x \leq 1\}$,

$$\Psi = 0, \quad \frac{\partial\Psi}{\partial y} = 0, \quad Q = -\gamma^2 \frac{\partial^2\Psi}{\partial y^2}, \quad \frac{\partial\theta}{\partial y} = \frac{-1}{\gamma}.$$

4. On $\{(0,y) \mid 0 < y < 1\}$,

$$\Psi = 0, \quad \frac{\partial\Psi}{\partial x} = 0, \quad Q = -\frac{\partial^2\Psi}{\partial x^2}, \quad \frac{\partial\theta}{\partial x} = -\frac{Q_2}{Q_1}.$$

Initial conditions

$$\Psi = 0, \ Q = 0, \ \theta = 0 \quad \text{in} \quad \{(x,y) \mid 0 \leq x \leq 1, 0 \leq y \leq 1\}.$$

An analytical solution to this coupled system of equations is not possible, so in the next chapter we shall look for a numerical solution.

CHAPTER 3
NUMERICAL PROCEDURE

§3.1 Choice for a numerical solution procedure

To the present, only a limited number of types of partial differential equations have been solved analytically and these solutions are normally restricted to problems in regions of simple geometrical shape. Exact analytical solutions of our governing equations are not feasible so approximate analytical methods or numerical solutions are the only methods available, apart from the use of analogue devices. Although analytical approximation methods can provide extremely useful information concerning the character of the solution for critical values of the dependent variables, it is not possible for our problem to find such solutions that are valid throughout the cavity. Therefore, in this thesis, a numerical solution procedure has been adopted. Of the numerical approximation methods available for solving differential equations those employing finite differences are more frequently used and will be employed here. Since the transport equations are of parabolic type and the Poisson equation is elliptic, the numerical techniques for these two types of equations will be discussed in the following sections.

3.2 An introduction to finite difference schemes

Let the arbitrary function f and its derivatives be single-valued, finite and continuous functions of the independent variable s
In other words $f \in C^{K}(\mathbb{R})$. Then by Taylor's theorem it follows that

$$f(s+h) = f(s) + h\frac{\partial f}{\partial s} + \frac{h^2}{2!}\frac{\partial^2 f}{\partial s^2} + o(h^3) \qquad (3.2.1)$$

and $$f(s-h) = f(s) - h\frac{\partial f}{\partial s} + \frac{h^2}{2!}\frac{\partial^2 f}{\partial s^2} + o(h^3) , \qquad (3.2.2)$$

where h is measured relative to the s -axis and $o(h^3)$ denotes terms containing third and higher power of h .

Addition of (3.2.1) and (3.2.2) gives

$$f(s+h) + f(s-h) = 2f(s) + h^2\frac{\partial^2 f}{\partial s^2} + o(h^4) . \qquad (3.2.3)$$

Assuming the magnitudes of the higher terms are negligible in comparison with lower order terms, it follows that

$$\frac{\partial^2 f}{\partial s^2} = \frac{1}{h^2}\left\{ f(s+h) - 2f(s) + f(s-h)\right\} , \qquad (3.2.4)$$

with a leading error on the right hand side of $o(h^2)$. In an analogous way subtraction of expansion (3.2.2) from (3.2.1) gives

$$\frac{\partial f}{\partial s} = \frac{1}{2h}\left\{ f(s+h) - f(s-h)\right\} , \qquad (3.2.5)$$

with an error of $o(h^2)$. Expression (3.2.5) is called the central-difference approximation for $\frac{\partial f}{\partial s}$.

Neglecting terms of order h^2 and higher in expansions (3.2.1) and (3.2.2), we obtain the following two expressions for $\frac{\partial f}{\partial s}$ respectively:

$$\frac{\partial f}{\partial s} = \frac{1}{h}\left\{ f(s+h) - f(s) \right\} \tag{3.2.6}$$

and

$$\frac{\partial f}{\partial s} = \frac{1}{h}\left\{ f(s) - f(s-h) \right\} . \tag{3.2.7}$$

Formulae (3.2.6) and (3.2.7) are called the forward-difference and backward-difference approximations respectively for $\frac{\partial f}{\partial s}$.

It is easily seen from expansions (3.2.1) and (3.2.2) that the errors in using the formulae (3.2.6) and (3.2.7) are both of $o(h)$.

If f is a function of more than one variable, then the above expressions can be used to obtain appropriate finite difference forms for the partial derivatives. Below we shall derive some basic finite difference formulae.

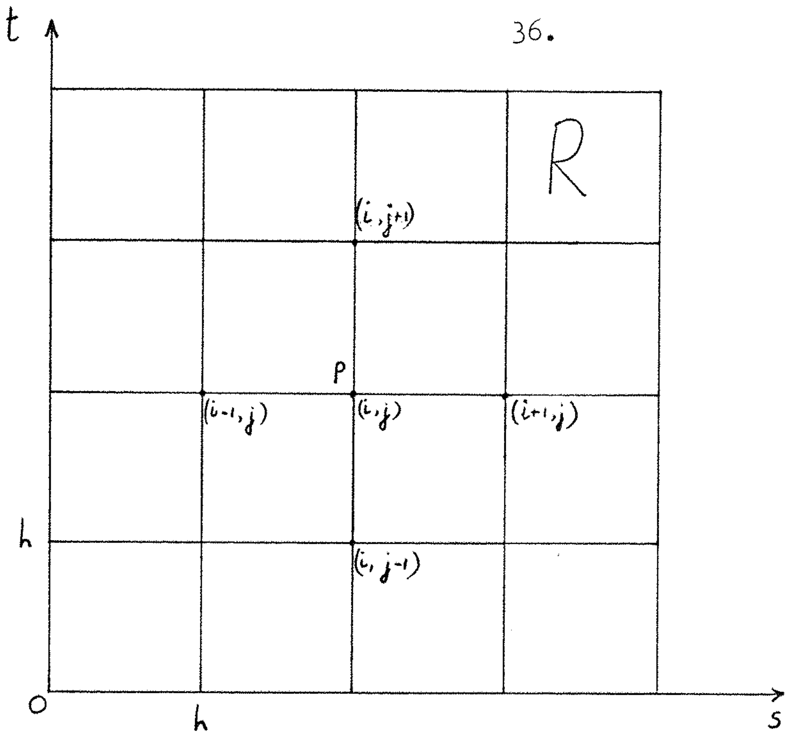

Fig 3.2.1 Discretization of a square region

Let $R \subset \mathbb{R}^2$ be a square finite region (see Fig. 3.2.1) and suppose f is a function of two variables s and t (t is not necessarily the time). Using expressions (3.2.4) - (3.2.7) we approximate the first and second derivatives of the function f on a set of discrete points within R . The discretization of R is done in the following way: subdivide the region R into sets of equal squares of sides $\delta s = h$, $\delta t = h$, as shown in Fig. 3.2.1 and let the co-ordinates (s, t) of the arbitrary mesh point P be

$$s = ih \; ; \quad t = jh \; , \tag{3.2.8}$$

where i and j are integers. Denoting the value of f at P by

$$f_P = f(ih, jh) = f_{i,j} \; ,$$

we have by (3.2.4):

$$\left[\frac{\partial^2 f}{\partial s^2}\right]_P = \frac{1}{h^2}\left\{f[(i+1)h, jh] - 2f[ih, jh] + f[(i-1)h, jh]\right\}, \quad (3.2.9)$$

ie
$$\left[\frac{\partial^2 f}{\partial s^2}\right]_{i,j} = \frac{1}{h^2}\left(f_{i+1,j} - 2f_{i,j} + f_{i-1,j}\right), \quad (3.2.10)$$

with an error of order h^2. Similarly

$$\left[\frac{\partial^2 f}{\partial t^2}\right]_{i,j} = \frac{1}{h^2}\left(f_{i,j+1} - 2f_{i,j} + f_{i,j-1}\right), \quad (3.2.11)$$

with an error again of order h^2.

With this notation the centred, forward and backward difference approximations for the first derivative at the point P are respectively

$$\left[\frac{\partial f}{\partial s}\right]_{i,j} = \frac{1}{2h}\left(f_{i+1,j} - f_{i-1,j}\right), \quad (3.2.12)$$

$$\left[\frac{\partial f}{\partial s}\right]_{i,j} = \frac{1}{h}\left(f_{i+1,j} - f_{i,j}\right) \quad (3.2.13)$$

and
$$\left[\frac{\partial f}{\partial s}\right]_{i,j} = \frac{1}{h}\left(f_{i,j} - f_{i-1,j}\right). \quad (3.2.14)$$

the last two with an error of $o(h)$. The corresponding expressions for $\partial f/\partial t$ can be written from the above in an obvious way. Expressions ((3.2.10) - (3.2.14)) are known as the finite-difference formulae for the first and second derivatives of f. The points of intersection of lines in the discretized region that are parallel to the S-axis and t-axis are called mesh points. Finite difference methods generally give solutions that are sufficiently accurate for the required purposes.

§3.3 Co-ordinate transformation. The ADI method

The finite difference formulae derived in the previous section shall be used in the solution of the governing equations for our particular problem.

Let Ω' be the region over which the governing equations (2.4.32) - (2.4.34) and the boundary conditions are defined.

$$\Omega' = \left\{ (x, y) \,\middle|\, 0 \leq x \leq 1, 0 \leq y \leq 1 \right\} . \tag{3.3.1}$$

Because of the expected steep temperature and velocity gradients in the fluid near the side walls, we would like in our numerical scheme to have good resolution in and near the boundary regions. One answer to the problem would be to introduce an extremely dense, but uniform, grid which naturally leads to a tremendous number of algebraic equations to be solved. An alternative, and better method, is to use a non-uniform grid by introducing suitable coordinate transformations

$$x \longleftrightarrow p(x) \quad , \quad y \longleftrightarrow q(y) .$$

which accumulate the grid points in the boundary regions.

With arbritrary transformation relations $p(x)$ and $q(y)$, one obtains for the first derivative of a dependent dummy variable Γ

$$\frac{\partial \Gamma}{\partial x} = A_x \frac{\partial \Gamma}{\partial p} , \tag{3.3.2}$$

$$\frac{\partial \Gamma}{\partial y} = A_y \frac{\partial \Gamma}{\partial q} , \tag{3.3.3}$$

where

$$A_x = \frac{\partial p}{\partial x} \quad , \qquad A_y = \frac{\partial q}{\partial y} \quad .$$

From (3.3.2), (3.3.3) one similarly obtains for the second derivatives

$$\frac{\partial^2 \Gamma}{\partial x^2} = A_x^2 \frac{\partial^2 \Gamma}{\partial p^2} + B_x \frac{\partial \Gamma}{\partial p} \quad ,$$

$$\frac{\partial^2 \Gamma}{\partial y^2} = A_y^2 \frac{\partial^2 \Gamma}{\partial q^2} + B_y \frac{\partial \Gamma}{\partial q} \quad , \tag{3.3.4}$$

where

$$B_x = \frac{\partial^2 p}{\partial x^2} \quad , \qquad B_y = \frac{\partial^2 q}{\partial y^2} \quad ,$$

Substituting (3.3.2) - (3.3.4) into governing equations (2.4.32) - (2.4.34) one obtains the following set of transformed equations

$$\frac{\partial Q}{\partial \tau} + A_x u \frac{\partial Q}{\partial p} + \gamma A_y v \frac{\partial Q}{\partial q} = P_r\left(A_x^2 \frac{\partial^2 Q}{\partial p^2} + \gamma^2 A_y^2 \frac{\partial^2 Q}{\partial q^2}\right) + \tag{3.3.5}$$

$$+ P_r\left(B_x \frac{\partial Q}{\partial p} + \gamma^2 B_y \frac{\partial Q}{\partial q}\right) + G_r P_r^2 A_x \frac{\partial \theta}{\partial p} \quad ,$$

$$\frac{\partial \theta}{\partial \tau} + A_x u \frac{\partial \theta}{\partial p} + \gamma A_y v \frac{\partial \theta}{\partial q} = A_x^2 \frac{\partial^2 \theta}{\partial p^2} + \gamma^2 A_y^2 \frac{\partial^2 \theta}{\partial q^2} + \tag{3.3.6}$$

$$+ B_x \frac{\partial \theta}{\partial p} + \gamma^2 B_y \frac{\partial \theta}{\partial q} \quad ,$$

$$A_x^2 \frac{\partial^2 \psi}{\partial p^2} + B_x \frac{\partial \psi}{\partial p} + \gamma^2\left(A_y^2 \frac{\partial^2 \psi}{\partial q^2} + B_y \frac{\partial \psi}{\partial q}\right) = -Q \quad . \tag{3.3.7}$$

where the velocities are calculated as follows:

$$u = \gamma A_y \frac{\partial \psi}{\partial q}, \qquad V = -A_x \frac{\partial \psi}{\partial p} . \tag{3.3.8}$$

It should be noted that the original equations are immediately recovered by setting

$$A_x = A_y = 1 , \qquad B_x = B_y = 0 .$$

The choice of the form of coordinate transformation may depend on the nature of the particular problems to be solved. Several useful transformations have been discussed (Roache, 1976; Phillips, 1984). For natural convection in a cavity, the relation

$$p(x) = \frac{1}{2}\left\{ 1 + \frac{\tan\left[\frac{\pi\epsilon}{2}(2x-1)\right]}{\tan\left(\frac{\pi\epsilon}{2}\right)} \right\} . \tag{3.3.9}$$

has been recommended (Kublbeck, 1980) and will be used in this thesis. Fig. 3.3.1 shows a graph of this relation for several values of the deformation parameter, ϵ .

Fig. 3.3.1 The transformation relation $p(x,\epsilon)$ for different values of the deformation parameter

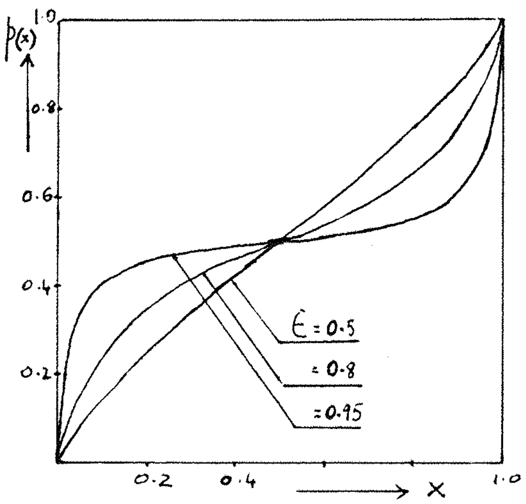

For our problem we shall choose

$$q(y) = y \ , \tag{3.3.10}$$

that is, the y -coordinate will not be transformed: this postulate will be discussed at the end of § 3.7. With the assumption (3.3.10) it follows that

$$A_y = 1 \quad \text{and} \quad B_y = 0 \ .$$

Also with the coordinate transformation, the discretization of the continuous region, Ω' gives the following grid system $\overline{\Omega}$:

$$\overline{\Omega} = \left\{ \left(p_i, y_j \right) : p_i = (i-1)h \ , \ y_j = (j-1)h \,\middle|\, i = 1,2,\ldots,N \, ; \ j = 1,2,\ldots,N \right\}, \tag{3.3.11}$$

where $h = 1/(N-1)$. p_i is related to X through expression (3.3.9). Next we define Ω as follows:

$$\Omega = \left\{ \left(p_i, y_j \right) : p_i = (i-1)h \ , \ y_j = (j-1)h \,\middle|\, i = 2,3,\ldots,N-1, \ j = 2,3,\ldots,N-1 \right\}. \tag{3.3.12}$$

For a numerical solution procedure finite difference formulae are used to approximate the derivates in the governing equations and boundary conditions. Thus the governing differential equations are converted into algebraic finite difference equations which are now defined over Ω . Similarly the boundary conditions are converted into algebraic finite difference equations defined over $\overline{\Omega} \setminus \Omega$.

The value of any function FN at any point in $\overline{\Omega}$ is defined as follows:

$$FN_{i,j} = FN\left(p_i, y_j\right), \tag{3.3.13}$$

where $p_i = (i-1)h$, $y_j = (j-1)h$; $i = 1,2,\ldots,N$, $j = 1,2,\ldots,N$.

The ADI method

In problems involving parabolic equations, one can construct numerical solutions step by step using an explicit scheme, because only two time levels are involved in the calculations: the new values at time ($n+1$) being calculated solely in terms of values at the previous time n . Although it would appear to be much simpler and computationally faster to obtain the numerical solution of parabolic equations with an explicit method than with an implicit method, explicit schemes do introduce a difficulty, since they are prone to instability. Most implicit schemes, on the other hand, are unconditionally stable and thus, for a given grid size, it is frequently possible to take time steps many times larger in implicit schemes than those allowed by the explicit schemes, and yet still obtain comparable accuracy. An obvious disadvantage of implicit methods is that it requires the simultaneous solutions of the N algebraic equations at a new time step. The final choice of which method to use for the vorticity and energy equations depends on many factors (Roache, 1972). In this thesis, the conservation equations are solved using an alternating direct implicit (ADI) finite difference method (Peaceman and Rachford, 1955).

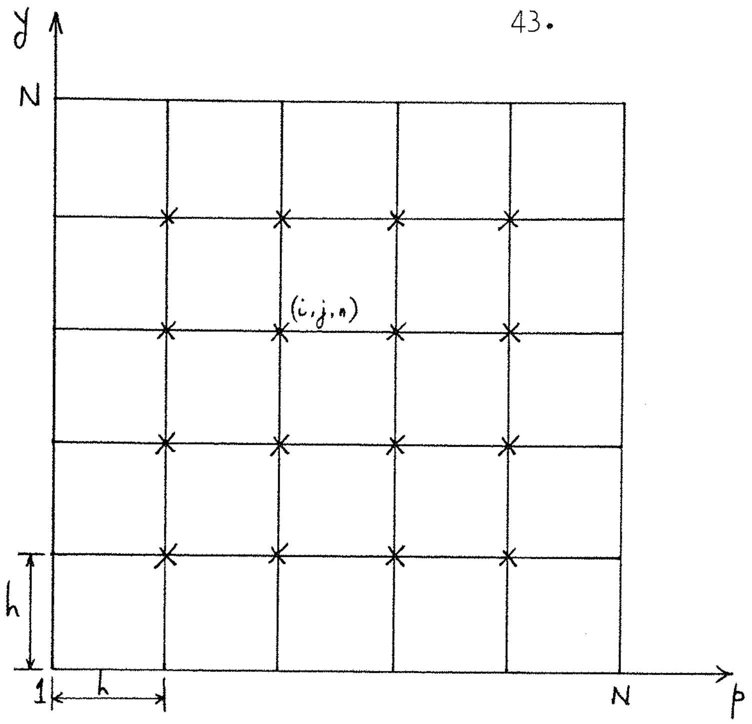

Fig. 3.3.2 Internal grid

Away from the boundaries centred space differences are used for all terms except the non-linear convection one. Since the central difference representation of the convection terms gives physically unrealistic results (Patankar, 1980) this unrealistic scheme may cause some of the stability problems encountered by earlier investigators who have used the central difference approximation. In the present work the second upwind difference scheme is used for the convection terms, because this method is always physically realistic and achieves numerical stability of the convection term by introducing false diffusion (Roache, 1972). False diffusion is a particular type of truncation error and it is a desirable one at large Grashof numbers to promote increased numerical stability (Torrance, 1968; Patankar, 1980).

The ADI method splits the time step into two obtaining at each time level a two-dimensional implicit method. The solution procedure is characterised by writing the finite difference equations in implicit form in the p -direction and solving these equations at the end of a half time step. Assuming the solution is known for time $\tau = n\,\delta\tau$, application of the corresponding finite difference equations to each of the $(N-2)$ mesh points along a row parallel to p -axis (see Fig. 3.3.2) gives $(N-2)$ equations for the $(N-2)$ unknown values of Γ , say at these mesh points for time $\tau = (n+\frac{1}{2})\,\delta\tau$. When there are $(N-2)$ rows parallel to -axis the advancement of the solution over the whole space (Ω) to the $(n+\frac{1}{2})$ th time step involves the solution of $(N-2)$ independent systems of equations, each system containing $(N-2)$ unknowns. The finite difference equations are then written in implicit form in the y -direction and, using similar arguments as above, the resulting $(N-2)$ independent systems of equations each containing $(N-2)$ unknowns are solved to give the solution at time $(n+1)$. Fig. 3.3.3 shows schematically the approach of the two-dimensional ADI scheme.

The advantage of the ADI over fully implicit methods is that at each time step the finite difference equation, although implicit, forms a tridiagonal system, which can be easily solved.

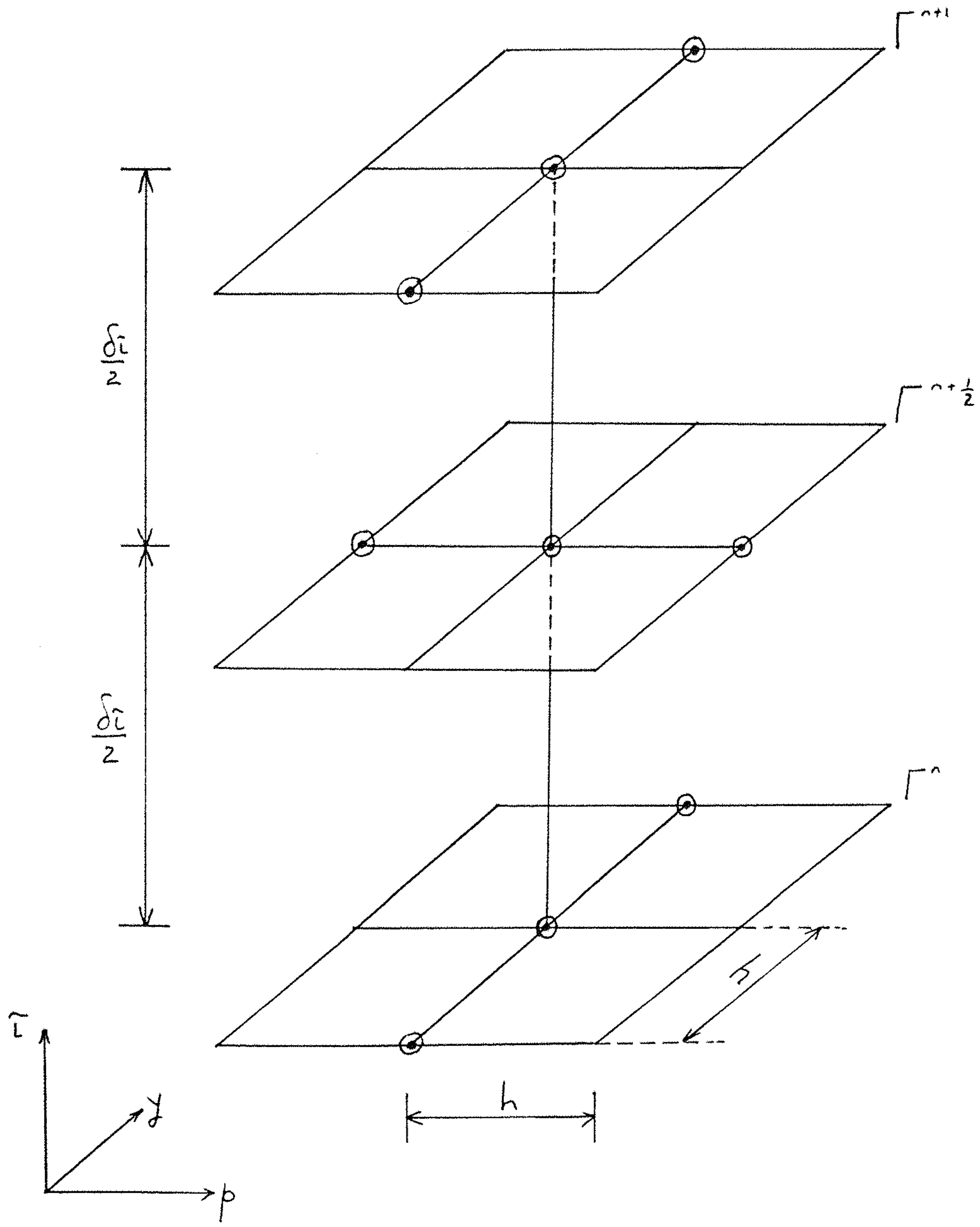

Fig. 3.3.3 Arrangement of time-step and grid point for ADI scheme

In the next section , we shall look at the second upwind differencing method and shall derive the appropriate finite difference equations.

§3.4 Second upwind difference scheme. Finite difference equations

Since equations (3.3.6) and (3.3.5) are similar in form, and recalling our assumptions $A_y = 1$, $B_y = 0$ it is convenient to represent both by the general equation

$$\frac{1}{\lambda}\frac{\partial\Gamma}{\partial\tau} + A_x u\frac{\partial\Gamma}{\partial p} + \gamma V\frac{\partial\Gamma}{\partial y} = \alpha\left(A_x^2\frac{\partial^2\Gamma}{\partial p^2} + \gamma^2\frac{\partial^2\Gamma}{\partial y^2} + B_x\frac{\partial\Gamma}{\partial p}\right) + \bar{\beta}, \quad (3.4.1)$$

where

$\alpha = 1$, $\bar{\beta} = 0$ and $\Gamma = \theta$ for the energy equation

and

$\alpha = P_r$, $\bar{\beta} = G_r P_r^2 A_x \frac{\partial\theta}{\partial p}$ and $\Gamma = Q$ for the momentum equation.

The constant λ influences the rate of convergence of equation (3.4.1) and may be set differently for the energy and vorticity equations.

To obtain an implicit scheme in the p -direction equation (3.4.1) can be written

$$\frac{\Gamma^{n+\frac{1}{2}} - \Gamma^n}{\lambda\,\Delta\tau/2} + A_x u^n\frac{\partial\Gamma^{n+\frac{1}{2}}}{\partial p} + \gamma V^n\frac{\partial\Gamma^n}{\partial y} =$$

$$= \alpha\left(A_x^2\frac{\partial^2\Gamma^{n+\frac{1}{2}}}{\partial p^2} + \gamma^2\frac{\partial^2\Gamma^n}{\partial y^2} + B_x\frac{\partial\Gamma^{n+\frac{1}{2}}}{\partial p}\right) + \bar{\beta}^n . \quad (3.4.2)$$

At the next half time step the corresponding equation in the y -direction is

$$\frac{\Gamma^{n+1} - \Gamma^{n+\frac{1}{2}}}{\lambda\,\Delta\tau/2} + A_x u^{n+\frac{1}{2}}\frac{\partial\Gamma^{n+\frac{1}{2}}}{\partial p} + \gamma V^{n+\frac{1}{2}}\frac{\partial\Gamma^{n+1}}{\partial y} =$$

$$= \alpha\left(A_x^2\frac{\partial^2\Gamma^{n+\frac{1}{2}}}{\partial p^2} + \gamma^2\frac{\partial^2\Gamma^{n+1}}{\partial y^2} + B_x\frac{\partial\Gamma^{n+\frac{1}{2}}}{\partial p}\right) + \bar{\beta}^{n+\frac{1}{2}}, \quad (3.4.3)$$

where the time derivatives have been approximated by the simple difference formula.

In the second upwind differencing scheme (Roache, 1976), the non-linear oonvective terms in (3.4.2) are approximated as follows:

$$\left(V\frac{\partial\Gamma}{\partial y}\right)^n_{i,j} = \begin{cases} \frac{1}{2h}\left(V_R^n\Gamma_{i,j}^n - V_L^n\Gamma_{i,j-1}^n\right) ; & V_R^n > 0,\ V_L^n > 0, \\ \frac{1}{2h}\left(V_R^n\Gamma_{i,j+1}^n - V_L^n\Gamma_{i,j}^n\right) ; & V_R^n < 0,\ V_L^n < 0, \\ \frac{1}{2h}\left(V_R^n\Gamma_{i,j}^n - V_L^n\Gamma_{i,j-1}^n\right) ; & V_R^n > 0,\ V_L^n < 0, \\ \frac{1}{2h}\left(V_R^n\Gamma_{i,j+1}^n - V_L^n\Gamma_{i,j-1}^n\right) ; & V_R^n < 0,\ V_L^n > 0, \end{cases} \quad (3.4.5)$$

where

$$V_R = \left(V_{i,j+1} + V_{i,j}\right) , \quad (3.4.6)$$

and

$$V_L = \left(V_{i,j} + V_{i,j-1}\right) . \quad (3.4.7)$$

We can rewrite (3.4.5) in the more compact form:

$$\left(V\frac{\partial\Gamma}{\partial y}\right)^n_{i,j} = \frac{\left(V_R^n - |V_R^n|\right)\Gamma_{i,j+1}^n + \left(V_R^n + |V_R^n| - V_L^n + |V_L^n|\right)\Gamma_{i,j}^n - \left(V_L^n + |V_L^n|\right)\Gamma_{i,j-1}^n}{4h} . \quad (3.4.8)$$

The same arguments are valid for the first velocity component giving

$$\left(U^n \frac{\partial \Gamma^{n+\frac{1}{2}}}{\partial p}\right)_{i,j} = \frac{\left(U_R^n - |U_R^n|\right)\Gamma_{i+1,j}^{n+\frac{1}{2}} + \left(U_R^n + |U_R^n| - U_L^n + |U_L^n|\right)\Gamma_{i,j}^{n+\frac{1}{2}} - \left(U_L^n + |U_L^n|\right)\Gamma_{i-1,j}^{n+\frac{1}{2}}}{4h} , \quad (3.4.9)$$

where $U_R = \left(U_{i+1,j} + U_{i,j}\right)$ and $U_L = \left(U_{i,j} + U_{i-1,j}\right)$.
Similarly, for the non-linear convective terms in (3.4.3), we have

$$\left(U\frac{\partial \Gamma}{\partial p}\right)_{i,j}^{n+\frac{1}{2}} = \frac{\left(U_R^{n+\frac{1}{2}} - |U_R^{n+\frac{1}{2}}|\right)\Gamma_{i+1,j}^{n+\frac{1}{2}} + \left(U_R^{n+\frac{1}{2}} + |U_R^{n+\frac{1}{2}}| - U_L^{n+\frac{1}{2}} + |U_L^{n+\frac{1}{2}}|\right)\Gamma_{i,j}^{n+\frac{1}{2}} - \left(U_L^{n+\frac{1}{2}} + |U_L^{n+\frac{1}{2}}|\right)\Gamma_{i-1,j}^{n+\frac{1}{2}}}{4h} \quad (3.4.10)$$

and

$$\left(V^{n+\frac{1}{2}} \frac{\partial \Gamma^{n+1}}{\partial y}\right)_{i,j} =$$

$$= \frac{\left(V_R^{n+\frac{1}{2}} - |V_R^{n+\frac{1}{2}}|\right)\Gamma_{i,j+1}^{n+1} + \left(V_R^{n+\frac{1}{2}} + |V_R^{n+\frac{1}{2}}| - V_L^{n+\frac{1}{2}} + |V_L^{n+\frac{1}{2}}|\right)\Gamma_{i,j}^{n+1} - \left(V_L^{n+\frac{1}{2}} + |V_L^{n+\frac{1}{2}}|\right)\Gamma_{i,j-1}^{n+1}}{4h} . \quad (3.4.11)$$

At each new time level U_L, U_R, V_L and V_R are calculated from the current values of the stream function using central differences.

The second derivatives of the diffusion terms are approximated by centred space evaluation with an error of $o(h^2)$,

$$\left(\frac{\partial^2 \Gamma}{\partial p^2}\right)_{i,j}^{n+\frac{1}{2}} = \frac{1}{h^2}\left(\Gamma_{i+1,j}^{n+\frac{1}{2}} - 2\Gamma_{i,j}^{n+\frac{1}{2}} + \Gamma_{i-1,j}^{n+\frac{1}{2}}\right) , \quad (3.4.12)$$

$$\left(\frac{\partial^2 \Gamma}{\partial y^2}\right)_{i,j}^{n} = \frac{1}{h^2}\left(\Gamma_{i,j+1}^{n} - 2\Gamma_{i,j}^{n} + \Gamma_{i,j-1}^{n}\right) . \quad (3.4.13)$$

The second derivatives on the right hand side of equation (3.4.3) are approximated in the same way but are not given here. The first derivatives of the diffusion terms are also approximated by centred space evaluation:

$$\left(\frac{\partial \Gamma}{\partial p}\right)_{i,j}^{n+\frac{1}{2}} = \frac{1}{2h}\left(\Gamma_{i+1,j}^{n+\frac{1}{2}} - \Gamma_{i-1,j}^{n+\frac{1}{2}}\right) \quad . \tag{3.4.14}$$

The derivative in the buoyancy term in (3.4.2) is approximated by centred space evaluation yielding

$$\left(\frac{\partial \theta}{\partial p}\right)_{i,j}^{n} = \frac{1}{2h}\left(\theta_{i+1,j}^{n} - \theta_{i-1,j}^{n}\right) . \tag{3.4.15}$$

The corresponding derivative in the buoyancy term in (3.4.3) is obtained from above simply by replacing n by $n+\frac{1}{2}$.

Substituting (3.4.8), (3.4.9) and (3.4.12) - (3.4.15) into (3.4.2) and bearing in mind that functions A_x and B_x are functions of the p -coordinate only, we have for the first half of the time step

$$\frac{\Gamma_{i,j}^{n+\frac{1}{2}} - \Gamma_{i,j}^{n}}{\lambda\,\Delta\tau/2} \quad +$$

$$A_{x}(i)\frac{\left[\left(U_R^n - |U_R^n|\right)\Gamma_{i+1,j}^{n+\frac{1}{2}} + \left(U_R^n + |U_R^n| - U_L^n + |U_L^n|\right)\Gamma_{i,j}^{n+\frac{1}{2}} - \left(U_L^n + |U_L^n|\right)\Gamma_{i-1,j}^{n+\frac{1}{2}}\right]}{4h} \quad +$$

$$+\,\gamma\;\frac{\left[\left(V_R^n - |V_R^n|\right)\Gamma_{i,j+1}^{n} + \left(V_R^n + |V_R^n| - V_L^n + |V_L^n|\right)\Gamma_{i,j}^{n} - \left(V_L^n + |V_L^n|\right)\Gamma_{i,j-1}^{n}\right]}{4h} \quad =$$

$$= \alpha\left[\frac{A_x^2(i)}{h^2}\left(\Gamma_{i+1,j}^{n+\frac{1}{2}} - 2\Gamma_{i,j}^{n+\frac{1}{2}} + \Gamma_{i-1,j}^{n+\frac{1}{2}}\right) + \frac{\gamma^2}{h^2}\left(\Gamma_{i,j+1}^{n} - 2\Gamma_{i,j}^{n} + \Gamma_{i,j-1}^{n}\right) + \frac{B_x(i)}{2h}\left(\Gamma_{i+1,j}^{n+\frac{1}{2}} - \Gamma_{i-1,j}^{n+\frac{1}{2}}\right)\right] +$$

$$+ G_r P_r^2 \frac{A_x(i)}{2h}\left(\Theta_{i+1,j}^{n} - \Theta_{i-1,j}^{n}\right) . \qquad (3.4.16)$$

Similarly, from (3.4.3), we obtain for the next half of the time step

$$\frac{\Gamma_{i,j}^{n+1} - \Gamma_{i,j}^{n+\frac{1}{2}}}{\lambda\, \Delta\tau/2} +$$

$$+ A_x(i)\frac{\left[\left(U_R^{n+\frac{1}{2}} - |U_R^{n+\frac{1}{2}}|\right)\Gamma_{i+1,j}^{n+\frac{1}{2}} + \left(U_R^{n+\frac{1}{2}} + |U_R^{n+\frac{1}{2}}| - U_L^{n+\frac{1}{2}} + |U_L^{n+\frac{1}{2}}|\right)\Gamma_{i,j}^{n+\frac{1}{2}} - \left(U_L^{n+\frac{1}{2}} + |U_L^{n+\frac{1}{2}}|\right)\Gamma_{i-1,j}^{n+\frac{1}{2}}\right]}{4h} +$$

$$+ \gamma\frac{\left[\left(V_R^{n+\frac{1}{2}} - |V_R^{n+\frac{1}{2}}|\right)\Gamma_{i,j+1}^{n+1} + \left(V_R^{n+\frac{1}{2}} + |V_R^{n+\frac{1}{2}}| - V_L^{n+\frac{1}{2}} + |V_L^{n+\frac{1}{2}}|\right)\Gamma_{i,j}^{n+1} - \left(V_L^{n+\frac{1}{2}} + |V_L^{n+\frac{1}{2}}|\right)\Gamma_{i,j-1}^{n+1}\right]}{4h} =$$

$$= \alpha\left[\frac{A_x^2(i)}{h^2}\left(\Gamma_{i+1,j}^{n+\frac{1}{2}} - 2\Gamma_{i,j}^{n+\frac{1}{2}} + \Gamma_{i-1,j}^{n+\frac{1}{2}}\right) + \frac{\gamma^2}{h^2}\left(\Gamma_{i,j+1}^{n+1} - 2\Gamma_{i,j}^{n+1} + \Gamma_{i,j-1}^{n+1}\right) + \frac{B_x(i)}{2h}\left(\Gamma_{i+1,j}^{n+\frac{1}{2}} - \Gamma_{i-1,j}^{n+\frac{1}{2}}\right)\right]$$

$$+ G_r P_r^2 \frac{A_x(i)}{2h}\left(\Theta_{i+1,j}^{n+\frac{1}{2}} - \Theta_{i-1,j}^{n+\frac{1}{2}}\right) . \qquad (3.4.17)$$

Rearranging Equations (3.4.16) and (3.4.17) one obtains finally for the ρ -component

$$R^{n}_{i,j}\Gamma^{n+\frac{1}{2}}_{i-1,j} + S^{n}_{i,j}\Gamma^{n+\frac{1}{2}}_{i,j} + T^{n}_{i,j}\Gamma^{n+\frac{1}{2}}_{i+1,j} = U^{n}_{i,j} \quad , \tag{3.4.18}$$

$$i,j = 2,3,\ldots,N-1$$

and for the y -component

$$R^{n+\frac{1}{2}}_{i,j}\Gamma^{n+1}_{i,j-1} + S^{n+\frac{1}{2}}_{i,j}\Gamma^{n+1}_{i,j} + T^{n+\frac{1}{2}}_{i,j}\Gamma^{n+1}_{i,j+1} = U^{n+\frac{1}{2}}_{i,j} \quad , \tag{3.4.19}$$

$$i,j = 2,3,\ldots,N-1$$

where

$$R^{n}_{i,j} = \frac{-A_{x(i)}}{4h}\left(U^{n}_{L}+|U^{n}_{L}|\right) - \alpha\left(\frac{A^{2}_{x(i)}}{h^{2}} - \frac{B_{x(i)}}{2h}\right) \quad , \tag{3.4.20}$$

$$S^{n}_{i,j} = \frac{2}{\Delta\tau\lambda} + \frac{A_{x(i)}}{4h}\left(U^{n}_{R}+|U^{n}_{R}| - U^{n}_{L}+|U^{n}_{L}|\right) + \frac{2\alpha A^{2}_{x(i)}}{h^{2}} \quad , \tag{3.4.21}$$

$$T^{n}_{i,j} = \frac{A_{x(i)}}{4h}\left(U^{n}_{R}-|U^{n}_{R}|\right) - \alpha\left(\frac{A^{2}_{x(i)}}{h^{2}} + \frac{B_{x(i)}}{2h}\right) \quad , \tag{3.4.22}$$

$$\begin{aligned} U^{n}_{i,j} = {} & \Gamma^{n}_{i,j+1}\left[\frac{\gamma}{4h}\left(-V^{n}_{R}+|V^{n}_{R}|\right) + \frac{\alpha\gamma^{2}}{h^{2}}\right] + \\ & +\Gamma^{n}_{i,j}\left[\frac{2}{\Delta\tau\lambda} - \frac{\gamma}{4h}\left(V^{n}_{R}+|V^{n}_{R}|-V^{n}_{L}+|V^{n}_{L}|\right) - \frac{2\alpha\gamma^{2}}{h^{2}}\right] + \\ & + \Gamma^{n}_{i,j-1}\left[\frac{\gamma}{4h}\left(V^{n}_{L}+|V^{n}_{L}|\right) + \frac{\alpha\gamma^{2}}{h^{2}}\right] + G_r P_r^{2}\frac{A_{x(i)}}{2h}\left(\theta^{n}_{i+1,j} - \theta^{n}_{i-1,j}\right) \end{aligned} \tag{3.4.23}$$

and

$$R^{n+\frac{1}{2}}_{i,j} = \frac{-\gamma}{4h}\left(V^{n+\frac{1}{2}}_{L}+\left|V^{n+\frac{1}{2}}_{L}\right|\right) - \frac{\alpha\gamma^{2}}{h^{2}} \quad , \tag{3.4.24}$$

$$S_{i,j}^{n+\frac{1}{2}} = \frac{\gamma}{4h}\left(V_R^{n+\frac{1}{2}} + \left|V_R^{n+\frac{1}{2}}\right| - V_L^{n+\frac{1}{2}} + \left|V_L^{n+\frac{1}{2}}\right|\right) + $$

$$+ \frac{2}{\Delta\tau\,\lambda} + \frac{2\alpha\gamma^2}{h^2} , \tag{3.4.25}$$

$$T_{i,j}^{n+\frac{1}{2}} = \frac{\gamma}{4h}\left(V_R^{n+\frac{1}{2}} - \left|V_R^{n+\frac{1}{2}}\right|\right) - \frac{\alpha\gamma^2}{h^2} , \tag{3.4.26}$$

$$U_{i,j}^{n+\frac{1}{2}} = \Gamma_{i+1,j}^{n+\frac{1}{2}}\left[\frac{A_{x(i)}}{4h}\left(-U_R^{n+\frac{1}{2}} + \left|U_R^{n+\frac{1}{2}}\right|\right) + \alpha\left(\frac{A_{x(i)}^2}{h^2} + \frac{B_{x(i)}}{2h}\right)\right] +$$

$$+\Gamma_{i,j}^{n+\frac{1}{2}}\left[-\frac{A_{x(i)}}{4h}\left(U_R^{n+\frac{1}{2}} + \left|U_R^{n+\frac{1}{2}}\right| - U_L^{n+\frac{1}{2}} + \left|U_L^{n+\frac{1}{2}}\right|\right) + \frac{2}{\Delta\tau\,\lambda} - \frac{2\alpha A_{x(i)}^2}{h^2}\right] +$$

$$+\Gamma_{i-1,j}^{n+\frac{1}{2}}\left[\frac{A_{x(i)}}{4h}\left(U_L^{n+\frac{1}{2}} + \left|U_L^{n+\frac{1}{2}}\right|\right) + \alpha\left(\frac{A_{x(i)}^2}{h^2} - \frac{B_{x(i)}}{2h}\right)\right] + G_r P_r^2 \frac{A_{x(i)}}{2h}\left(\theta_{i+1,j}^{n+\frac{1}{2}} - \theta_{i-1,j}^{n+\frac{1}{2}}\right). \tag{3.4.27}$$

Equations (3.4.18) and (3.4.19) are valid at every mode $\{i,j\}$ inside the boundary. Given a row with N grid points one obtains for each j a tridiagonal matrix of size ($N-2$) x ($N-2$) to determine the ($N-2$) unknowns. A similar type of matrix occurs on using (3.4.19) for a fixed i . In the next two sections we shall deal with the construction of the tridiagonal matrix and shall look at a particular method of solving the finite difference equations.

§3.5 Boundary conditions in finite difference form

The construction of the tridiagonal matrix requires the inclusion of the boundary conditions. Therefore, we shall devote this section to the formulation of the boundary conditions in finite difference form, recalling that the cavity considered has been shown on Fig. 2.4.2.

1. On $\left\{ (p_i, N) \mid p_i = (i-1)h, \ i = 1,2,\ldots,N \right\}$, the dependent variables satisfy

$$\psi = 0 \ , \quad \theta = 0 \ , \quad Q = 0 \ .$$

The finite difference form of these conditions are

$$\psi_{i,N} = 0 \ , \quad \theta_{i,N} = 0 \ , \quad Q_{i,N} = 0 \ ; \quad i = 1,2,\ldots,N \ . \qquad (3.5.1)$$

2. On $\left\{ (N, y_j) \mid y_j = (j-1)h \ , \ j = 2,3,\ldots,N-1 \right\}$, the required boundary conditions are

$$\frac{\partial \theta}{\partial p} = 0 \ , \quad \psi = 0 \ , \quad Q = 0 \ . \qquad (3.5.2)$$

The latter two equations can be written

$$\psi_{N,j} = 0 \ , \quad Q_{N,j} = 0 \ , \quad j = 2,3,\ldots,N-1 \ . \qquad (3.5.3)$$

but the temperature condition needs careful treatment. It was shown by numerical experimentation that the results obtained from our numerical procedure depend crucially on the accuracy of the expressions used to represent the heat input at the boundaries. Hence, for greater accuracy, we assume that the temperature in the immediate vicinity of the line of symmetry can be approximated by a parabola.

To formulate the necessary expression we return temporarily to the continuous region, Ω (see (3.3.1) in x-y space before applying the conditions obtained to the grid system $\overline{\Omega}$ (in p-y space).

Suppose that near the axis of symmetry

$$\theta(x) = ax^2 + bx + c \quad , \tag{3.5.4}$$

where x is measured from the centre line, then from (3.5.4) we find that $\theta(0) = c$. (3.5.5)

The temperature condition immediately yields

$$b = 0 \quad . \tag{3.5.6}$$

In $\overline{\Omega}$, $\forall j$ in the range $2 \leq j \leq N-1$, (3.5.4) - (3.5.6) imply that

$$\theta_{N-1,j} = a_j x_1^2 + b_j x_1 + c_j \quad , \tag{3.5.7}$$

$$\theta_{N-2,j} = a_j (x_2)^2 + b_j x_2 + c_j \quad , \tag{3.5.8}$$

$$\theta_{N,j} = c_j \quad , \tag{3.5.9}$$

$$b_j = 0 \quad , \tag{3.5.10}$$

where x_1 , x_2 are measured in x-space and $(1-x_1)$, $(1-x_2)$ correspond to the points $(N-2)h$, $(N-3)h$ in p-space respectively.

Assuming that $\Theta_{N-1,j}$ and $\Theta_{N-2,j}$ are known, equations (3.5.7) - (3.5.10) represent a system of linear algebraic equations for a_j , b_j , c_j and $\Theta_{N,j}$ with solution

$$\Theta_{N,j} = \Theta_{N-1,j}(1-E) + E\,\Theta_{N-2,j} , \qquad (3.5.11)$$

where

$$E = -(X_1)^2/\left((X_2)^2-(X_1)^2\right). \qquad (3.5.12)$$

(3.5.11) represents the temperature condition at the line of symmetry.

3. On $\{(p_i,1) \mid p_i = (i-1)h ,\ i = 1,2,\ldots,N\}$, the boundary conditions to be satisfied are

$$\Psi = \frac{\partial \Psi}{\partial y} = 0 , \quad Q = -\gamma^2\frac{\partial^2\Psi}{\partial y^2} , \ \gamma\frac{\partial\theta}{\partial y} = -1 . \qquad (3.5.13)$$

Clearly zero stream function implies that

$$\Psi_{i,1} = 0 , \qquad i = 1,2,\ldots,N .$$

Next we shall find an approximation for $\frac{\partial^2\Psi}{\partial y^2}$ from the Taylor's series expansion.

$$\Psi_{i,2} = \Psi_{i,1} + h\frac{\partial\Psi}{\partial y}\bigg|_{i,1} + \frac{h^2}{2!}\frac{\partial^2\Psi}{\partial y^2}\bigg|_{i,1} + o(h^3) . \qquad (3.5.14)$$

Dividing by h^2 on both sides of (3.5.14) and using

$$\Psi_{i,1} = \frac{\partial\Psi}{\partial y}\bigg|_{i,1} = 0 ,$$

we have

$$\left.\frac{\partial^2 \psi}{\partial y^2}\right|_{i,1} = 2\psi_{i,2}/h^2 + o(h) . \qquad (3.5.15)$$

Although the truncation error in (3.5.15) is of order h , Kublbeck et al (1979) and Roache (1976) certify that the resulting numerical procedure is essentially more stable than it would be with the corresponding approximation due to Woods (1954)

$$\left.\frac{\partial^2 \psi}{\partial y^2}\right|_{i,1} = \frac{3\psi_{i,2}}{h^2} + \frac{1}{2}\left.\frac{\partial^2 \psi}{\partial y^2}\right|_{i,2} ,$$

which is accurate to $o(h^2)$. Other approximations are suggested by Roache (1976) but shall use the expression (3.5.15). With this choice the finite difference form of the vorticity boundary condition can be written

$$Q_{i,1} = \frac{-2\gamma^2 \psi_{i,2}}{h^2} , \quad i = 1,2,\ldots,N . \qquad (3.5.16)$$

As stated earlier, numerical results are found to be very sensitive to the accuracy of expressions used to represent the heat input at the boundaries. Hence, for greater accuracy, we assume that the temperature at the walls also has a parabolic profile.

As in the case of the temperature at the centre line, we suppose that

$$\theta(y) = ay^2 + by + c , \qquad (3.5.17)$$

which immediately gives

$$\Theta(0) = c \ , \quad \left.\frac{\partial\theta}{\partial y}\right|_{y=0} = b \ . \tag{3.5.18}$$

Hence from (3.5.13) we find that

$$b = -\frac{1}{\gamma} \ . \tag{3.5.19}$$

Then in $\bar{\Omega}$, $\forall i$, such that $1 \leq i \leq N$ expressions (3.5.17) - (3.5.19) imply that

$$\theta_{i,2} = a_i h^2 + b_i h + c_i \ , \tag{3.5.20}$$

$$\theta_{i,3} = a_i (2h)^2 + b_i (2h) + c_i \ , \tag{3.5.21}$$

$$\theta_{i,1} = c_i \ , \tag{3.5.22}$$

$$b_i = -\frac{1}{\gamma} \ . \tag{3.5.23}$$

Assuming that $\theta_{i,2}$ and $\theta_{i,3}$ are known equations (3.5.20) - (3.5.23) represent a system of linear algebraic equations, the unknowns being a_i , b_i , c_i and $\theta_{i,1}$.

Solving the system, we obtain for the temperature at the base:

$$\theta_{i,1} = \frac{1}{3}\left(4\,\theta_{i,2} - \theta_{i,3} + 2h/\gamma\right) \ . \tag{3.5.24}$$

4. Finally on $\left\{(1, y_j) \mid y_j = (j-1)h \ , \ j = 2,3,\dots,N-1\right\}$, with our coordinate transformation the non dimensional variables satisfy

$$\Psi = \frac{\partial\Psi}{\partial p} = 0 \ ;$$

$$Q = -\left(A_x^2 \frac{\partial^2\Psi}{\partial p^2} + B_x \frac{\partial\Psi}{\partial p}\right) ; \tag{3.5.25}$$

$$A_x \frac{\partial\theta}{\partial p} = -\frac{Q_2}{Q_1} \quad . \tag{3.5.26}$$

The first condition is obviously written

$$\Psi_{i,1} = \left.\frac{\partial\Psi}{\partial p}\right|_{1,j} = 0 \ , \quad j = 2,3,\ldots, N-1 \ . \tag{3.5.27}$$

Using a Taylor series expansion an approximation for $\frac{\partial^2\Psi}{\partial p^2}$ is obtained in a similar way to that for $\frac{\partial^2\Psi}{\partial y^2}$ in the previous sub-section: Thus

$$\Psi_{2,j} = \Psi_{1,j} + h\left.\frac{\partial\Psi}{\partial p}\right|_{1,j} + \frac{h^2}{2!}\left.\frac{\partial^2\Psi}{\partial p^2}\right|_{1,j} + o(h^3) \tag{3.5.28}$$

and using (3.5.27) it follows that

$$\left.\frac{\partial^2\Psi}{\partial p^2}\right|_{1,j} = 2\Psi_{2,j}/h^2 + o(h) \ . \tag{3.5.29}$$

From (3.5.25), (3.5.27) and (3.5.29) we obtain the following expression for the wall vorticity:

$$Q_{1,j} = -2A_x^2(1)\,\Psi_{2,j}/h^2 \ . \tag{3.5.30}$$

Again for greater accuracy we assume that the temperature near the wall has a parabolic distribution following the same argument as in sub-section 2 but recalling that the appropriate boundary condition is now $\left(\partial\theta/\partial x\right)_{x=0} = -Q_2/Q_1$ we deduce that the expression for the wall temperature is

$$\theta_{1,j} = E_1\theta_{2,j} + E_2\theta_{3,j} + E_3 \quad , \tag{3.5.31}$$

where

$$E_1 = (x_2)^2/\left((x_2)^2-(x_1)^2\right) \quad , \tag{3.5.32}$$

$$E_2 = -(X_1)^2 / ((X_2)^2 - (X_1)^2) , \tag{3.5.33}$$

$$E_3 = \left[X_1 X_2 / (X_1 + X_2) \right] Q_2 / Q_1 , \tag{3.5.34}$$

with the quantities X_1 and X_2 corresponding to the points h and $2h$ in p-space.

§3.6 Construction of Tridiagonal matrices. Solution of Finite Difference equations (FDE)

We shall now construct the tridiagonal matrix for the first half of the time step. We recall that the FDE corresponding to the transport equation for the first half of the time step is given by (3.4.18), which yields the following system of linear algebraic equations.

$$
\begin{aligned}
R^n_{2,j}\Gamma^{n+\frac{1}{2}}_{1,j} + S^n_{2,j}\Gamma^{n+\frac{1}{2}}_{2,j} + T^n_{2,j}\Gamma^{n+\frac{1}{2}}_{3,j} &= U^n_{2,j}\,, \\
R^n_{3,j}\Gamma^{n+\frac{1}{2}}_{2,j} + S^n_{3,j}\Gamma^{n+\frac{1}{2}}_{3,j} + T^n_{3,j}\Gamma^{n+\frac{1}{2}}_{4,j} &= U^n_{3,j}\,, \\
&\vdots \\
R^n_{N-1,j}\Gamma^{n+\frac{1}{2}}_{N-2,j} + S^n_{N-1,j}\Gamma^{n+\frac{1}{2}}_{N-1,j} + T^n_{N-1,j}\Gamma^{n+\frac{1}{2}}_{N,j} &= U^n_{N-1,j}\,.
\end{aligned}
\qquad (3.6.1)
$$

For the momentum equation the boundary conditions just discussed in 3.5 give

$$\Gamma^n_{1,j} = Q^n_{1,j} = -2\Psi_{2,j}\, A^2_{x(1)}/k^2 \,, \qquad (3.6.2)$$

$$\Gamma^n_{N,j} = Q^n_{N,j} = 0 \,. \qquad (3.6.3)$$

Since it is not possible to know beforehand the wall vorticity at $(n+\frac{1}{2})$, we have taken its value to be the one at time n.

This indicates that the wall vorticity lags behind by half a time step. This will occur at all time levels. Since we are aiming at a steady state solution, this difference in time levels does not affect the numerical results at steady state.

System (3.6.1) can be written as

$$AX = B \qquad , \qquad (3.6.4)$$

where A is the following tridiagonal matrix

$$\begin{bmatrix} S^n_{2,j} & T^n_{2,j} & 0 & \cdots & & 0 \\ R^n_{3,j} & S^n_{3,j} & T^n_{3,j} & 0 & & 0 \\ 0 & \ddots & \ddots & \ddots & & \vdots \\ \vdots & & \ddots & \ddots & \ddots & 0 \\ 0 & \cdots & 0 & R^n_{N-2,j} & S^n_{N-2,j} & T^n_{N-2,j} \\ 0 & \cdots & & 0 & R^n_{N-1,j} & S^n_{N-1,j} \end{bmatrix} \qquad , \qquad (3.6.5)$$

$$X = \begin{bmatrix} Q^{n+\frac{1}{2}}_{2,j} \\ Q^{n+\frac{1}{2}}_{3,j} \\ \vdots \\ Q^{n+\frac{1}{2}}_{N-1,j} \end{bmatrix} , \qquad B = \begin{bmatrix} U^n_{2,j} - R^n_{2,j} Q^n_{1,j} \\ U^n_{3,j} \\ \vdots \\ U^n_{N-1,j} \end{bmatrix} . \qquad (3.6.6)$$

For the energy equation, we refer to expressions (3.5.11) and (3.5.31) which define the temperature at the wall and at the line of symmetry respectively.

The tridiagonal matrix , A , for the energy equation therefore is

$$\begin{bmatrix} (E_1 R^n_{2,j} + S^n_{2,j}) & (T^n_{2,j} + E_2 R^n_{2,j}) & 0 & \cdots & 0 \\ R^n_{3,j} & S^n_{3,j} & T^n_{3,j} & \ddots & \vdots \\ 0 & \ddots & \ddots & \ddots & 0 \\ \vdots & & R^n_{N-2,j} & S^n_{N-2,j} & T^n_{N-2,j} \\ 0 & \cdots & 0 & (R^n_{N-1,j} + T^n_{N-1,j} E) & (S^n_{N-1,j} + T^n_{N-1,j}(1-E)) \end{bmatrix},$$

where E , E_1 , E_2 are defined through (3.5.12), (3.5.32), (3.5.33) respectively. The corresponding vector B is

$$\begin{bmatrix} U^n_{2,j} - E_3 R^n_{2,j} \\ U^n_{3,j} \\ \vdots \\ U^n_{N-1,j} \end{bmatrix}, \qquad (3.6.10)$$

where E_3 is defined through (3.5.34)

The matrices corresponding to the momentum equation for the second half of the time step have essentially the same structure as those discussed above. The only difference in A lies in interchanging i's and j's in the subscripts and because of the modified version for the base vorticity, only the first element of the column vector B is different. There are also slight changes in the matrices A and B for the energy equation. As discussed earlier we have (see 3.5)

$$\Theta_{i,1}^{n+1} = \frac{4}{3}\Theta_{i,2}^{n+1} - \frac{1}{3}\Theta_{i,3}^{n+1} + \frac{2h}{3\gamma} ;$$

and $$\Theta_{i,N}^{n+1} = 0$$

Hence, for the case of the temperature the matrices are A =

$$= \begin{bmatrix} \left(\frac{4}{3}R_{i,2}^{n+\frac{1}{2}} + S_{i,2}^{n+\frac{1}{2}}\right) & T_{i,2}^{n+\frac{1}{2}} - \frac{1}{3}R_{i,2}^{n+\frac{1}{2}} & 0 & \cdots & 0 \\ R_{i,3}^{n+\frac{1}{2}} & S_{i,3}^{n+\frac{1}{2}} & T_{i,3}^{n+\frac{1}{2}} & \ddots & \vdots \\ 0 & \ddots & \ddots & \ddots & 0 \\ \vdots & \ddots & R_{i,N-2}^{n+\frac{1}{2}} & S_{i,N-2}^{n+\frac{1}{2}} & T_{i,N-2}^{n+\frac{1}{2}} \\ 0 & \cdots & 0 & R_{i,N-1}^{n+\frac{1}{2}} & S_{i,N-1}^{n+\frac{1}{2}} \end{bmatrix} \quad (3.6.11)$$

and

$$B = \begin{bmatrix} U_{i,2}^{n+\frac{1}{2}} - R_{i,2}^{n+\frac{1}{2}}\, 2h/3\gamma \\ U_{i,3}^{n+\frac{1}{2}} \\ \vdots \\ U_{i,N-1}^{n+\frac{1}{2}} \end{bmatrix} . \quad (3.6.12)$$

Having completed the construction of the tridiagonal matrices for all relevant cases we shall now look at a particular way of solving the equations using the tridiagonality of the matrices. The Crout decomposition method (Bajpai, Mustoe, Walker; 1977) is a general method for solving systems of equations that yields particularly simple results when A is tridiagonal.

In brief, if $A = (a_{mk})_{\substack{m=1,\dots,M \\ k=1,\dots,M}}$ is a tridiagonal matrix,

then there exist a lower triangular matrix

$L = (l_{mk})_{\substack{m=1,\dots,M \\ k=1,\dots,M}}$ and an upper triangular matrix

$U = (u_{mk})_{\substack{m=1,\dots,M \\ k=1,\dots,M}}$ with $u_{mk} = 1$ when $m = k$,

such that

$$A = LU .$$

In that case the non-zero components in the matrices L and U are readily calculated through

(i) $\quad l_{m1} = a_{m1} \quad , \quad m = 1, 2 \;;$

(ii) $\quad u_{1k} = a_{1k}/l_{11} \quad , \quad k = 2 \;;$

$$\left.\begin{aligned} &\text{(iii)} \quad l_{kk} = a_{kk} - l_{k\,k+1}\,u_{k\,k+1}, \\ &\qquad\;\; l_{k+1\,k} = a_{k+1\,k}, \\ &\text{(iv)} \quad u_{k\,k+1} = a_{k\,k+1}/l_{kk}, \end{aligned}\right\} \text{for } k = 2, 3, \dots, M .$$

This procedure is termed triangular decomposition. To solve the system of equations

$$A\underline{\Gamma} = \underline{B} \qquad , \text{ where } A \text{ is tridiagonal}$$

we first factorise A into LU so that

$$(LU)\underline{\Gamma} = \underline{B} = L(U\underline{\Gamma}).$$

Then if we write

$$U\underline{\Gamma} = \underline{y}, \tag{3.6.13}$$

then the original equation is equivalent to

$$L\underline{y} = \underline{B} . \tag{3.6.14}$$

Since L is a triangular matrix with only one non-zero sub diagonal, $\underline{y}$ can be easily found from (3.6.14) to be given by

$$y_1 = B_1/\ell_{11} ,$$

$$y_K = B_K - \ell_{K\,K-1}\, y_{K-1}/\ell_{K\,K} , \quad K = 2,3,\ldots,M$$

Having found $\underline{y}$ we then use (3.6.13) to find $\underline{\Gamma}$. Again the triangular nature of U makes the solution an easy task. We obtain

$$\begin{aligned} \Gamma_M &= y_M , \\ \Gamma_K &= y_K - U_{K\,K+1}\, \Gamma_{K+1} , \quad K = M-1, M-2, \ldots, 2,1 \end{aligned} \tag{3.6.15}$$

Having determined the solution of the conservation equations, we shall, in the next paragraph, look at the solution of the Poisson equation.

§3.7 Solution of Poisson equation - Block Cyclic Reduction method

We shall now consider the elliptic Poisson equation (2.4.34) for the stream function. A review of the literature shows that many attempts have been made to find a solution. The iteration methods are very easy to understand and program. Frankel (1950) has developed a method of applying over relaxation to the Gauss-Seidel method: this procedure is called Successive Overrelaxation (SOR). In recent years the slightly more complicated ADI methods have become popular. The procedure here is to convert the elliptic equation into a parabolic one, by including the unsteady terms which can then be integrated in time by the previously described ADI method until steady state is reached.

Due to intensive research direct inversion methods are now coming into wider use. These methods are extremely accurate since in theory they yield the exact solution to the difference equations. They need considerably less computation time than ADI methods, but they often place some limitations on the boundary conditions and grid size. Kublbeck, Merker and Straub (1980) conclude that a reasonable compromise between computation time, freedom with boundary conditions and a suitable grid size is obtained with the method of cyclic reduction of Schumann and Sweet (1976). Buzbee et al (1970) examined the method of cyclic reduction with the Buneman variants to obtain greater numerical stability. In this work, the Poisson equation will be solved by the method of cyclic reduction using the Buneman variant.

An introduction to the idea of cyclic reduction

Consider the system of equations

$$M\underline{x} = \underline{y} \ , \qquad (3.7.1)$$

where M is a $q \times q$ real symmetric matrix of block tridiagonal form:

$$M = \begin{pmatrix} A & T & 0 & \cdots & 0 \\ T & A & T & \ddots & \vdots \\ 0 & \ddots & \ddots & \ddots & 0 \\ \vdots & \ddots & \ddots & \ddots & T \\ 0 & \cdots & 0 & T & A \end{pmatrix} . \tag{3.7.2}$$

We assume that T is symmetric and that the ($p \times p$) matrices A and T commute. To maintain consistency with the form of matrix M, we write the vectors $\underline{x}$ and $\underline{y}$ in partitioned form,

$$\underline{x} = \begin{pmatrix} \underline{x}_1 \\ \hline \underline{x}_2 \\ \hline \vdots \\ \hline \underline{x}_q \end{pmatrix} , \quad \underline{y} = \begin{pmatrix} \underline{y}_1 \\ \hline \underline{y}_2 \\ \hline \vdots \\ \hline \underline{y}_q \end{pmatrix} . \tag{3.7.3}$$

Furthermore it is then quite natural to write

$$\underline{x}_j = \begin{pmatrix} x_{1j} \\ x_{2j} \\ \vdots \\ x_{pj} \end{pmatrix} , \quad \underline{y}_j = \begin{pmatrix} y_{1j} \\ y_{2j} \\ \vdots \\ y_{pj} \end{pmatrix} , \quad j = 1, 2, \ldots, p . \tag{3.7.4}$$

With the use of expressions (3.7.2), (3.7.3) system (3.7.1) may be expressed as

$$\begin{aligned} A\underline{x}_1 + T\underline{x}_2 &= \underline{y}_1 , \\ T\underline{x}_{j-1} + A\underline{x}_j + T\underline{x}_{j+1} &= \underline{y}_j , \quad j = 2, 3, \ldots, q-1 , \\ T\underline{x}_{q-1} + A\underline{x}_q &= \underline{y}_q . \end{aligned} \tag{3.7.5}$$

Consider a j such that $2 < j < N-1$, then the equations for $(j-1)$, j and $(j+1)$ are

$$\left.\begin{aligned} T\underline{x}_{j-2} + A\underline{x}_{j-1} + T\underline{x}_{j} &= \underline{y}_{j-1}, \\ T\underline{x}_{j-1} + A\underline{x}_{j} + T\underline{x}_{j+1} &= \underline{y}_{j}, \\ T\underline{x}_{j} + A\underline{x}_{j+1} + T\underline{x}_{j+2} &= \underline{y}_{j+1}. \end{aligned}\right\} \tag{3.7.6}$$

Multiplying the first and third equations of above system by T, the second by $(-A)$ and adding we have

$$T^2\underline{x}_{j-2} + \left(2T^2 - A^2\right)\underline{x}_j + T^2\underline{x}_{j+2} = T\underline{y}_{j-1} - A\underline{y}_j + T\underline{y}_{j+1}. \tag{3.7.7}$$

This is a single equation of the same form as each equation in (3.7.6) but with the unknowns $\underline{X}_{j-1}$ and $\underline{X}_{j+1}$ not appearing. By choosing even values for j a new smaller system of equations involving $\underline{X}_j$'s with even indices is produced. The process of reducing the number of equations in this fashion is known as cyclic reduction. It should be noted, however, that the calculation of the right hand sides of equations (3.7.7) is subject to severe rounding off errors in many cases of interest. This difficulty is almost eliminated by using the more stable Buneman variants of the Cyclic Reduction method.

Recall the Poisson equation in transformed coordinates, equation (3.3.7), which, with $A_y = 1$ and $B_y = 0$, reduces to

$$A_x^2 \frac{\partial^2 \Psi}{\partial p^2} + B_x \frac{\partial \Psi}{\partial p} + \gamma^2 \frac{\partial^2 \Psi}{\partial y^2} = -Q, \tag{3.7.8}$$

subject to $\Psi = 0$ on all boundaries.

Next, we convert equation (3.7.8) into finite difference form using central differences obtaining

$$\frac{A_x^2(i)}{h^2}\left(\Psi_{i+1,j}-2\Psi_{i,j}+\Psi_{i-1,j}\right)+\frac{B_x(i)}{2h}\left(\Psi_{i+1,j}-\Psi_{i-1,j}\right)+\frac{\gamma^2}{h^2}\left(\Psi_{i,j+1}-2\Psi_{i,j}+\Psi_{i,j-1}\right)=$$
$$=-Q_{i,j}\quad,\qquad i,j=2,3,\ldots,N-1 \qquad (3.7.9)$$

with boundary conditions

$$\left.\begin{aligned}\Psi_{1,j}&=0\quad,\\ \Psi_{N,j}&=0\quad,\\ \Psi_{i,1}&=0\quad,\\ \Psi_{i,N}&=0\end{aligned}\right\}\quad i=1,2,\ldots,N\ ;\ j=1,2,\ldots,N\ . \qquad (3.7.10)$$

Equations(3.7.9)and(3.7.10)can be put into the form (3.7.1) and the corresponding matrices M and $\underline{y}$ are now determined.

Let
$$\left.\begin{aligned} a_i &= A_x^2(i)-\tfrac{1}{2}h\,B_x(i)\quad,\\ b_i &= -2\left(A_x^2(i)+\gamma^2\right)\quad,\\ c_i &= A_x^2(i)+\tfrac{1}{2}h\,B_x(i)\ ,\\ QH'_{i,j} &= -h^2 Q_{i,j}\ .\end{aligned}\right. \qquad (3.7.11)$$

Then equation (3.7.9) can be written in a simplified way:

$$a_i\Psi_{i-1,j}+b_i\Psi_{i,j}+c_i\Psi_{i+1,j}+\gamma^2\Psi_{i,j-1}+\gamma^2\Psi_{i,j+1}=QH'_{i,j},\qquad (3.7.12)$$
$$i,j=2,3,\ldots,N-1$$

but the boundary conditions are unchanged. With $j = 2$ equations (3.7.10) and (3.7.12) yield the set of equations

$$
\begin{aligned}
b_2 \Psi_{2,2} + c_2 \Psi_{3,2} + \gamma^2 \Psi_{2,3} &= QH'_{2,2}, \\
a_3 \Psi_{2,2} + b_3 \Psi_{3,2} + c_3 \Psi_{4,2} + \gamma^2 \Psi_{3,3} &= QH'_{3,2}, \\
&\vdots \\
a_{N-1} \Psi_{N-2,2} + b_{N-1} \Psi_{N-1,2} + \gamma^2 \Psi_{N-1,3} &= QH'_{N-1,2}.
\end{aligned}
\tag{3.7.13}
$$

Furthermore for general j in the range $3 \leq j \leq N-2$ equations (3.7.10) and (3.7.12) yield

$$
\begin{aligned}
b_2 \Psi_{2,j} + c_2 \Psi_{3,j} + \gamma^2 \Psi_{2,j-1} + \gamma^2 \Psi_{2,j+1} &= QH'_{2,j}, \\
a_3 \Psi_{2,j} + b_3 \Psi_{3,j} + c_3 \Psi_{4,j} + \gamma^2 \Psi_{3,j-1} + \gamma^2 \Psi_{3,j+1} &= QH'_{3,j}, \\
&\vdots \\
a_{N-1} \Psi_{N-2,j} + b_{N-1} \Psi_{N-1,j} + \gamma^2 \Psi_{N-1,j-1} + \gamma^2 \Psi_{N-1,j+1} &= QH'_{N-1,j}.
\end{aligned}
\tag{3.7.14}
$$

Finally when $j = N-1$, the corresponding set of equations is

$$
\begin{aligned}
b_2 \Psi_{2,N-1} + c_2 \Psi_{3,N-1} + \gamma^2 \Psi_{2,N-2} &= QH'_{2,N-1}, \\
a_3 \Psi_{2,N-1} + b_3 \Psi_{3,N-1} + c_3 \Psi_{4,N-1} + \gamma^2 \Psi_{3,N-2} &= QH'_{3,N-1}, \\
&\vdots \\
a_{N-1} \Psi_{N-2,N-1} + b_{N-1} \Psi_{N-1,N-1} + \gamma^2 \Psi_{N-1,N-2} &= QH'_{N-1,N-1}.
\end{aligned}
\tag{3.7.15}
$$

Define the vectors $\underline{\Psi}_j$ and $\underline{QH}'_j$ through

$$\underline{\Psi}_j = \begin{pmatrix} \Psi_{2,j} \\ \Psi_{3,j} \\ \vdots \\ \Psi_{N-1,j} \end{pmatrix} \quad \text{and} \quad \underline{QH}'_j = \begin{pmatrix} QH'_{2,j} \\ QH'_{3,j} \\ \vdots \\ QH'_{N-1,j} \end{pmatrix}, \quad j = 2,3,\dots,N-1 \tag{3.7.16}$$

then systems (3.7.13), (3.7.14) and (3.7.15) can be written respectively

$$A\underline{\Psi}_2 + I\underline{\Psi}_3 + 0\cdot\underline{\Psi}_4 + \cdots + 0\cdot\underline{\Psi}_{N-1} = \underline{QH}_2, \tag{3.7.17}$$

$$\left.\begin{aligned} I\underline{\Psi}_{j-1} + A\underline{\Psi}_j + I\underline{\Psi}_{j+1} + 0\cdot\underline{\Psi}_{j+2} + \cdots + 0\cdot\underline{\Psi}_{N-1} = \underline{QH}_j, \\ 3 \le j \le N-2 \end{aligned}\right\} \tag{3.7.18}$$

and

$$0\cdot\underline{\Psi}_2 + \cdots + 0\cdot\underline{\Psi}_{N-3} + I\underline{\Psi}_{N-2} + A\underline{\Psi}_{N-1} = \underline{QH}_{N-1}, \tag{3.7.19}$$

where

$$A = \frac{1}{\gamma^2}\begin{bmatrix} b_2 & c_2 & 0 & \cdots & 0 \\ a_3 & b_3 & c_3 & \ddots & \vdots \\ 0 & \ddots & \ddots & \ddots & 0 \\ \vdots & & \ddots & \ddots & c_{N-2} \\ 0 & \cdots & 0 & a_{N-1} & b_{N-1} \end{bmatrix}, \tag{3.7.20}$$

$$\underline{QH}_i = \frac{1}{\gamma^2}\underline{QH}'_i. \tag{3.7.21}$$

and $\underline{I}$ is the identity matrix of order $(N-2)$. Hence, the systems of equations (3.7.17) - (3.7.19) are equivalent to the block matrix equation

$$M\underline{X} = \underline{f}\ , \tag{3.7.22}$$

where

$$M = \begin{bmatrix} A & \underline{I} & 0 & \cdots & 0 \\ \underline{I} & A & \underline{I} & \ddots & \vdots \\ 0 & & \ddots & \ddots & 0 \\ \vdots & \ddots & & & \underline{I} \\ 0 & \cdots & 0 & \underline{I} & A \end{bmatrix}, \tag{3.7.23}$$

$$\underline{X} = \begin{pmatrix} \underline{\Psi_2} \\ \hline \underline{\Psi_3} \\ \hline \vdots \\ \hline \underline{\Psi_{N-1}} \end{pmatrix} \quad \text{and} \quad \underline{f} = \begin{pmatrix} \underline{QH_2} \\ \hline \underline{QH_3} \\ \hline \vdots \\ \hline \underline{QH_{N-1}} \end{pmatrix}. \tag{3.7.24}$$

The basic idea for reducing the system (3.7.22) was given at the beginning of this section, although the precise details depend on the value of N. For convenience we choose

$$N = 2^{K+1} + 1\ , \tag{3.7.25}$$

where K is a positive integer. System(3.7.22) may be written

$$\begin{aligned} A\underline{\Psi_2} + \underline{I}\,\underline{\Psi_3} &= \underline{QH_2}\,, \\ \underline{I}\,\underline{\Psi_{j+1}} + A\underline{\Psi_j} + \underline{I}\,\underline{\Psi_{j+1}} &= \underline{QH_j}\,, \quad j = 3,\ldots,N-2\,, \\ \underline{I}\,\underline{\Psi_{N-2}} + A\underline{\Psi_{N-1}} &= \underline{QH_{N-1}} \end{aligned} \tag{3.7.26}$$

and it is this system that is now subjected to the process of cyclic reduction. Recalling result (3.7.7), after one stage of cyclic reduction we have

$$\underline{\Psi}_{j-1} + (2I-A^2)\underline{\Psi}_{j+1} + \underline{\Psi}_{j+3} = \underline{QH}_j + \underline{QH}_{j+2} - A\,\underline{QH}_{j+1}, \quad (3.7.27)$$

for $j = 2,4, \ldots, N-3$ with $\underline{\Psi}_1 = \underline{\Psi}_N = \underline{0}$.

Since system (3.7.27) is block tridiagonal and is of the form of system (3.7.22) with

$$A^{(1)} = 2I - [A]^2 \quad , \quad (3.7.28)$$

$$\underline{f}^{(1)} = \underline{QH}_j + \underline{QH}_{j+2} - A\,\underline{QH}_{j+1} \quad , \quad (3.7.29)$$

we can apply the reduction process repeatedly until we are left with one block equation (this is possible with our choice of N). In general after $(r+1)$ reductions we have

$$A^{(r+1)} = 2I - \left[A^{(r)}\right]^2 \quad \text{with} \quad A^{(0)} = A \quad (3.7.30)$$

and the right hand side is obtained from

$$\underline{f}_j^{(r+1)} = \underline{f}_{j-2^r}^{(r)} + \underline{f}_{j+2^r}^{(r)} - A^{(r)}\underline{f}_j^{(r)} \quad , \quad (3.7.31)$$

where $r = 0, \ldots, K-1$, (K is defined through (3.7.25)) and

$$j = 1\cdot 2^{r+1}, 2\cdot 2^{r+1}, \ldots, (2^{K-r}-1)2^{r+1} .$$

After K steps, we obtain the single block equation

$$A^{(K)}\underline{\Psi}_{2^K+1} = \underline{f}_{2^K}^{(K)} . \quad (3.7.32)$$

In general system (3.7.32) can easily be inverted but, as stated earlier, in practice the calculation of the right hand sides introduces acute instabilities. The Buneman variant requires that the right hand sides resulting from the reduction process are not computed directly but defined implicitly by two auxiliary vectors $\underline{p}_j^{(r)}$ and $\underline{q}_j^{(r)}$

First, note that the right hand side of (3.7.27) may be written as

$$\underline{f}_j^{(1)} = \underline{QH}_j + \underline{QH}_{j+2} - A\underline{QH}_{j+1} =$$

$$= A^{(1)}[A]^{-1}\underline{QH}_{j+1} + \underline{QH}_j + \underline{QH}_{j+2} - 2[A]^{-1}\underline{QH}_{j+1} \,, \qquad (3.7.33)$$

where $j = 2, 4, \ldots, N-3$ and we have used equation (3.7.28)

Next let us define

$$\underline{p}_j^{(1)} = [A]^{-1}\underline{QH}_{j+1} \,, \qquad (3.7.34)$$

$$\underline{q}_j^{(1)} = \underline{QH}_j + \underline{QH}_{j+2} - 2\underline{p}_j^{(1)} \,, \qquad (3.7.35)$$

then from (3.7.3) we have

$$\underline{f}_j^{(1)} = A^{(1)}\underline{p}_j^{(1)} + \underline{q}_j^{(1)} \,. \qquad (3.7.36)$$

Writing

$$\underline{f}_j^{(r)} = A^{(r)}\underline{p}_j^{(r)} + \underline{q}_j^{(r)} \,, \qquad (3.7.37)$$

we can obtain expressions for $\underline{p}_j^{(r)}$ and $\underline{q}_j^{(r)}$ by substituting (3.7.37) into (3.7.31) and making use of the identity (3.7.30). The following relationships are obtained:

$$\underline{p}_j^{(r+1)} = \underline{p}_j^{(r)} - [A^{(r)}]^{-1}\left(\underline{p}_{j-2^r}^{(r)} + \underline{p}_{j+2^r}^{(r)} - \underline{q}_j^{(r)}\right) \,, \qquad (3.7.38)$$

$$\underline{q}_j^{(r+1)} = \underline{q}_{j+2^r}^{(r)} + \underline{q}_{j-2^r}^{(r)} - 2\underline{p}_j^{(r+1)}, \tag{3.7.39}$$

for $j = i\,2^{r+1}$, $i = 1, 2, \ldots, 2^{K-r}-1$, with

$$\underline{p}_0^{(r)} = \underline{p}_{2^{K+1}}^{(r)} = \underline{q}_0^{(r)} = \underline{q}_{2^{K+1}}^{(r)}. \tag{3.7.40}$$

After K reductions, one therefore has the equation

$$A^{(K)}\,\underline{\Psi}_{2^K+1} = A^{(K)}\,\underline{p}_{2^K}^{(K)} + \underline{q}_{2^K}^{(K)}$$

and hence

$$\underline{\Psi}_{2^K+1} = \underline{p}_{2^K}^{(K)} + \left[A^{(K)}\right]^{-1}\underline{q}_{2^K}^{(K)}. \tag{3.7.41}$$

To compute $\underline{\Psi}_{2^K+1}$ in (3.7.41) we solve the system of equations

$$A^{(K)}\left(\underline{\Psi}_{2^K+1} - \underline{p}_{2^K}^{(K)}\right) = \underline{q}_{2^K}^{(K)}, \tag{3.7.42}$$

where $A^{(r)}$ is given by the factorization

$$A^{(r)} = -\prod_{j=1}^{2^r}\left(A + 2\cos\theta_j^{(r)} I\right) \tag{3.7.43}$$

and $\theta_j^{(r)} = (2j-1)\pi/2^{r+1}$. (Buzbee et al, 1970). It should be pointed out that in the derivation of (3.7.43) the authors have assumed that the matrix A can be diagonalised. We note that each of the matrices forming the product $A^{(r)}$ in (3.7.43) is tridiagonal. Hence, for equation (3.7.41) we have

$$[A_1][A_2]\cdots[A_{2^r}]\left(\underline{\Psi}_{2^K+1} - \underline{p}_{2^K}^{(K)}\right) = \underline{q}_{2^K}^{(K)},$$

where for a given r

$A_j = A + 2\cos\theta_j^{(r)} I$, with $\theta_j^{(r)}$ defined above.

Define η_i through

$$\eta_i = [A_i][A_{i+1}]\cdots[A_{2^r}]\left(\underline{\Psi}_{2^K+1} - \underline{p}^{(K)}_{2^K}\right). \quad (3.7.44)$$

Then we successively solve the system

$$A_i \eta_{i+1} = \mathcal{X}_i \ , \qquad i = 1, 2, \ldots, 2^r ,$$

where $\mathcal{X}_1 = \underline{q}^{(K)}_{2^K} \ , \quad \eta_{2^r+1} = \Psi_{2^K+1} - \underline{p}^{(K)}_{2^K} \ ,$

$$\mathcal{X}_i = \eta_i \ , \qquad i = 2, 3, \ldots, 2^r \ ,$$

at each stage obtaining the solution by using the Crout decomposition method described earlier. At the end of this cyclic procedure, a solution is determined for $\underline{\Psi}_{2^K+1}$: Having found $\underline{\Psi}_{2^K+1}$, we then back-solve to successively find the eliminated unknowns. To achieve this we use the relationship

$$\underline{\Psi}_{j-2^r+1} + A^{(r)}\underline{\Psi}_{j+1} + \underline{\Psi}_{j+2^r+1} = A^{(r)}\underline{p}^{(r)}_j + \underline{q}^{(r)}_j \ , \quad (3.7.45)$$

for $j = i2^r$, $i = 1, 2, \ldots, 2^{K+1-r} - 1$ with $\underline{\Psi}_1 = \underline{\Psi}_{2^{K+1}+1} = \underline{0}$.

Hence to find the eliminated unknowns we solve the system of equations

$$A^{(r)}\left(\underline{\Psi}_{j+1} - \underline{p}^{(r)}_j\right) = \underline{q}^{(r)}_j - \left(\underline{\Psi}_{j+2^r-1} + \underline{\Psi}_{j+2^r+1}\right), \quad (3.7.46)$$

where $j = 2^r, 3\cdot 2^r, \ldots, 2^{K+1} - 2^r$, using the factorization of $A^{(r)}$ and the procedure described earlier.

To summarise, the Buneman algorithm for the solution of the Poisson equation with the boundary conditions proceeds as follows:

1. Compute the sequence

$$\left\{ \underline{p}_j^{(r)} , \underline{q}_j^{(r)} \right\}$$ by (3.7.38) and (3.7.39) for

$r = 1, 2, \ldots, K$ with $\underline{p}_j^{(0)} = \underline{0}$ for $j = 0, 1, \ldots, 2^{K+1}$ and

$\underline{q}_j^{(0)} = \underline{QH}_{j+1}$, $j = 1, 2, \ldots, 2^{K-1} - 1$.

2. Determine $\underline{\Psi}_{2^K+1}$ from (3.7.41).

3. Back-solve for other $\underline{\Psi}_j$'s using (3.7.46).

The scheme described in this section is valid only for the case $N = 2^{K+1} + 1$. Schumann and Sweet (1976) have examined the case for general N : the basic method is unaltered but the details of the reduction process are changed.

It should be emphasised that the complications introduced with the use of Buneman's variants were judged worthwhile since they provide greater numerical stability.

Ideally, we would like to transform the coordinates in both x and y-directions since we would then obtain, for a fixed number of mesh points, a more accurate description of the flow in the boundary layer at the bottom of the container and in the shear layer near the free surface of the fluid than we get with mesh points that are equally spaced in the y-direction. Unfortunately, the use of stretched co-ordinates in both directions gives rise to an asymmetric block tridiagonal matrix and the 'simple' reduction process outlined above does not work. It might be possible to amend the method to circumvent this difficulty but such a change is not attempted in this thesis.

CHAPTER 4
NUMERICAL RESULTS AND DISCUSSION

§ 4.1 Stability criteria of the ADI scheme

Generally speaking, implicit methods are unconditionally stable: that is, round off errors introduced at time level n are not magnified in modulus when values of the dependent variable are computed at time level ($n+\frac{1}{2}$). This is clearly demonstrated by various stability analysis methods (Roache, 1976). These methods however make use of some simplifying assumptions; that the velocity be a positive constant along any given row or column, for instance. These assumptions are not generally valid and therefore, in practice, one does experience certain restrictions on the time step. These restrictions certainly arise with the ADI scheme.

Roache (1976) argues that the Courant-Friederick-Lewy (CFL) condition is a reliable stability criterion for most numerical methods. The CFL condition states that

$$\Delta \tau \leqslant \frac{1}{2}\frac{h^2}{\alpha} , \qquad (4.1.1)$$

where α is some diffusion coefficient.

Since the CFL condition is a very general one, its application to our problem does not necessarily guarantee that round off errors are not amplified.

There is another condition that must be obeyed in order to obtain accurate solutions to the system of linear algebraic equations using the Crout algorithm; that the coefficient matrix on the left hand side of (3.6.4) be diagonally dominant. In order to be more explicit, we first recall that the transport equation in transformed coordinates along a given row as $n \longrightarrow n+\frac{1}{2}$ can be written

$$\frac{1}{\lambda}\frac{\partial \Gamma}{\partial \tau} + A_x u \frac{\partial \Gamma}{\partial p} = \alpha A_x^2 \frac{\partial^2 \Gamma}{\partial p^2} + \alpha B_x \frac{\partial \Gamma}{\partial p} + \frac{\partial f}{\partial y}(p,y), \quad (4.1.2)$$

where α is a positive constant and $\frac{\partial f}{\partial y}(p,y)$ is some known quantity. Using forward time and centred space approximations we obtain from (4.1.2) the following finite difference equation (FDE).

$$R_i \Gamma_{i-1}^{n+\frac{1}{2}} + S_i \Gamma_i^{n+\frac{1}{2}} + T_i \Gamma_{i+1}^{n+\frac{1}{2}} = U_i^n, \quad (4.1.3)$$

$$i = 2,3,\ldots,N-1$$

where

$$R_i = -\left[\frac{(u A_x(i) - \alpha B_x(i))}{2h} + \alpha \frac{A_x^2(i)}{h^2}\right], \quad (4.1.4)$$

$$S_i = \frac{2}{\Delta\tau\cdot\lambda} + \frac{2\alpha A_x^2(i)}{h^2}, \quad (4.1.5)$$

$$T_i = \frac{(u A_x(i) - \alpha B_x(i))}{2h} - \frac{\alpha A_x^2(i)}{h^2} \quad (4.1.6)$$

and U_i^n is a known quantity.

Diagonal dominance of the system of equation 4.1.3 requires that

$$|S_i| \geqslant |R_i| + |T_i| \quad . \quad (4.1.7)$$

If (4.1.7) is not obeyed, then the loss of accuracy in the solution of the algebraic equations may make the results from an application of the Crout method quite worthless. Throughout the following analysis let us assume that u is constant at all nodes in a particular row.

Suppose $uA_x(i) - \alpha B_x(i) \geqslant 0$. Then, if

$$\left(uA_x(i) - \alpha B_x(i)\right)/2 \leqslant \frac{\alpha A_x^2(i)}{h} \quad , \qquad (4.1.8)$$

inequality (4.1.7) is satisfied (that is the matrix is diagonally dominant) for all values of $\Delta\tau$. The inequality (4.1.8) is equivalent to

$$\frac{\left(uA_x(i) - \alpha B_x(i)\right)h}{\alpha A_x^2(i)} \leqslant 2 \quad , \qquad (4.1.9)$$

or

$$R_c \leqslant 2 \ ,$$

where R_c denotes the cell Reynolds number for the transformed equations.

When inequality (4.1.8) is not satisfied diagonal dominance requires that

$$\frac{uA_x(i) - \alpha B_x(i)}{h} < \frac{2}{\Delta\tau\lambda} + \frac{2\alpha A_x^2(i)}{h^2} \ , \qquad \text{yielding}$$

$$\lambda\Delta\tau\left[\frac{uA_x(i) - \alpha B_x(i)}{h} - \frac{2\alpha A_x^2(i)}{h^2}\right] < 2 \ . \qquad (4.1.10)$$

Suppose now $uA_x(i) - \alpha B_x(i) \leqslant 0$. In this case if $\dfrac{\alpha B_x(i) - uA_x(i)}{2h} \leqslant \dfrac{\alpha A_x^2(i)}{h^2}$ (or $R_c > -2$) then (4.1.7) is always satisfied irrespective the value of $\Delta\tau\,(>0)$. However, if $R_c < -2$ then inequality (4.1.7) is satisfied only if the time step $\Delta\tau$ is chosen such that

$$\Delta\tau\lambda\left[\frac{\alpha B_x(i) - uA_x(i)}{h} - \frac{2\alpha A_x^2(i)}{h^2}\right] < 2 \ . \qquad (4.1.11)$$

Conditions (4.1.10) and (4.1.11) may be more conveniently written as the single equation

$$\lambda \Delta \tau \left[\frac{|u A_x(i) - \alpha B_x(i)|}{h} - \frac{2\alpha A_x^2(i)}{h^2} \right] < 2 \cdot \qquad (4.1.12)$$

Similarly the conditions on R_c that yield unconditional stability can be combined to give $|R_c| \leqslant 2$.

As $n+\frac{1}{2} \rightarrow n+1$, we have the following FDE corresponding to the transport equation, where is assumed to be constant along a given column

$$R_j \Gamma_{j-1}^{n+1} + S_j \Gamma_j^{n+1} + T_j \Gamma_{j+1}^{n+1} = U_j^{n+\frac{1}{2}} , \qquad (4.1.13)$$

where

$$R_j = -\left(\frac{V}{2h} + \frac{\alpha}{h^2}\right) , \qquad (4.1.14)$$

$$S_j = \frac{2}{\Delta\tau\lambda} + \frac{2\alpha}{h^2} , \qquad (4.1.15)$$

$$T_j = \frac{V}{2h} - \frac{\alpha}{h^2} \qquad (4.1.16)$$

and $U_j^{n+\frac{1}{2}}$ is a known quantity. Diagonal dominance of the system of equations (4.1.13) again requires that (4.1.7) be satisfied.

Using the same arguments as for the case when $n \longrightarrow n+\frac{1}{2}$, we find that the coefficient matrix is diagonally dominant for all values of $\Delta\tau$ if $|R_c| \leqslant 2$, where $R_c = Vh/\alpha$. On the other hand, if $|R_c| > 2$ the system is diagonally dominant when the time step satisfies

$$\lambda \Delta \tau \left[\frac{|V|}{h} - \frac{2\alpha}{h^2} \right] < 2 \quad . \qquad (4.1.17)$$

It was found by numerical experimentation that a variable time step enabled the steady state solution to be reached faster than with a constant step. In view of the fact that a large part of the computational calculations in the program involved inversion of tridiagonal systems, diagonal dominance of the matrices was found to be a key element for numerical stability. In our numerical procedure the CFL condition (4.1.7) was used to provide an initial value of the time step and any subsequent changes in $\Delta \tau$ were made through the use of conditions (4.1.10) and (4.1.17).

§ 4.2 Computational procedure

The procedure that was adopted for obtaining solutions using the finite difference equations derived in § 3.5 is now described. First, it was necessary to choose values for N (the number of mesh points in a row or column), for the small convergence parameters EP1, EP2 and EP3 (defined later in this section), for the initial time step $\Delta\tau$, the Prandtl number P_r and the Grashof number Gr . Then the dependent variables Q, θ and Ψ were initialized.

Suppose the solution for (3.4.1) had been calculated at time level n . Then the temperature at the bottom and sides of the container were updated using the prescribed constant heat fluxes on these surfaces (conditions (3.5.24) and (3.5.31)). Next, the components of the matrices A appropriate to the solution of the momentum and energy equations along the first row ($j = 2$) were calculated from equations (3.4.18). Using the Crout algorithm (see § 3.6) the vorticity and temperature at time level ($n+\frac{1}{2}$) were found consecutively at all internal nodes along that particular row, using the boundary conditions at the ends of the row. This procedure was repeated for the other rows ($j = 3, 4, \ldots, N-1$). The vorticity at time level ($n+\frac{1}{2}$) was then substituted into the right hand side of the Poisson equation (2.4.34). Using the Block Cyclic Reduction Method given in § 3.7, the Poisson Equation was solved to give the stream function at time level ($n+\frac{1}{2}$). The time step was then set to its correct value according to (4.1.12).

After updating the values of the temperature and vorticity on the boundary the procedure described in the above paragraph was repeated, except that now the vorticity and temperature were calculated in column order through (3.4.19), this time using the boundary conditions at the base and top surface. With this method the vorticity, temperature and stream function were found at time level ($n+1$).

A convergence test was now performed. Let Q, θ, Ψ be the calculated values of the respective variables at an arbitrary point (i,j) at time level $(n+1)$, $(i,j) \in \Omega$, Ω being defined through (3.3.12);
Q_2, θ_2, Ψ_2 to be the corresponding values at the same point at time level n
and Q_M, θ_M, Ψ_M be the maximum values of the variables over the whole grid at time level $(n+1)$. Then we assumed that convergence of our solution was achieved when all the inequalities

$$\left.\begin{array}{ll} \dfrac{|Q - Q_2|}{Q_M} < \text{EP1}, \\[2ex] \dfrac{|\theta - \theta_2|}{\theta_M} < \text{EP2}, \\[2ex] \dfrac{|\Psi - \Psi_2|}{\Psi_M} < \text{EP3} \end{array}\right\} \quad \forall \, (i,j) \in \Omega$$

were satisfied, where EP1, EP2 and EP3 were prescribed constants. If the convergence test was satisfied, the velocity field was calculated from the stream function using equations (2.2.18) and the solution was printed out. However, if one or more inequalities was violated, the value of n was increased by one with the time step set according to (4.1.17) and the procedure for updating the dependent variables was repeated.

§4.3 On convergence, accuracy and converged solution

In this section we shall describe the steps, which we have taken to enhance the rate of convergence of the numerical solution and shall discuss the accuracy achieved. For simplicity, let us take the measure of the rate of convergence to be inversely proportional to the number of iteration steps required to achieve the steady state solution.

Effect of parameter λ

A parameter λ was introduced earlier (see (3.4.1)). Various sets of numerical results were produced for different values of λ and it was found that changing λ did significantly affect the rate of convergence. An optimal value of $\lambda = 0.25$ for the energy equation was found by numerical experimentation.

Choice of time step

The program was run initially with a constant time step ($\Delta\tau = c$) set by the CFL condition (see § 4.1). Numerous sets of numerical results were produced with different constant values of $\Delta\tau$ and different sets of error parameters. For a given Grashof number and a given set of error parameters results obtained with a smaller value of $\Delta\tau$ were generally less accurate, as might have been anticipated, since the solution was being truncated before it had properly converged. The values chosen for $\Delta\tau$ and the convergence parameters (EP1, etc) should therefore increase (or decrease) in tandem. However, a variable time step (discussed in § 4.1) had positive advantages on the rate of convergence, though some extra computations were required at each time step. The advantages on the rate of convergence of having a variable time step seemed to outweigh the disadvantages, but care has to be taken to ensure the solution has fully converged.

Other approximations for temperature boundary conditions and some derivatives of ψ

Various sets of numerical results were also produced with different finite difference expressions for approximating both the heat input at the solid boundaries and the temperature condition at the centre line. Initially, linear expressions were used at all three boundaries. With parabolic approximations, however, (see § 3.5) the solution converged faster and one expects them to provide increased accuracy in the velocity and thermal boundary layers. It should be pointed out that the extra computations needed for the parabolic approximations were insignificant. It is possible that exponential expressions for the variation in temperature near the boundaries would lead to more accurate results, but such variations have not been investigated in this work.

Expressions for the derivatives of the stream function near the solid boundaries, more accurate than those introduced in § 3.7, were obtained by exploiting fully the boundary conditions on the stream function and velocity. The modified expressions are derived as follows: Using Taylor's expansion we have for $j = 1, 2, \ldots, N$

$$\psi_{2,j} = \psi_{1,j} + h\frac{\partial\psi}{\partial p}(1,j) + \frac{h^2}{2!}\frac{\partial^2\psi}{\partial p^2} + \frac{h^3}{3!}\frac{\partial^3\psi}{\partial p^3} + o(h^4) \quad (4.3.1)$$

and

$$\psi_{3,j} = \psi_{1,j} + (2h)\frac{\partial\psi}{\partial p}(1,j) + \frac{(2h)^2}{2!}\frac{\partial^2\psi}{\partial p^2}(1,j) + \frac{(2h)^3}{3!}\frac{\partial^3\psi}{\partial p^3} + o(h^4) \quad (4.3.2)$$

From (4.3.1) and (4.3.2) and with the use of the boundary conditions

$$\psi_{1,j} = \frac{\partial\psi}{\partial p}(1,j) = 0 \quad , \quad \text{(see § 3.5)} \quad (4.3.3)$$

it follows that

$$\frac{\partial^2 \psi}{\partial p^2}(1,j) = \left(8\psi_{2,j} - \psi_{3,j}\right)\Big/2h^2 + o(h^2) \qquad (4.3.4)$$

and

$$\frac{\partial^3 \psi}{\partial p^3}(1,j) = \frac{3}{2}\left(\psi_{3,j} - 4\psi_{2,j}\right)\Big/h^3 + o(h) \,. \qquad (4.3.5)$$

Furthermore, another Taylor expansion yields

$$\frac{\partial \psi}{\partial p}(2,j) = \frac{\partial \psi}{\partial p}(1,j) + h\frac{\partial^2 \psi}{\partial p^2} + \frac{h^2}{2!}\frac{\partial^3 \psi}{\partial p^3} + o(h^3) \,, \qquad (4.3.6)$$

and expressions (4.3.3) to (4.3.6) then imply that

$$\frac{\partial \psi}{\partial p}(2,j) = \left(\psi_{2,j} + \frac{1}{4}\psi_{3,j}\right)\Big/h + o(h^3) \,. \qquad (4.3.7)$$

In an analogous way it can be shown that

$$\frac{\partial \psi}{\partial y}(i,2) = \left(\psi_{i,2} + \frac{1}{4}\psi_{i,3}\right)\Big/h + o(h^3) \,. \qquad (4.3.8)$$

Although the expressions for the first derivatives are modified as above, a simple Taylor's expansion analysis reveals that the second derivatives $\frac{\partial^2 \psi}{\partial p^2}(2,j)$ and $\frac{\partial^2 \psi}{\partial y^2}(i,2)$ retain their usual finite difference expressions. On the introduction of expressions (4.3.7) and (4.3.8) the solution converged much faster and, consequently, a more accurate picture was revealed.

It should be emphasized that the inclusion of (4.3.7) and (4.3.8) into the FDE for the Poisson equation did create some difficulties, since the diagonal elements of the block matrix M were changed from A (see (3.7.23)). The original form was restored by moving the 'extra' terms to the right hand side of equation (3.7.12) for the case when $i = 2$, giving the following scheme:

(reference is made to expressions (3.7.11) and (3.7.12))

$$\left(b_2/\gamma^2\right)\Psi_{2,j} + \left(c_2/\gamma^2\right)\Psi_{3,j} + \Psi_{2,j-1} + \Psi_{2,j+1} =$$

$$= QH_{2,j} - B_x(2)\,h\left(\Psi_{2,j} - \tfrac{1}{4}\Psi_{3,j}\right). \qquad (4.3.9)$$

More accurate solutions could have been obtained by representing the derivatives in the governing equations by finite difference approximations to a higher order of accuracy, thus reducing the truncation error, but the technique has not been used in this thesis.

Changes in grid spacing

Another technique commonly used for improving the accuracy of the solution is to reduce the grid spacing. No specific formula which connects the magnitude of the discretization error to the size of the grid spacing has yet been found. However, numerical experimentation has shown that, in general, errors decrease as the grid spacing is reduced. One therefore expects that using smaller and smaller grid spacings will eventually produce successive finite difference solutions that differ from the true solution by decreasing amounts. This approach is usually very uneconomic, however, and this was confirmed from a careful consideration of our program run with different mesh sizes. It was found that on halving the grid spacing the computational time increased approximately by a factor of r^2, where r is the ratio of the respective numbers of grid points (i.e. $r = (2^{K+2}+1)/(2^{K+1}+1)$ for the appropriate K). In practical terms this meant, for instance, that the program could be run satisfactorily on the local computer for a (17 x 17) mesh but had to be run on a super computer (CRAY-1S) if a (33 x 33) mesh were used. To decrease cost (and turn-round time) the program was developed and run mostly on the local computer but some runs on the CRAY-1S were carried out.

Heat and mass balance

We shall look now at ways of checking whether steady state has been reached, recalling that, at steady state, all the physical variables at each point are independent of time. One method is based on heat balance. Since we are assuming no evaporation at the free surface, all the heat passing through the solid boundaries of the container must leave through the top surface in the steady state. Therefore, a necessary condition for the numerical solution to satisfy in the steady state is the balance of heat in the container. A method of testing whether such a balance has been established is outlined below.

If Q_3 is the heat flux leaving the top surface in the real cavity, then

$$\left.\frac{\partial\theta}{\partial y}\right|_{y=1} = -\frac{Q_3}{\gamma Q'} = -\frac{\overline{Q}_3}{\gamma \overline{Q}_1} \quad \text{(see § 2.4)}, \qquad (4.3.10)$$

where $\overline{Q}_3$ and $\overline{Q}_1$ correspond to the respective heat fluxes in the non-dimensional cavity (N.B $Q_i = \overline{Q}_i$ for $i = 1, 2, 3$).

Introducing the variable $\overline{y} = 1 - y$, $\overline{y}$ is the distance measured into the fluid from the free surface, the boundary condition (4.3.10) can be written

$$\left.\frac{\partial\theta}{\partial \overline{y}}\right|_{\overline{y}=0} = \overline{Q}_3 / \gamma \overline{Q}_1 .$$

Assuming a parabolic distribution for the temperature at the free surface,

$$\theta = a\bar{y}^2 + b\bar{y} + c \quad , \qquad (4.3.11)$$

we then deduce that

$$b = \frac{\bar{Q}_3}{\gamma \bar{Q}_1} \quad . \qquad (4.3.12)$$

On the free surface we require (see (3.5.1)) that $\theta\big|_{\bar{y}=0} = 0$ and hence we find from (4.3.11) that

$$c = 0 \quad . \qquad (4.3.13)$$

Assuming $\theta_{i,N-1}$, $\theta_{i,N-2}$ are known, then $\forall i$ in the range $1 \le i \le N$, equations (4.3.11) to (4.3.13) imply that

$$\theta_{i,N-1} = a_j h^2 + \bar{Q}_3(i,N)\, h \big/ \gamma \bar{Q}_1 \quad , \qquad (4.3.14)$$

$$\theta_{i,N-2} = a_j (2h)^2 + \bar{Q}_3(i,N)\, 2h \big/ \gamma \bar{Q}_1 \quad , \qquad (4.3.15)$$

from which we deduce

$$\bar{Q}_3(i,N) = \frac{\gamma \bar{Q}_1}{2h}\left(4\theta_{i,N-1} - \theta_{i,N-2}\right) \quad . \qquad (4.3.16)$$

A simple analysis shows that, when $Q' = Q_2$ (see 4.3.10), we obtain the following expression for $\bar{Q}_3$: $\bar{Q}_3(i,N) = \left(\gamma\, \bar{Q}_2 \big/ 2h\right)\left(4\,\theta_{i,N-1} - \theta_{i,N-2}\right)$, where $\bar{Q}_2$ is the corresponding heat flux in the non-dimensional cavity.

Using the trapezoidal rule to evaluate the amount of heat leaving the free surface, QS say, we have

$$QS = \sum_{i=1}^{N-1} \left(\left(\bar{Q}_3(i,N) + \bar{Q}_3(i+1,N)\right)\big/ 2\right)\left(X_{i+1} - X_i\right), \qquad (4.3.17)$$

where X_i, measured in non-dimensional X-space, corresponds to $(i-1)h$ in p-space.

Since $\overline{Q}_1$ and $\overline{Q}_2$ are both constants, for heat balance we require

$$QS = \overline{Q}_1 + \overline{Q}_2 \quad . \tag{4.3.18}$$

Expression (4.3.17) is one criteria that helps us decide whether steady state has been reached. The accuracy of the heat balance was calculated by comparing QS and ($\overline{Q}_1 + \overline{Q}_2$). More precisely, a percentage value

$$P = \left| \frac{QS - (\overline{Q}_1 + \overline{Q}_2)}{\overline{Q}_1 + \overline{Q}_2} \right| \times 100 \tag{4.3.19}$$

was evaluated. For the numerical results presented later condition (4.3.19) was satisfied at 1% accuracy for most cases and, at worst, at 3% accuracy. Similar checks were also performed on the mass balance within the liquid. In the steady state the total mass flow across any line x = const or y = const must be zero. The accuracy of the mass balance relative to the vertical velocity for instance, was found by comparing the mass M_1 of liquid going upwards and the mass M_2 of liquid going downwards. A percentage value P_1 given by

$$P_1 = \left| \frac{M_2 - M_1}{\max(M_1, M_2)} \right| \times 100$$

was then evaluated. Relative to both velocity components balance was obtained within 1% accuracy. It is not surprising that, on the whole, the mass balance was more accurate than the heat balance, since accurate calculations for the heat flux at the free surface were not possible because of the relative scarcity of grid points in the thermal shear layer.

Check with known solutions

Another important way of checking major parts of our program was to change our problem to one commonly used in this area to assess numerical schemes: namely, a square region with differentially heated end walls and adiabalic top and bottom solid surfaces. This conversion was easily carried out and the resulting numerical solution obtained with our method was compared with the very accurate results that are available in the literature. Fig. 4.3.1 shows the vertical velocity profile, obtained using our numerical scheme along $y=\frac{1}{2}$ for Ra = 10^6 and Pr = 0.73. The figure clearly shows a centro-symmetric pattern: a necessary feature in view of the symmetry of the problem. Our values for the horizontal and vertical velocities were within 1% of those obtained in the bench mark solution of Markatos et al (1983) and De Vahl Davis (1982).

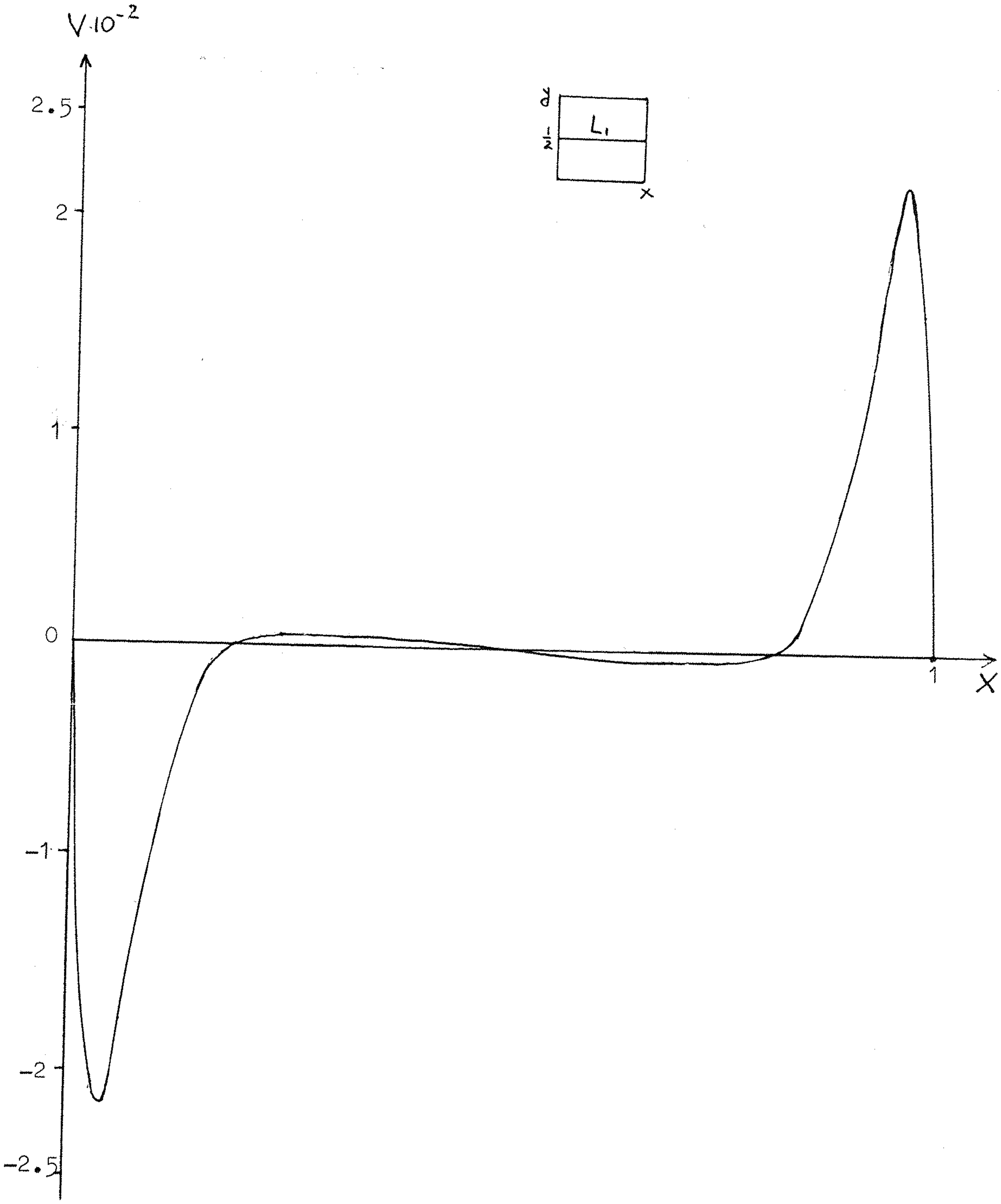

Fig 4.3.1 Comparison problem. Vertical velocity, Ra = 10^6

§ 4.4 Numerical results and analysis

Numerical results were obtained on the different mesh sizes (9 x 9), (17 x 17) and (33 x 33). Convergent solutions could not be obtained for the (33 x 33) mesh on the local computer (ICL 2976), so some runs for this mesh size were performed on the CRAY-1S at the University of London Computer Centre. Although the latter results showed little qualitative difference from the ones obtained on the (17 x 17) mesh, the results did reveal a more accurate description of the velocity and thermal boundary layers and varied at the most by 10% from the results recorded on the (17 x 17) mesh. Most of the numerical results were obtained locally on a (17 x 17) mesh size for Grashof numbers up to 10^8 and it is mainly these results that are presented in this thesis.

A few runs were performed for Grashof numbers of 10^9 to 10^{12}. Although instabilities did not arise for these values of Gr it is possible that the velocities become sufficiently large for the flow to be turbulent. Since the Reynolds number is defined by Re = $\rho V d/\mu$, the transition to turbulence clearly depends on the properties of the liquid under consideration and the size of the container. Because of the close similarity of the results for Gr = 10^6 and Gr = 10^8, we shall concentrate on presenting numerical results at steady state for Gr = 10^4 and Gr = 10^8, with a few plots for Gr = 10^{12}. In all cases, the Prandtl number is equal to unity which is a reasonable value for cryogenic liquids.

The program was run with different values of the stretching parameter ϵ (see Fig. 3.3.1). With ϵ = 0.95, it was found that the X-coordinate was overstretched and, consequently, the results suffered from loss of accuracy in the core region. However, as ϵ is decreased, the numerical error increases. The choice of ϵ = 0.8 seemed to be the best for our problem and is the one used for our numerical results.

Numerical results are presented for different values of the aspect ratio ($\gamma = H/W$). It was found that the aspect ratio had a major influence on the stability of the numerical method. This dependence was already revealed for similar problems almost two decades ago by Elder (1966). For our problem it did not prove possible to obtain accurate results with our numerical method for $\gamma < 0.25$. It was assumed in § 2.4 that Q_1 and Q_2 the heat fluxes at the base and sides of the container respectively were both constant. In practice, there may be spatial variations in these heat fluxes, particularly in Q_1 but although these would seem comparatively simple to introduce we do not do so here.

Some numerical results are presented for cases when there is no heat flux at the base. In these situations, a change of heat flux scale is necessary, in that Q' (see § 2.3) may no longer be set equal to Q_1 : we can however, set Q' equal to Q_2 .

The initial conditions were set as stated in § 2.3. These conditions provide an initial guess for the dependent variables. In view of the limited computational time on the local computer it was found necessary, in some cases, where the rate of convergence was slow to perform numerical computation in 2 stages. The outputted transient solution, for a given Grashof number, from the first stage was then used as initial conditions for another run at the same Grashof number.

The temperature and velocity profiles shown on Figures in this section are accompanied by small squares or rectangles that indicate the line along which the temperature or velocity is plotted. In order to make the diagrams more explicit for cases, where $\gamma \neq 1$, small rectangles representing the real configurations of the left half of the cavity, are drawn. In these rectangles, for instance, the line $y = 1$ would represent the top surface of the liquid, its height being given by H/γ , where $2H$ is the width of the cavity.

We shall now examine in some detail the numerical solutions obtained, grouping these solutions in a convenient way.

1. $\gamma = 1$, $\frac{Q_2}{Q_1} = 1$.

Here we are looking at a rectangular region of liquid with an equal influx of heat per unit area at the sides and bottom. Fig. 4.4.1 shows streamline patterns for Gr = 10^4. Since we are at steady state, the streamlines coincide with the particle paths and, therefore, the flow pattern is roughly speaking a cylindrical vortex, rotating clockwise in the region shown. The vortex is generated by the horizontal temperature gradient across the cavity since the heat transfer is still mostly by conduction. In the V-plots in Fig. 4.4.5, the curve corresponding to Gr = 10^4 demonstrates that the boundary layer is comparatively thick. This is not unexpected because we are dealing with a low Grashof number, for which viscous effects outweigh convection effects and, consequently, the liquid is still slowly moving.

As the Grashof number is increased to 10^8 (which, in our case, would mean that more heat is being applied at the base and sides of the cavity) buoyancy effects dominate the flow and, as a result, the boundary layer becomes thinner and the maximum velocity moves closer to the wall. Also, more of the motion of the liquid now occurs close to the boundaries and there is correspondingly less activity in the core region. At Gr = 10^{12}, the boundary layer is thinner and much more pronounced and the velocity gradient in that layer is very high, thus confirming the high values of the vorticity in that region. Again, we find that, at Gr = 10^{12}, more of the motion of the liquid is shifted towards the boundaries. The effect of increasing the Grashof number on the flow pattern can be observed by comparing Fig. 4.4.1 and Fig. 4.4.3 and inspecting the plots in Fig. 4.4.5. As Gr increases by a factor of 10^4, the vertical velocity increases by about 10^2 and, as is evident in Fig. 4.4.5, we find that there is a downward and relatively strong jet at the centre line. This phenomenon, which was not expected by experimentalists, has now been frequently observed during experiments with cryogenic liquids.

Fig. 4.4.4 shows temperature profiles along the line $X = \frac{1}{2}$. For Gr = 10^4, the curve corresponds to the conduction solution as the velocities are still small. Furthermore, we find that, along this curve, the vertical temperature gradient changes sign twice indicating the variation of the temperature with distances in the middle of the cavity. However, as Gr is increased to 10^8 and further to 10^{12}, the corresponding temperature profiles in Fig. 4.4.4 show that the vertical temperature gradient in the middle is almost zero. In these cases, because of the predominance of convective effects, the liquid moves faster and the flow becomes more uniform. The temperature in the core region is found to be constant. Peaks arise in the temperature close to the free surface (the ones for Gr = 10^8 and Gr = 10^{12} being more obvious).

It should be pointed out that the temperature profiles (or velocity profiles) measured along a constant value of y are not expected to be so accurate as those along a constant value of X , because the y -coordinate is not transformed so as to accumulate grid points near the boundaries.

As stated earlier, only a few solutions were obtained on a (33 x 33) mesh. Although these solutions took much longer time to converge, they did give more accurate results, in particular providing a better description of the thermal boundary layer at the free surface. Moreover, a very interesting fact was noted on comparing Fig. 4.4.3 and the streamline pattern for the finer mesh.

Fig. 4.4.3 shows that on increasing the Grashof number from 10^4 to 10^8, the single circular vortex is conserved. However, the flow pattern for $Gr = 10^8$ on the (33 x 33) grid showed the formation of a small secondary vortex in the bottom left hand corner of the cavity. A close look at the temperature distribution in that particular region showed a high concentration of isotherms similar in shape to that of a plume. These results suggest the existence of plume convection, thus confirming experimental observations by Scurlock et al (1984).

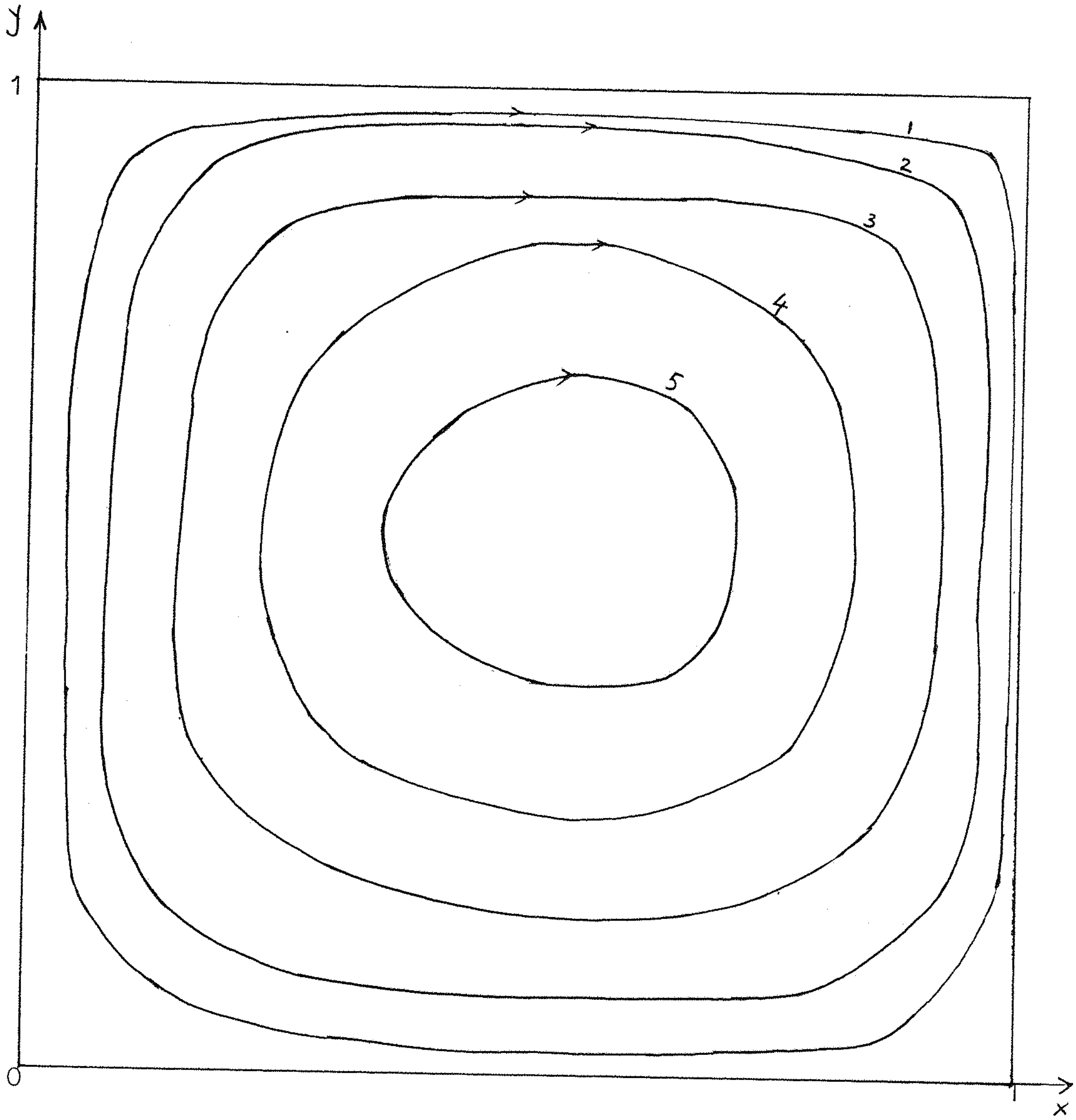

Fig. 4.4.1 Streamline pattern, Gr = 10^4

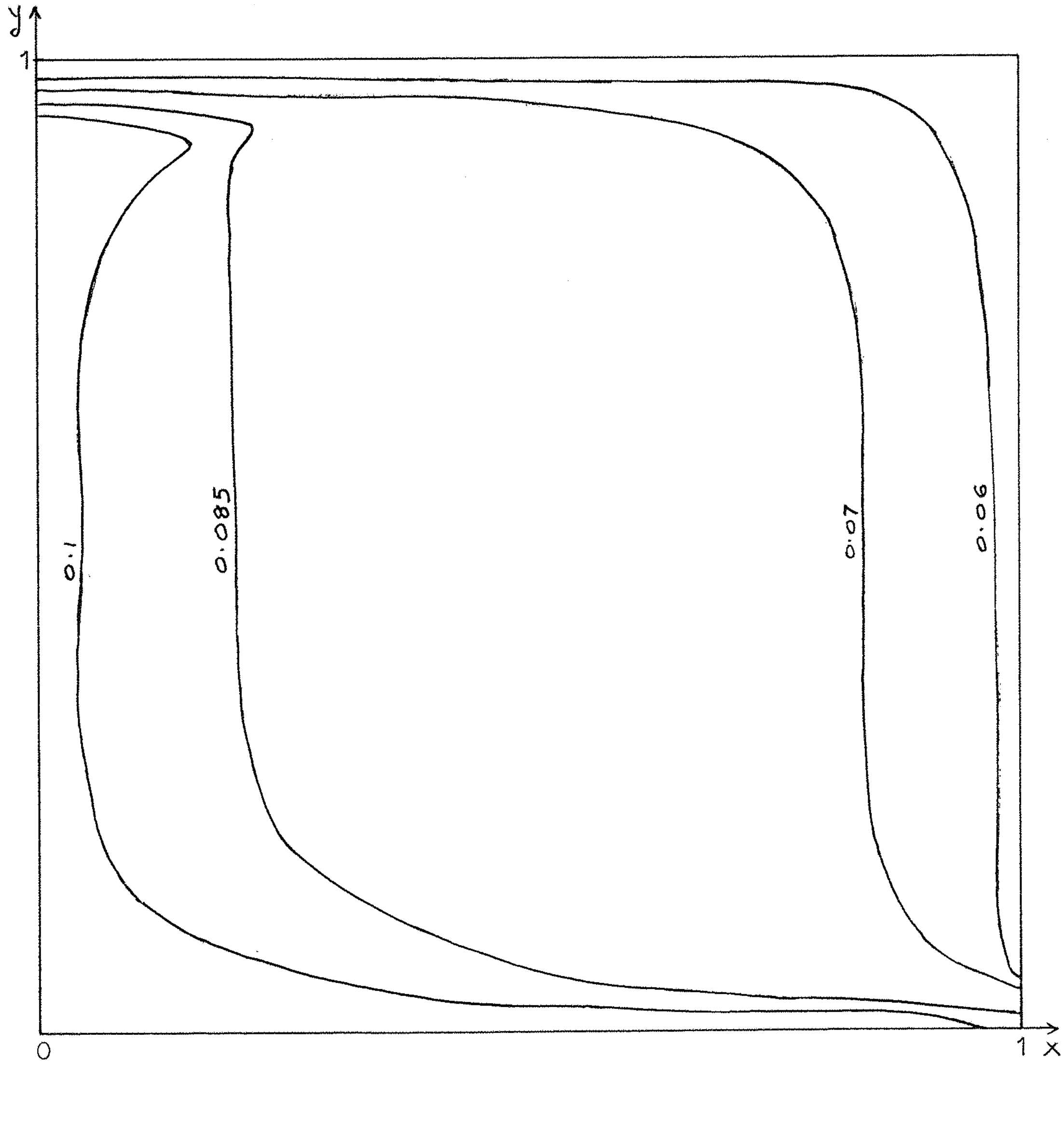

Fig. 4.4.2 Isotherms, Gr = 10^4

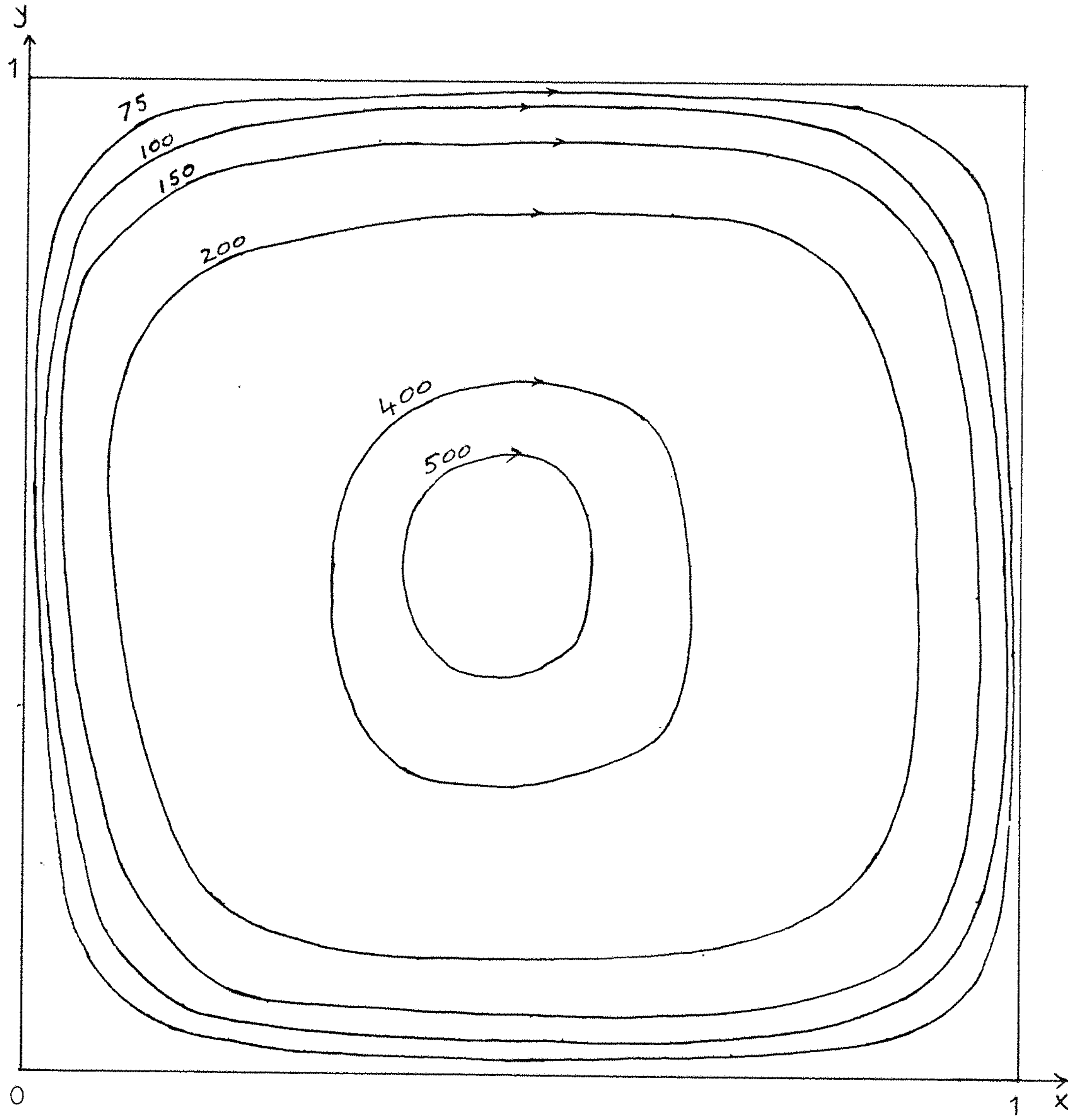

Fig. 4.4.3 Streamline pattern, Gr = 10^8

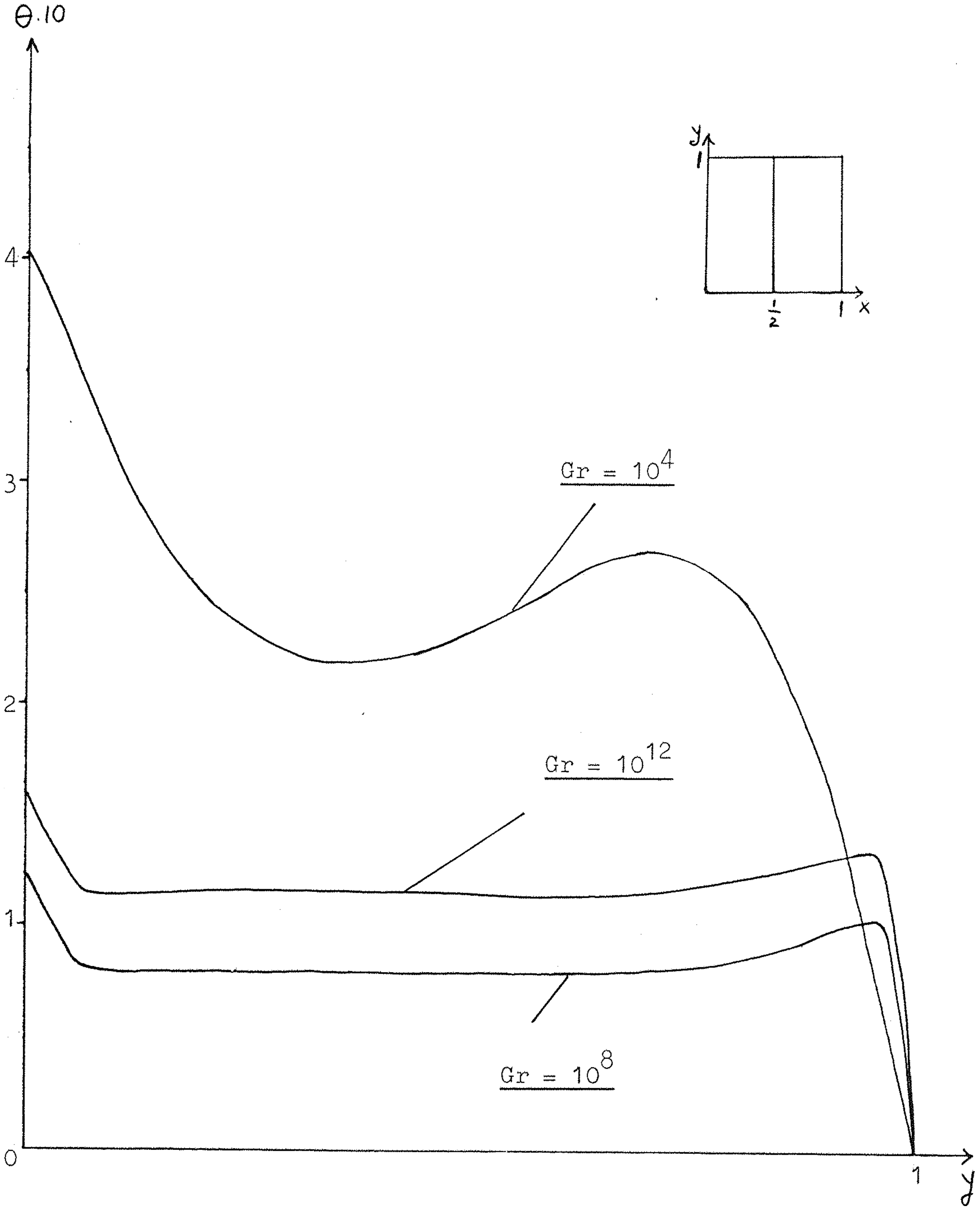

Fig. 4.4.4 Temperature profiles

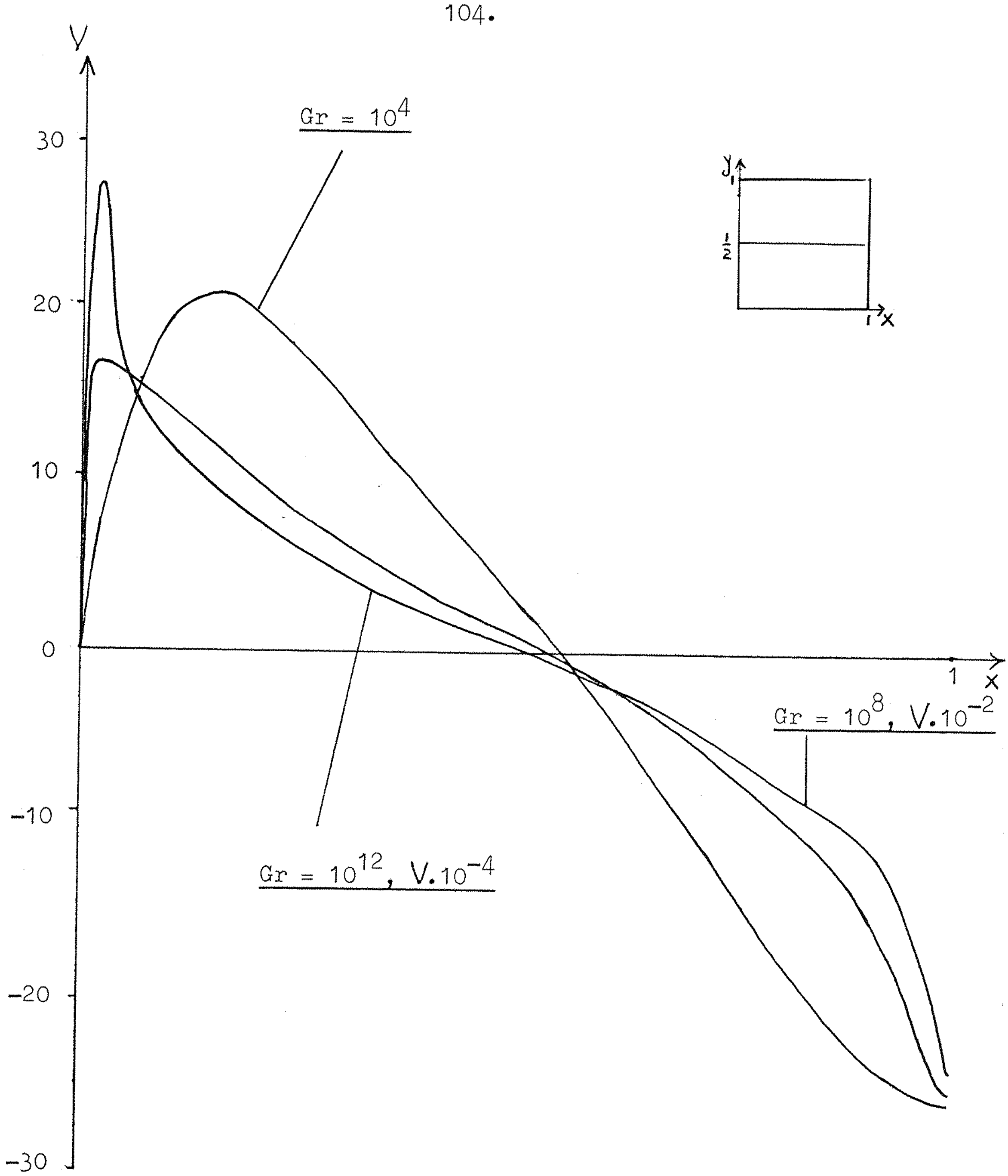

Fig. 4.4.5 Vertical velocity profiles

2. $\gamma = 1,\ Q_1 = 0$

Here we are looking at the same cavity as before but without any influx of heat at the base. There is not much qualitative difference in the numerical results from those of the previous case. Fig. 4.4.6 shows vertical velocity profiles for Gr = 10^4, 10^8 and we observe the marked difference in the boundary layer thickness as the Grashof number is increased. Comparing Fig.'s 4.4.5 and 4.4.6, we find that, when Gr = 10^8, the velocity profile is considerably flatter in the region $0.25 < X < 0.8$. This implies that, for Gr = 10^8, there is relatively less motion in the core region when the heat flux at the base is switched off. Also, as expected, the magnitudes of the velocities in this subsection are lower than those in subsection 1 as buoyancy effects are less strong. Although the scales are different, a comparison of Fig.'s 4.4.8 and 4.4.4 naturally reveals that the temperature gradient near the free surface is lower when there is no heat flux at the base. It is interesting to note from Fig. 4.4.7 that, even though no heat source is present at the base, a boundary layer still arises there. The isotherms for Gr = 10^8 (which are not shown here) reveal an almost vertical stratification pattern, which is not too dissimilar from the one shown later in Fig. 4.4.14 except for there being slightly thicker boundary layers in this case. Vertical motion in the core region is considerably reduced, therefore as shown in Fig. 4.4.6.

The numerical results mentioned above are not inconsistent with experimental data. However, in a laboratory situation the containers are narrow cylinders and so it seems appropriate to look next at numerical results for cavities with a smaller aspect ratio.

3. $\gamma = 0.25$, $Q_1 = 0$.

In this cavity, the height of the fluid is twice the width. Results are presented for Gr = 10^8 only since the latter value corresponds more closely to experimental data and, also, results obtained for Gr = 10^4 were found to be closely similar to the corresponding ones presented in subsection 1. In Fig. 4.4.9 the vertical velocity profile reveals a sharp definition of the boundary layer and the central downward jet is evident. The other interesting feature is the almost flat portion in the middle. Almost the same picture is revealed in Fig. 4.4.11 for the horizontal velocity. These results indicate that the motion of the liquid is, to a large extent, confined close to the boundaries and to the free surface and the liquid in the core region is relatively static. Recirculation exists mostly within the boundary layers and the flow along the sidewall contributes to the thermal layer formation at the top as shown in Fig. 4.4.10. No obvious reason is found for this behaviour, but these results are in good agreement with experimental results from the Institute of Cryogenics, University of Southampton.

4. $\gamma = 0.5$, $Q_1 = 0$.

In this cavity the height of the liquid is equal to the width of the cavity. Velocity and temperature profiles for Gr = 10^8 are shown in Fig. 4.4.12 and 4.4.13 respectively and these are qualitatively similar to the ones corresponding to γ = 0.25 plotted on Fig. 4.4.9 and Fig. 4.4.10. Fig. 4.4.12 reveals once again that the velocity boundary layer and central jet are clearly defined and the middle portion is almost flat. Hence, the motion of the liquid is mostly confined to the boundaries, the central jet is very close to the line of symmetry and the remainder of the liquid is relatively stagnant.

The isotherms shown in Fig. 4.4.14 reveal a thermal stratification in the core region. This vertical stratification in the temperature distribution with increasing values from the bottom to the top of the cavity inhibits the vertical motion in the core region and so is consistent with the velocity profile shown in Fig. 4.4.12. The boundary layers are quite noticeable in Fig. 4.4.14. Results for Gr = 10^4 are qualitatively similar to those given in subsection 2 for a different aspect ratio and are not presented.

We can deduce from the results presented in subsections 3 and 4, therefore, that some variations in the aspect ratio have little influence on the velocity and temperature distributions in the liquid.

5. $\gamma = 1, \quad \frac{Q_1}{Q_2} = 2$

In a real large storage tank, the presence of support devices at the base mean that, on average, the influx of heat at the base is higher than that at the walls and consequently our program was run with the ratio of the heat fluxes as stated above. The results showed little qualitative change from the ones given in subsection 1. However, the isotherms plotted in Fig. 4.4.15, for Gr = 10^8, reveal an interesting fact: for comparison of Fig.'s 4.4.14 and 4.4.15 reveals that the application of an external heat flux at the base totally disrupts the vertical thermal stratification. Sidewall heating, therefore, produces the greatest amount of stratification, a result first noted experimentally by Fan and Chu (1968). This subsection completes our analysis of the numerical results for the rectangular cavity.

In general, the coordinate transformation, $p(x)$ decreases the numerical error in the solutions, but increases the computational time by approximately 30%. As stated earlier, test runs have shown that numerical results are essentially grid independent. Hence, one could suggest that numerical results, for a given Grashof number, on a crude mesh be interpolated (assuming a linear or parabolic distribution of the dependent variable between grid points), to be subsequently defined as initial conditions for the same Grashof number on a finer mesh. This procedure would be easier to implement on a regular grid than on a non-equidistant one. Whether or not this procedure would save overall computational time is debatable since the interpolations introduce extra computations particularly so if they are to be used on a high order interpolation scheme.

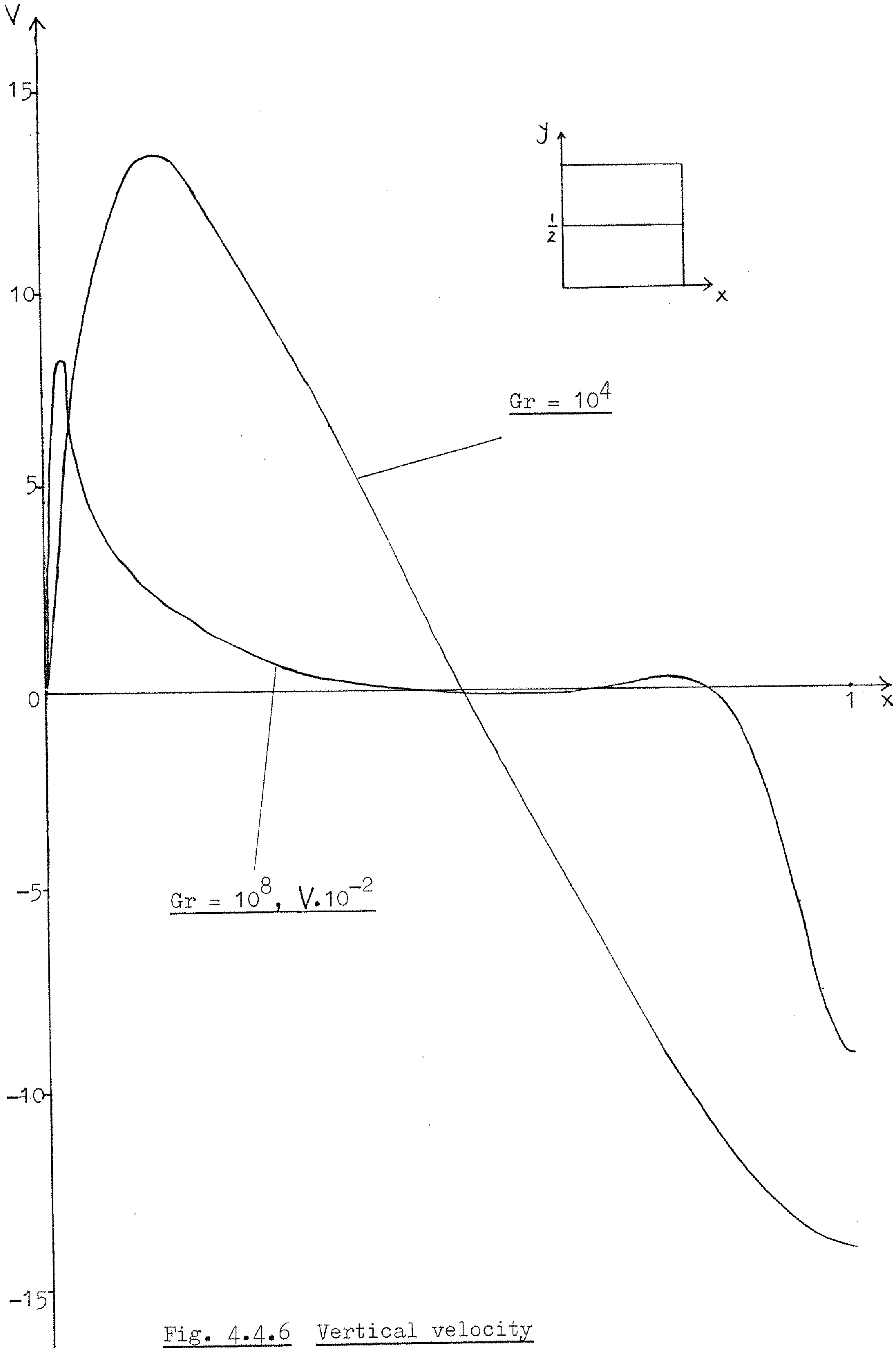

Fig. 4.4.6 Vertical velocity

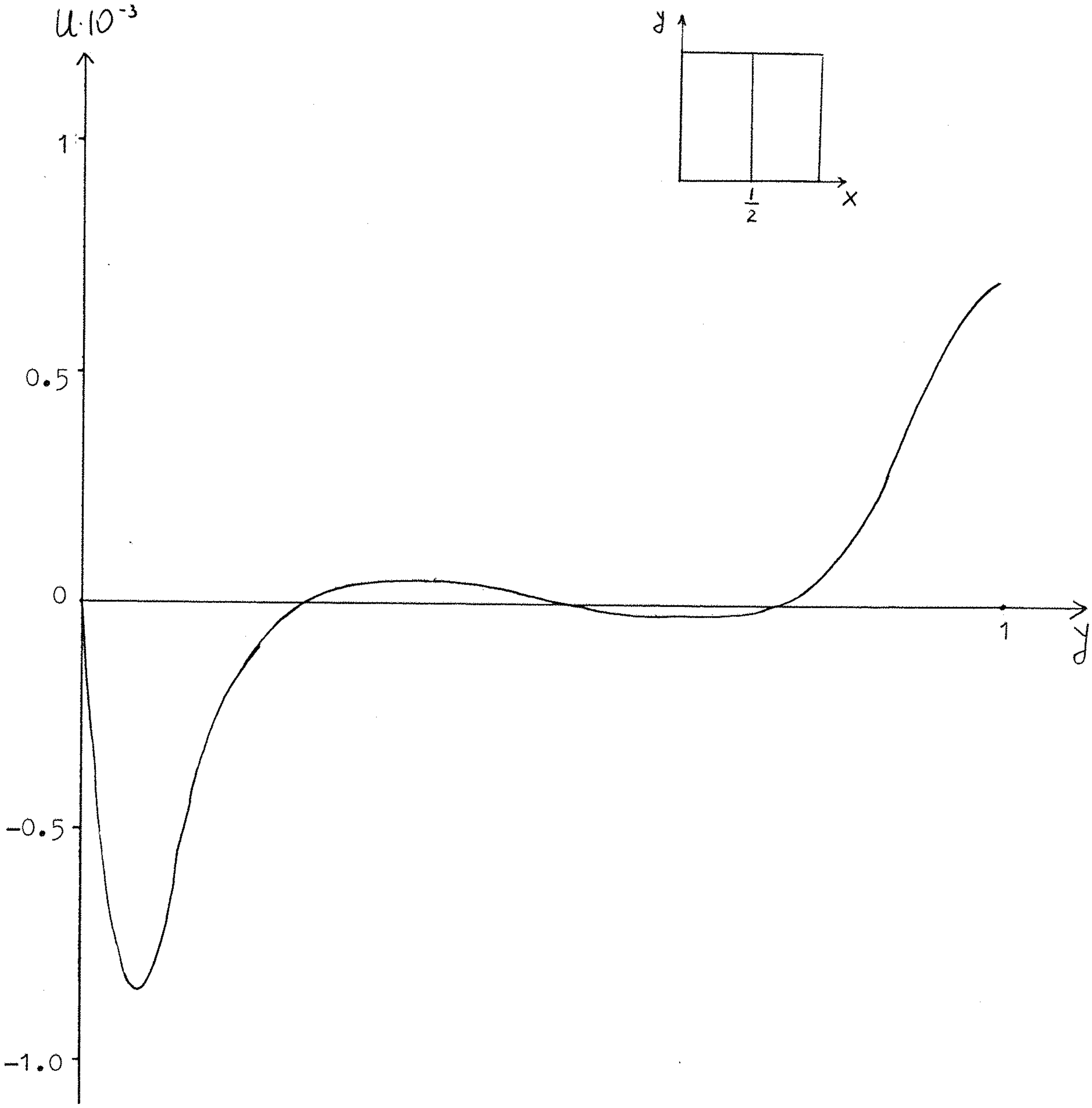

Fig. 4.4.7 Horizontal velocity profile, Gr = 10^8

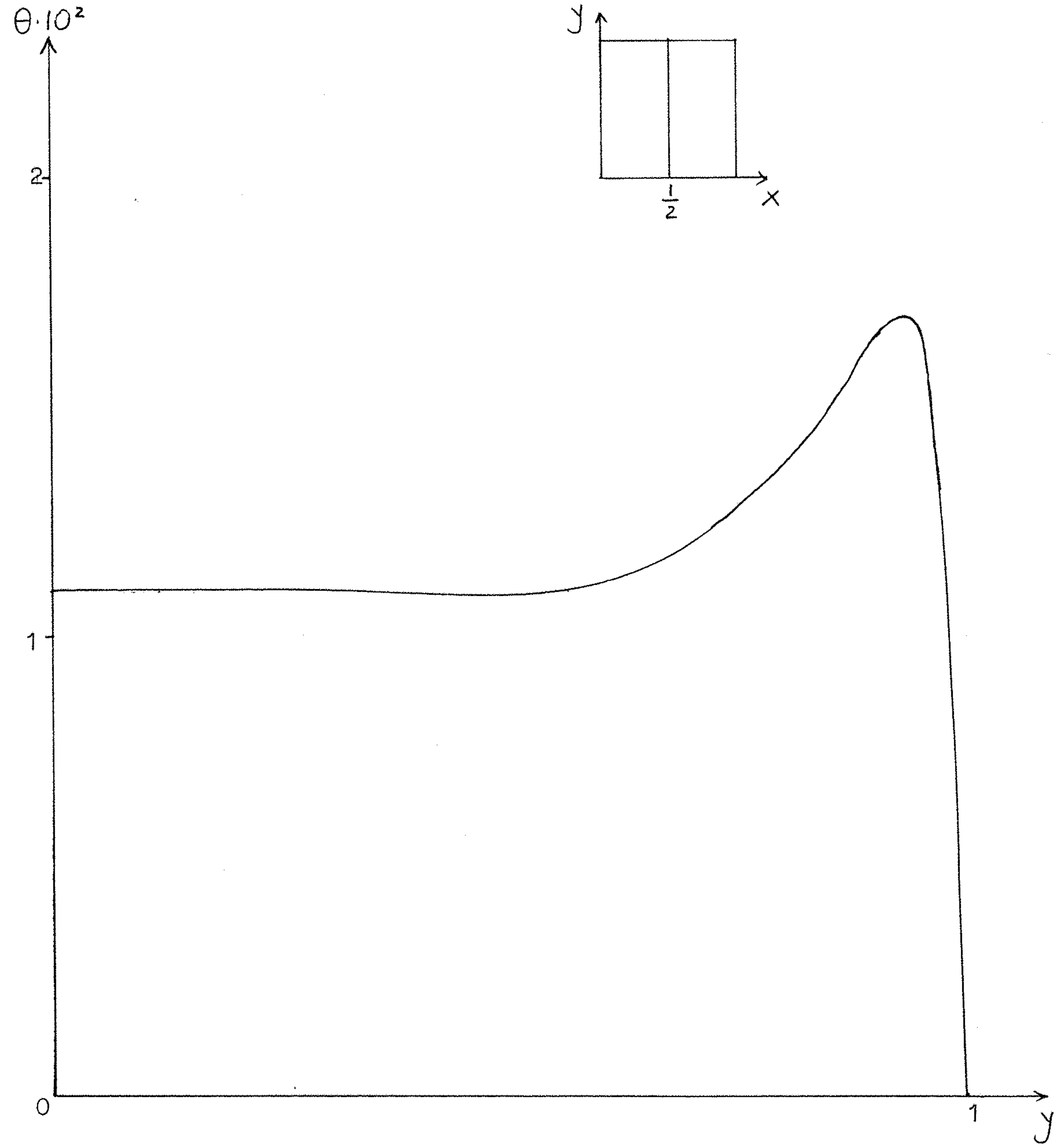

Fig. 4.4.8 Temperature profile, Gr = 10^8

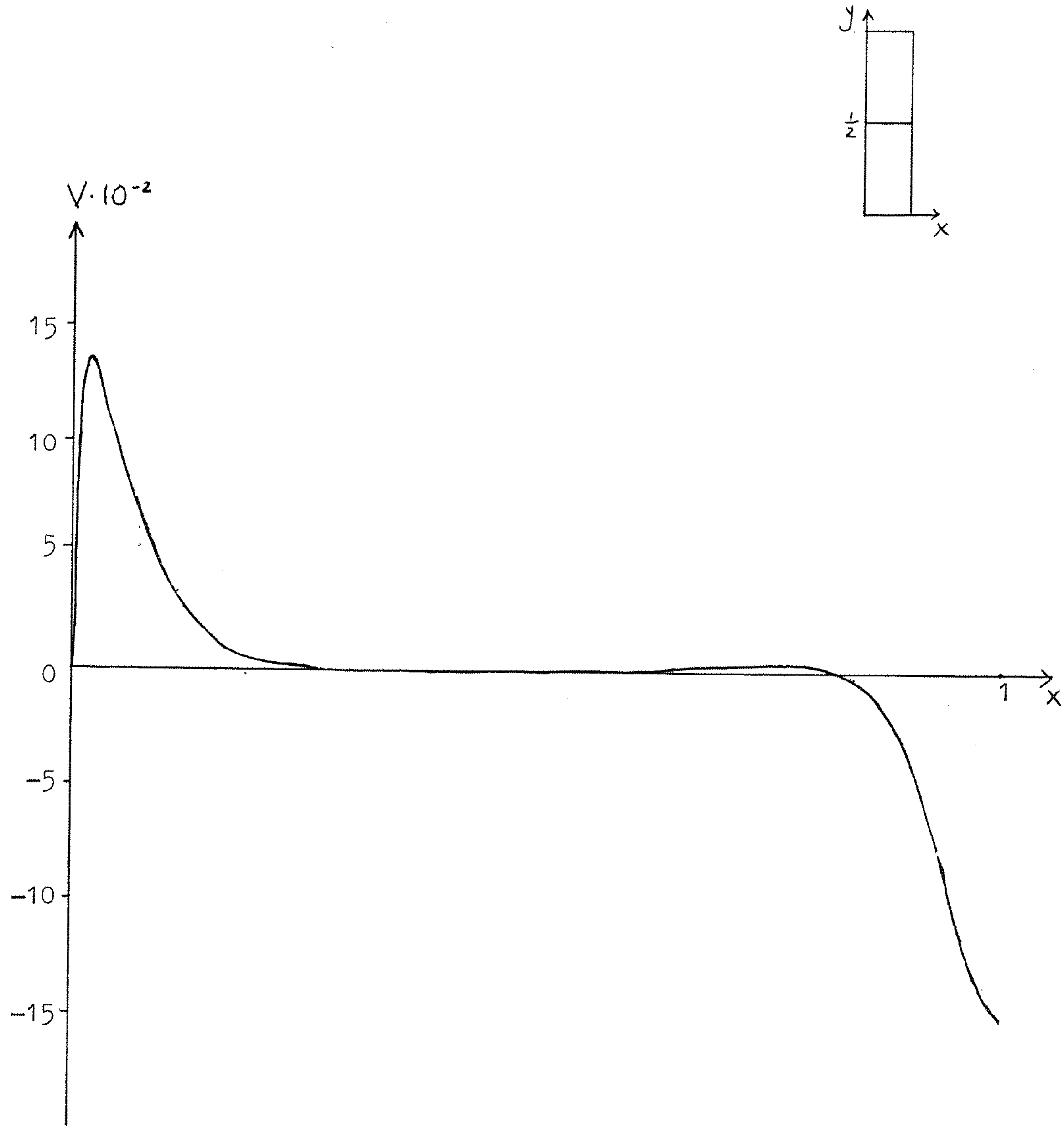

Fig. 4.4.9 Vertical velocity profile, Gr = 10^8

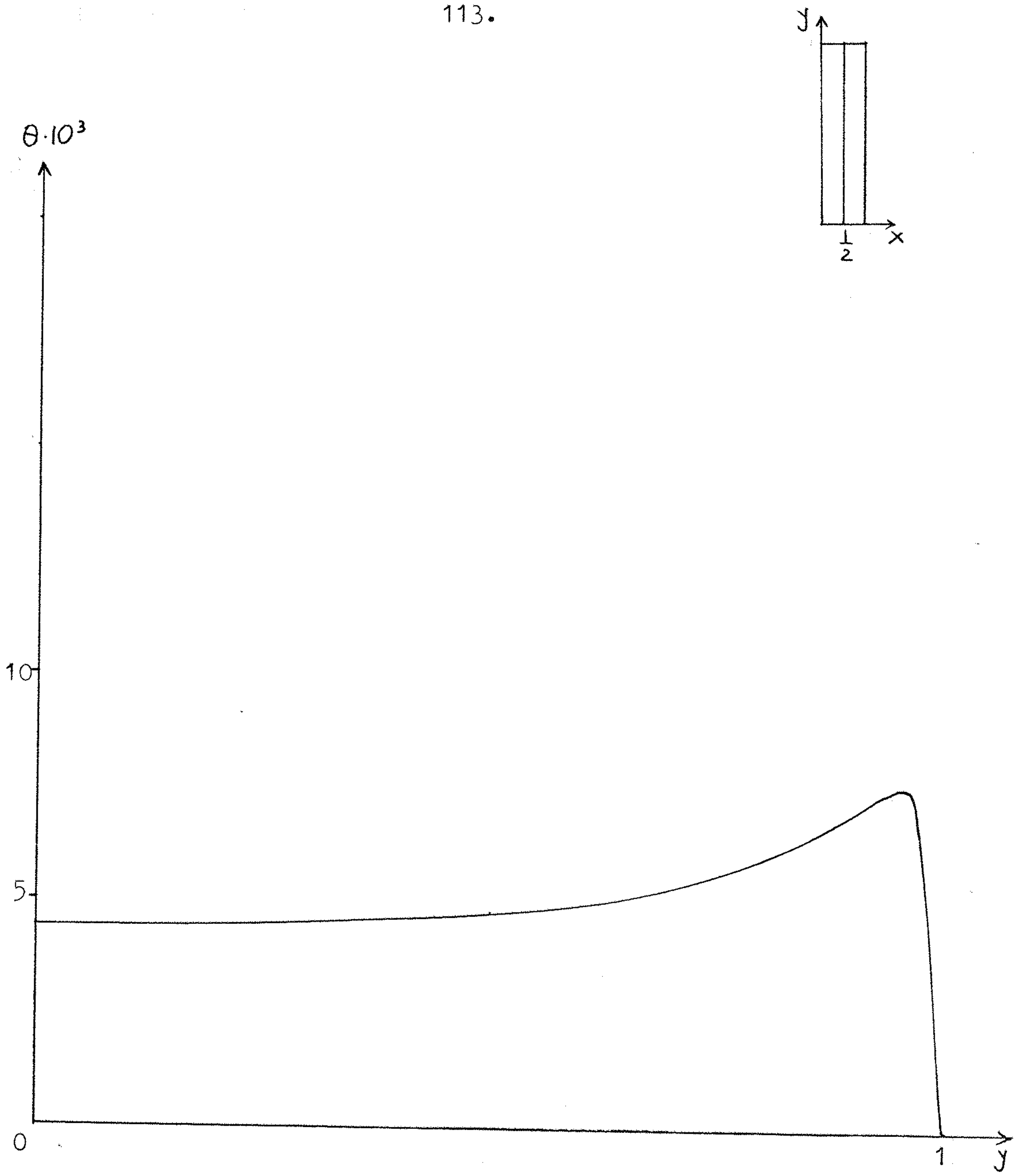

Fig. 4.4.10 Temperature profile, Gr = 10^8

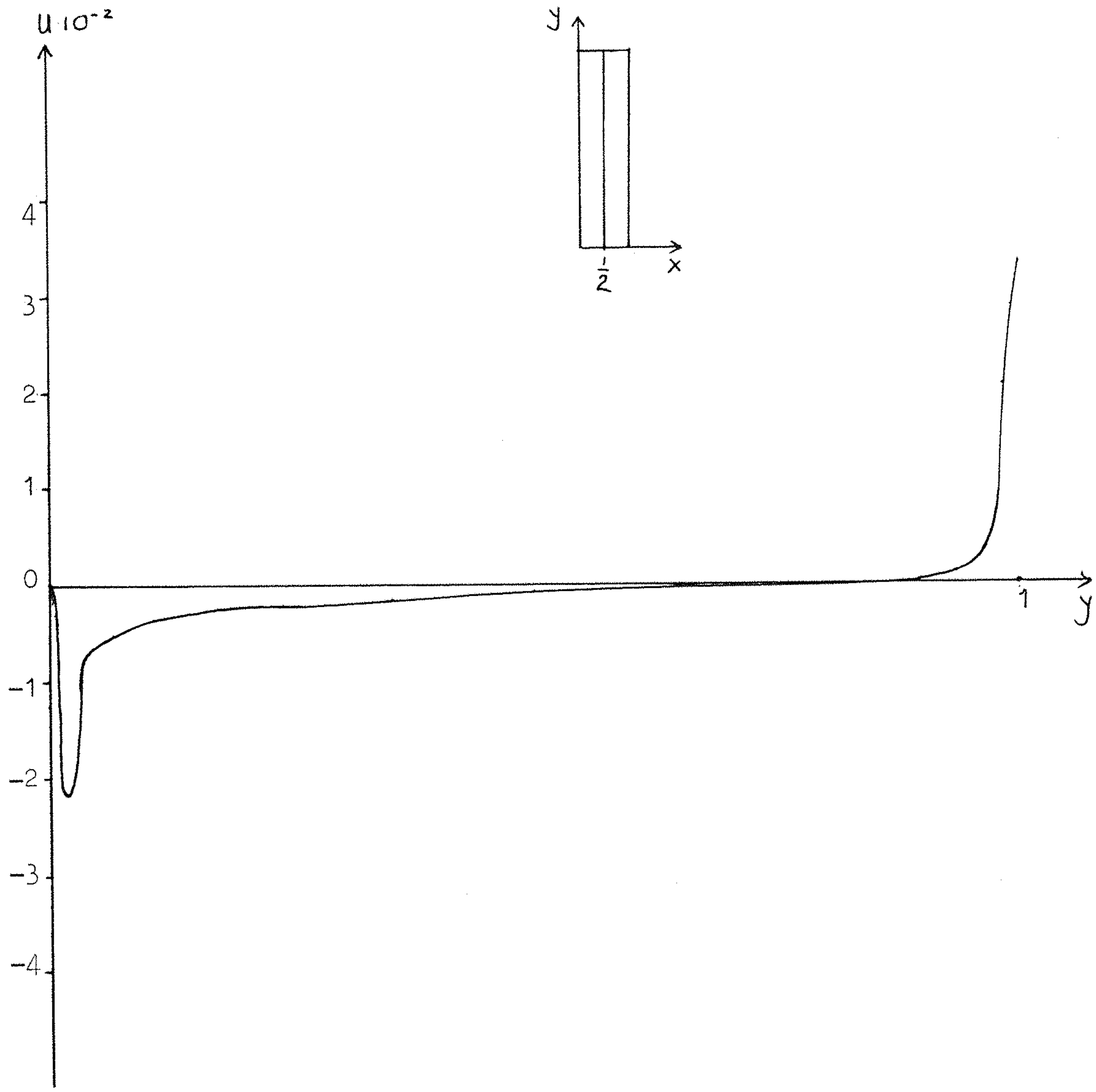

Fig. 4.4.11 Horizontal velocity profile, Gr = 10^8

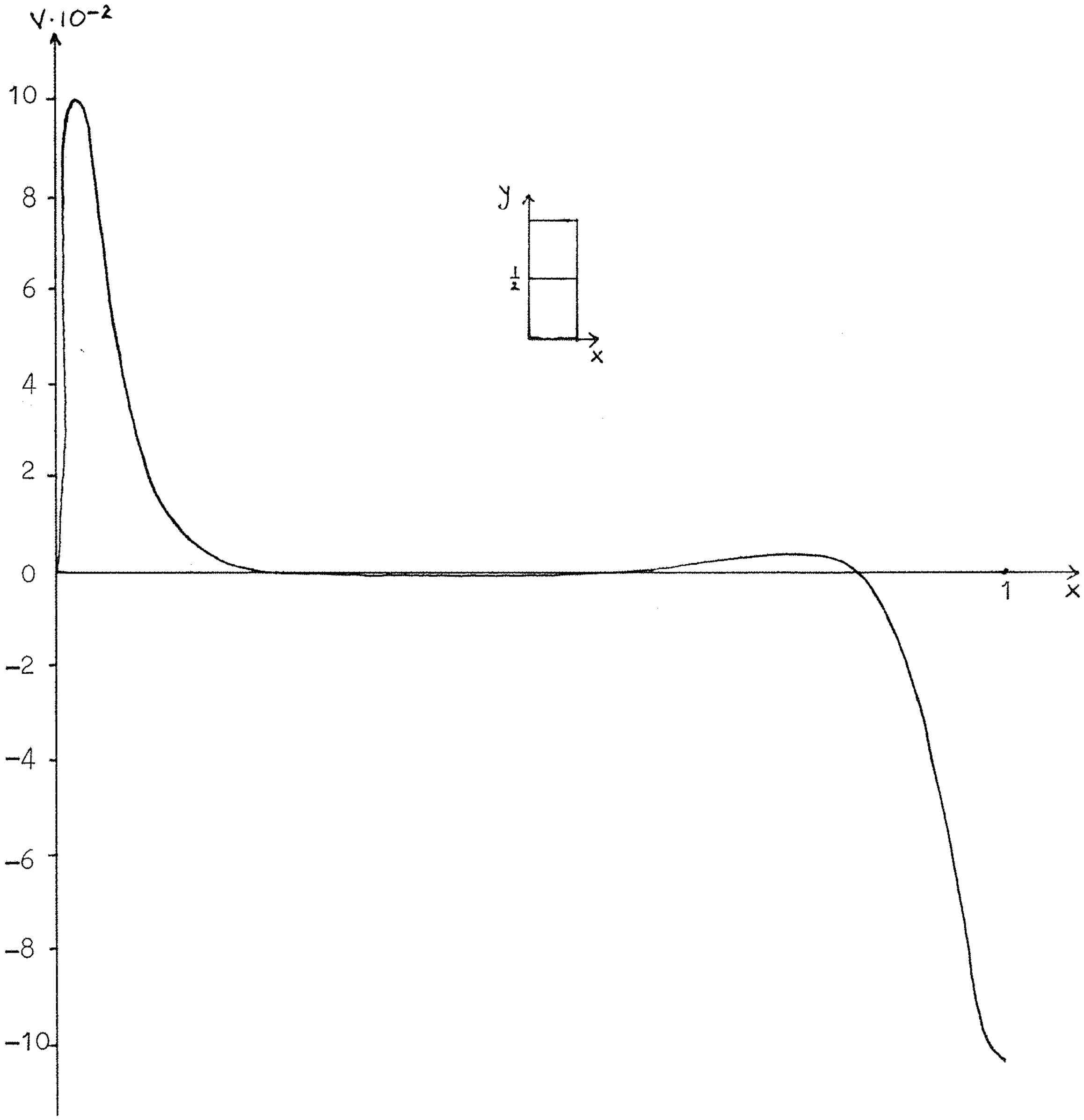

Fig. 4.4.12 Vertical velocity profile, Gr = 10^8

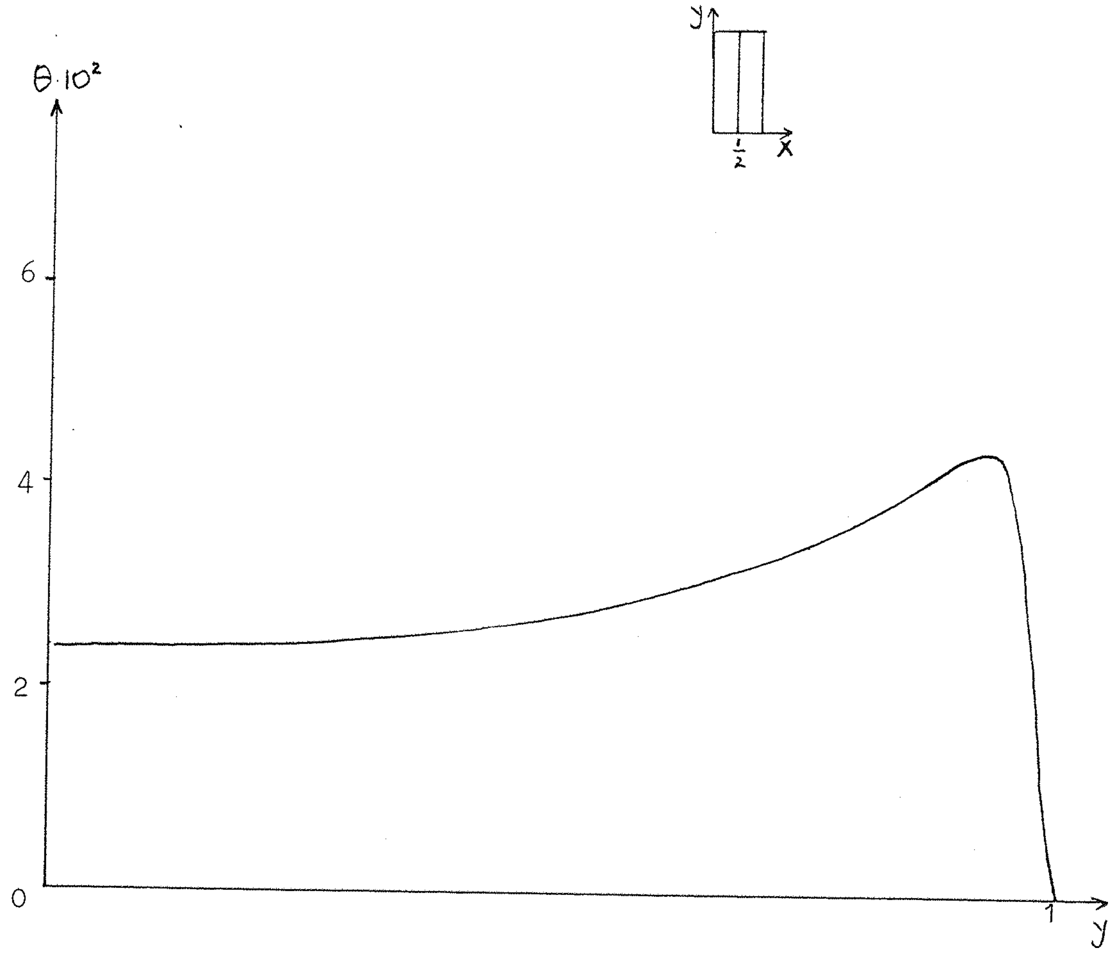

Fig. 4.4.13 Temperature profile, Gr = 10^8

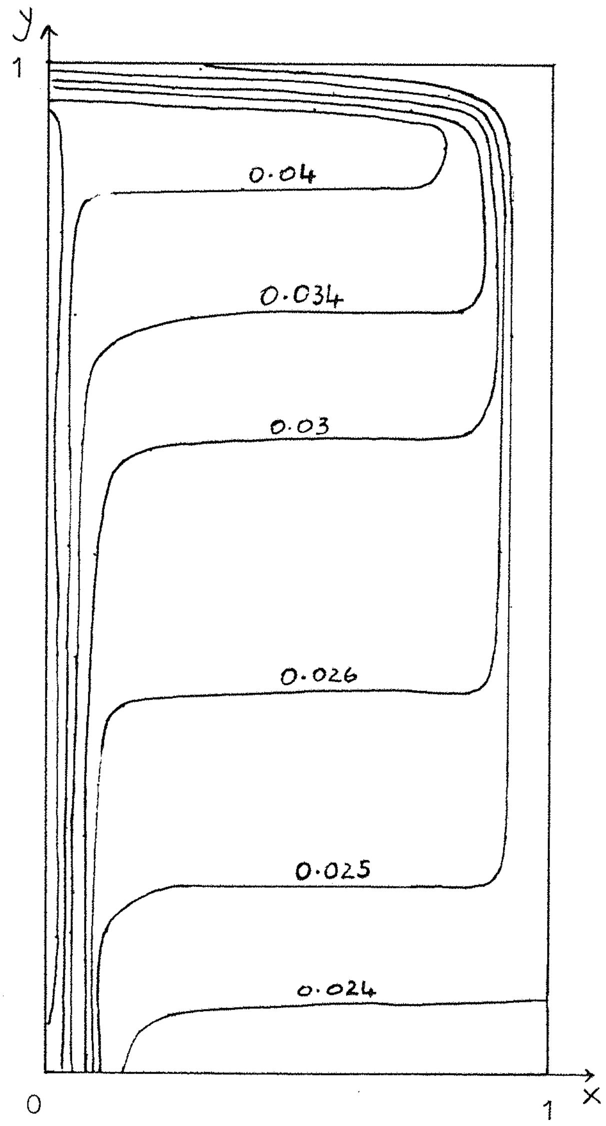

Fig. 4.4.14 Isotherms, Gr = 10^8

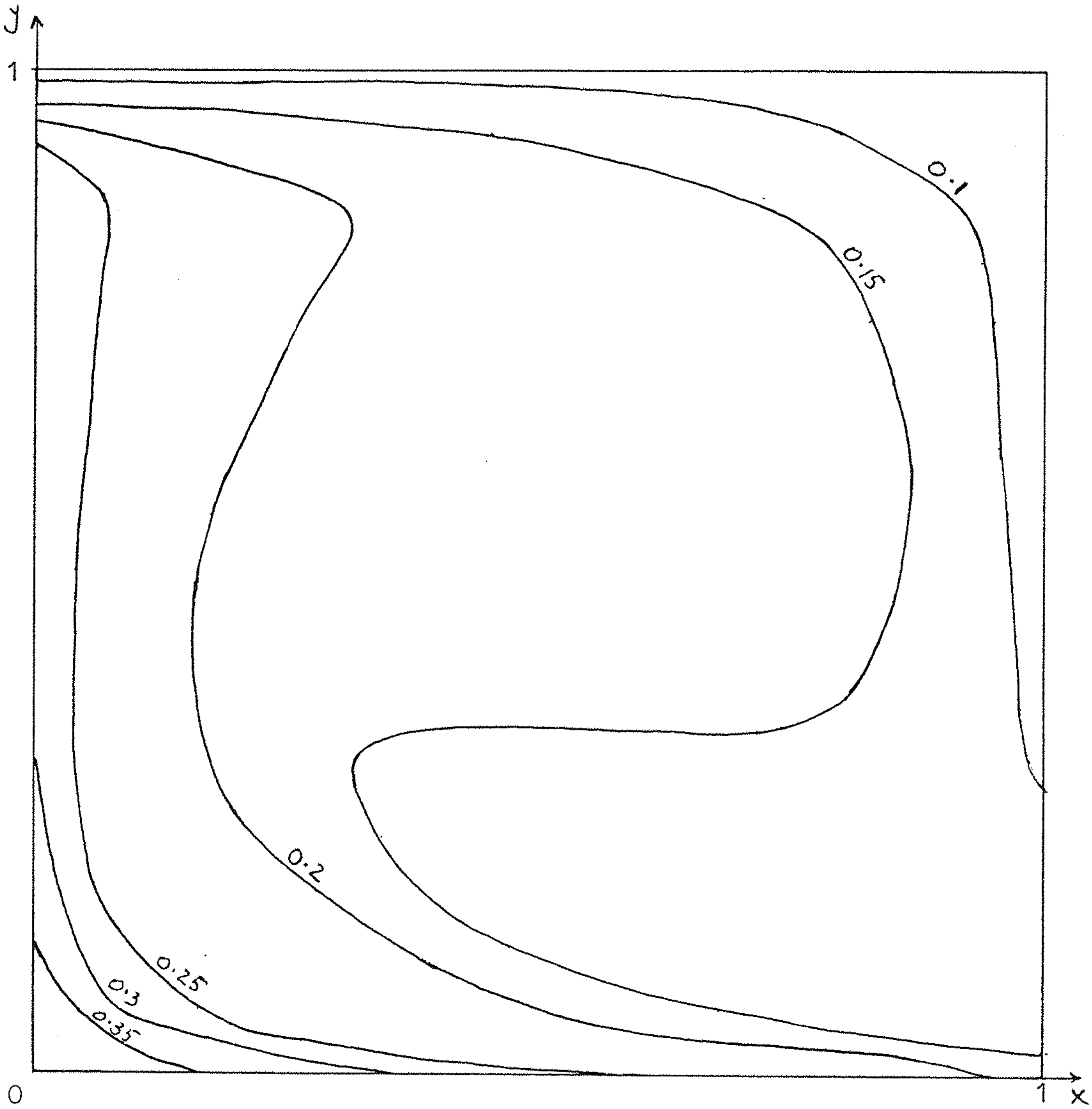

Fig. 4.4.15 Isotherms, Gr = 10^8

§ 4.5 Comparison of numerical results with experimental data

After discussing practical situations in Chapter 1, a transition was then made from the physical world to the mathematical one by constructing a mathematical model and solving the resulting equations. In order to test the usefulness of this mathematical model a comparison must be made between the numerical results and experimental data. Such a comparison is not easy to carry out, however, since as stated in the introduction experimental data on natural convection in cryogenic fluids is limited.

Experimental data on natural convection in Liquid Nitrogen (LIN) was recorded by Beresford (1984) and Scurlock et al (1984) at the Institute of Cryogenics, University of Southampton. In one experiment a Dewar flask containing LIN was subjected to a constant and uniform lateral heat flux while at the bottom a heat shield was provided by an external LIN pool. The boundary conditions and aspect ratio in this experiment correspond closely to those mentioned in subsection 3 of § 4.4, but it must be emphasized that the numerical results presented in § 4.4 refer only to Cartesian geometry whereas in the experiment a cylindrical configuration is appropriate. Fig. 4.5.1 shows the temperature profile measured by Scurlock et al (1984) along the axis of the container, while Fig. 4.5.2 shows the vertical velocity profile measured by Beresford (1984) at midheight. Qualitative agreement between Fig. 4.4.10 and Fig. 4.5.1 is evident, the most striking feature being the common thermal boundary layer at the free surface, although it should be noted that we have assumed zero evaporation in our model. Comparison of the velocity profiles in Fig. 4.4.9 and Fig. 4.5.2 also reveals qualitative agreement. Moreover, with the substitution of the figures relevant to LIN, it was found that the magnitudes of the velocities in Fig. 4.5.2 were of the same order as those obtained from our results with $Gr = 10^8$. With the aid of a Video Camera Scurlock and his co-workers also confirmed from experiments that the motion of Liquid Nitrogen was mainly confined to regions close to the boundaries while, in the core region, the liquid was essentially stagnant.

Some time ago Fan and Chu (1968) carried out a theoretical and experimental analysis of thermal stratification in closed cryogenic containers. Experimental observations suggested that lateral heat flux is responsible for creating stratification. Unfortunately, their theoretical model was not sufficiently sophisticated to enable them to predict the effect on stratification of applying a heat flux at the base of the container. Numerical results derived from our model and presented earlier in subsections 3 and 5 of § 4.4 show not only that side wall heating creates a well defined vertical stratification pattern but also that this pattern is disturbed in a major way when a heat flux is applied to the bottom. This observation could have significant implications in cryogenic engineering.

It is generally believed within the cryogenic industry that stratification leads to major problems in cryogenic storage tanks with the unavoidable influx of some heat, the temperature of the liquid at the free surface frequently rises more rapidly than that of the bulk of the liquid. Since the warmer liquid has a lower density and the liquid is a poor thermal conductor a stable stratification pattern is created, similar to that shown in Fig. 4.4.14. Since the pressure in the vapour above the liquid is determined by the temperature of the liquid surface, stratification is accompanied by a corresponding rise in vapour pressure, and the length of time that the liquid can be stored without venting vapour is greatly reduced. Vertical heat paths can be created by providing thermal conductors. Stratification can also be reduced by stirring the liquid, but carrying out this stirring in huge storage tanks may not be straightforward.

Fig. 4.4.15 showed us that almost vertical heat paths from the bottom to the top of the vessel can be created through the application of additional heating at the bottom. This process can in practice, sometimes lead to an instability, however, as the liquid becomes superheated in the lower region of the container. Ideally therefore one would like to apply heating at the base, sufficient just to disturb the stratification pattern but not so high as to cause superheating of the liquid.

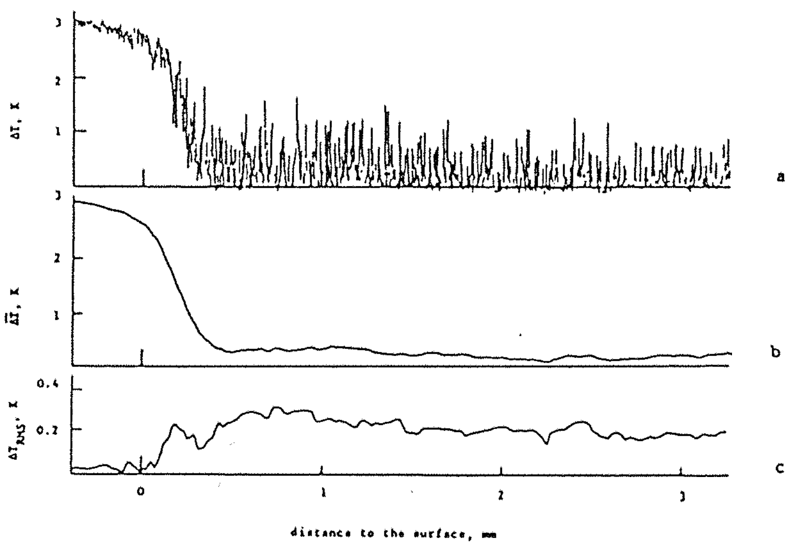

a) Temperature fluctuations ΔT = Tbulk - T
b) Moving mean of ΔT, c) RMS of ΔT

Fig. 4.5.1 Temperature profile, Scurlock et al (1984)

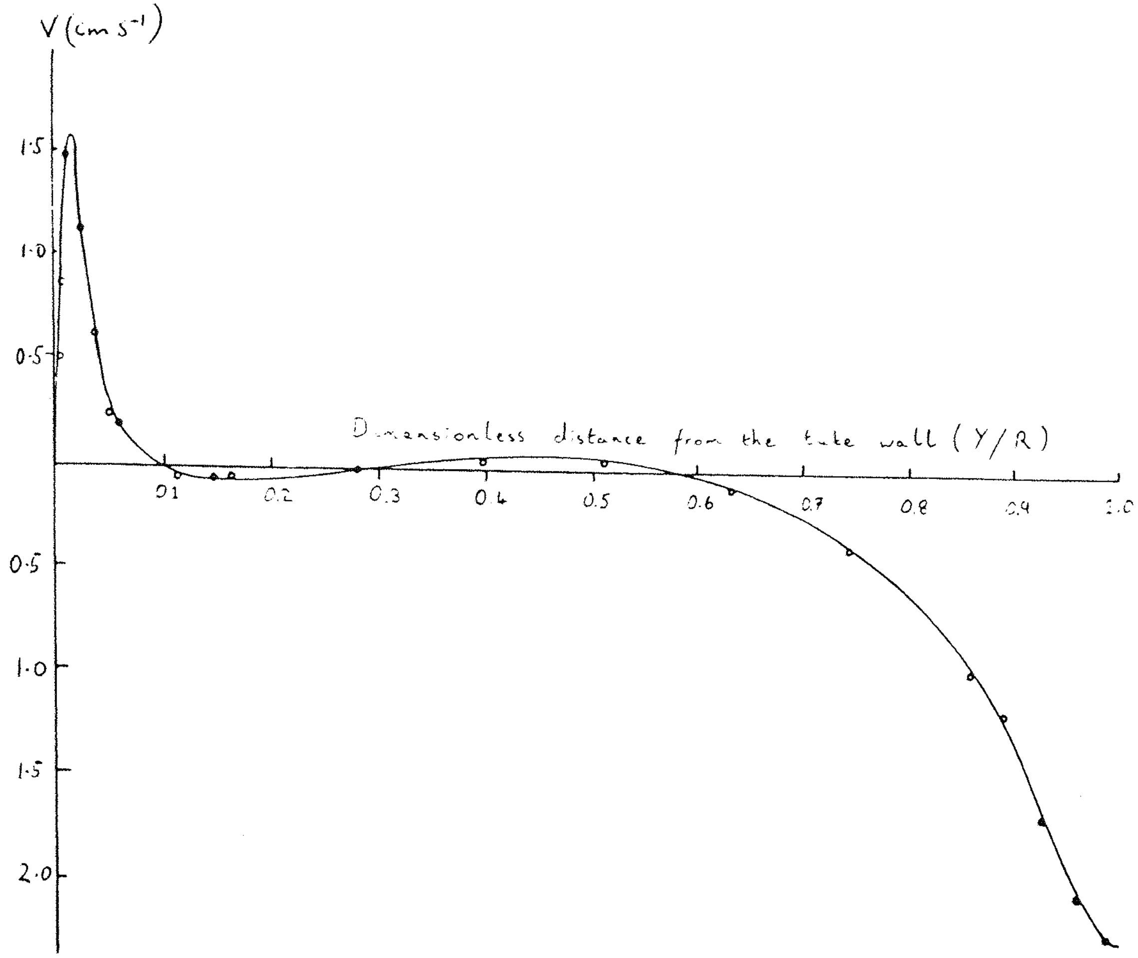

Fig. 4.5.2 Velocity profile in the liquid pool, Beresford (1984)

CHAPTER 5
NATURAL CONVECTION IN CYLINDRICAL GEOMETRY

§5.1 Choice of Coordinate axes

This chapter is devoted to the study of laminar natural convection in cryofluids in a cylindrical container subject to an influx of heat through the container's base and walls. Solutions in this geometry are important to obtain since as stated in the introduction to this thesis, cylindrical containers often arise in practice. However, Roache (1976) mentions that the solution of the transport equations in cylindrical coordinates introduces many complications and the task is far from simple. For instance, numerical instabilities often arise from singularities inherent to the equations. In this chapter we present some numerical results on a regular grid for Grashof numbers $\leqslant 10^4$.

The mathematical model considered here is the cylindrical analogue of the problem investigated in earlier chapters of this thesis. A cross-section of the cylindrical tank is shown in Fig. 5. 1.1.

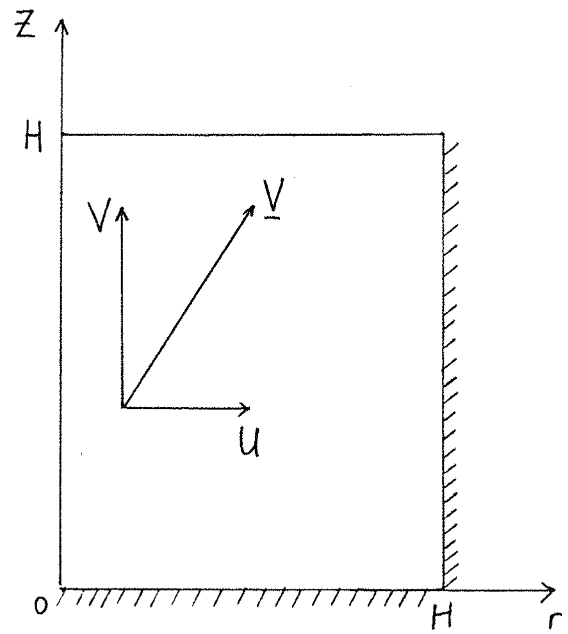

Fig. 5.1.1 Cylindrical representation

Note that in our simplified model

H is the radius of the cylinder and the height of fluid;

the base of the cylinder is represented by the axis Or ,

the axis of the cylinder lies along axis Oz ;

and $\underset{\sim}{V} = (U, V, 0)$, where U is the radial velocity and V is the axial velocity.

Our investigation of the cylindrical case is based on the same assumptions introduced in the previous two chapters. These are:-

1. The problem is axisymmetric;
2. Viscous dissipation is unimportant;
3. There are no internal heat sources;
4. The Boussinesq approximation is valid;
5. The thermal conductivity, coefficient of viscosity etc. are independent of temperature;
6. The top surface is flat and isothermal;
7. No evaporation occurs;
8. There is no shear stress at the top surface;
9. The cryogenic liquid is Newtonian.

§5.2 The governing equations and boundary conditions

The governing equations for our axisymmetric problem (see, for instance, Li·Lam, 1966) are

The radial momentum equation

$$\rho\left(\frac{\partial u}{\partial t} + u\frac{\partial u}{\partial r} + v\frac{\partial u}{\partial z}\right) = -\frac{\partial p}{\partial r} + \mu\left(\frac{\partial^2 u}{\partial z^2} - \frac{u}{r^2} + \frac{1}{r}\frac{\partial u}{\partial r} + \frac{\partial^2 u}{\partial r^2}\right) \quad (5.2.1)$$

and the axial momentum equation

$$\rho\left(\frac{\partial v}{\partial t} + u\frac{\partial v}{\partial r} + v\frac{\partial v}{\partial z}\right) = -\rho g - \frac{\partial p}{\partial z} + \mu\left(\frac{\partial^2 v}{\partial z^2} + \frac{1}{r}\frac{\partial v}{\partial r} + \frac{\partial^2 v}{\partial r^2}\right), \quad (5.2.2)$$

coupled with the energy equation

$$\frac{\partial T}{\partial t} + u\frac{\partial T}{\partial r} + v\frac{\partial T}{\partial z} = K\left(\frac{\partial^2 T}{\partial r^2} + \frac{1}{r}\frac{\partial T}{\partial r} + \frac{\partial^2 T}{\partial z^2}\right) \quad (5.2.3)$$

and the equation of continuity

$$\frac{\partial u}{\partial r} + \frac{\partial v}{\partial z} + \frac{u}{r} = 0 \ . \quad (5.2.4)$$

It should be noted that in writing the above equations some of the assumptions stated in § 5.1 have been used.

As earlier since the pressure boundary conditions are difficult to specify, we shall work with the vorticity and stream function. Differentiating (5.2.1) with respect to z and (5.2.2) with respect to r, adding both resulting equations to eliminate the pressure terms and then using equation (5.2.4) and the Boussinesq approximation we obtain

$$\frac{\partial Q}{\partial t} + U\frac{\partial Q}{\partial r} + V\frac{\partial Q}{\partial Z} =$$

$$= \nu\left(\frac{\partial^2 Q}{\partial r^2} + \frac{1}{r}\frac{\partial Q}{\partial r} + \frac{\partial^2 Q}{\partial Z^2} - \frac{Q}{r^2}\right) + \frac{UQ}{r} + g\beta\frac{\partial T}{\partial r}, \quad (5.2.5)$$

where Q, the only non-zero component of the vorticity, is defined through

$$Q = \frac{\partial V}{\partial r} - \frac{\partial U}{\partial Z} \quad , \quad (5.2.6)$$

ν is the kinematic viscosity, and β is the thermal volumetric expansion coefficient. The stream function, Ψ is defined by

$$U = -\frac{1}{r}\frac{\partial \Psi}{\partial Z} \quad ; \quad V = \frac{1}{r}\frac{\partial \Psi}{\partial r} \quad . \quad (5.2.7)$$

Equation (5.2.4) is then satisfied identically and from (5.2.6) and (5.2.7) we obtain the Poisson equation for the stream function

$$\frac{\partial^2 \Psi}{\partial r^2} - \frac{1}{r}\frac{\partial \Psi}{\partial r} + \frac{\partial^2 \Psi}{\partial Z^2} = Qr \quad . \quad (5.2.8)$$

We shall next proceed with the non-dimensionalization of the governing equations. Put

$$U^* = UH/K \quad , \quad V^* = VH/K \quad ; \quad (5.2.9)$$

$$R = \frac{r}{H} \quad , \quad Z^* = Z/H \quad , \quad \tau = tK/H^2 \quad ; \quad (5.2.10)$$

$$\Psi^* = \Psi/KH \quad , \quad Q^* = QH^2/K \quad (5.2.11)$$

and

$$\theta = T - T_0 \Big/ \frac{Q'H}{k} \quad , \quad (5.2.12)$$

where, we recall that K is thermal diffusivity, T_0 is surface temperature of the fluid and Q' is a reference heat flux. Substituting (5.2.9) - (5.2.11) into (5.2.5) we obtain the non-dimensional momentum equation

$$\frac{\partial Q^*}{\partial \tau} + U^* \frac{\partial Q^*}{\partial R} + V^* \frac{\partial Q^*}{\partial Z^*} = P_r \left(\frac{\partial^2 Q^*}{\partial R^2} + \frac{1}{R}\frac{\partial Q^*}{\partial R} + \frac{\partial^2 Q^*}{\partial Z^{*2}} - \frac{Q^*}{R^2} \right) +$$

$$+ \frac{U^* Q^*}{R} + G_r P_r^2 \frac{\partial \theta}{\partial R} , \tag{5.2.13}$$

where $P_r = \dfrac{\nu}{K}$

and $$Q^* = \frac{\partial V^*}{\partial R} - \frac{\partial U^*}{\partial Z^*} \tag{5.2.14}$$

Substituting (5.2.11) into (5.2.8) we obtain the non-dimensional Poisson equation for the stream function

$$\frac{\partial^2 \Psi^*}{\partial R^2} - \frac{1}{R}\frac{\partial \Psi^*}{\partial R} + \frac{\partial^2 \Psi^*}{\partial Z^{*2}} = Q^* R . \tag{5.2.15}$$

Likewise, we obtain the non-dimensional energy equation

$$\frac{\partial \theta}{\partial \tau} + U^* \frac{\partial \theta}{\partial R} + V^* \frac{\partial \theta}{\partial Z^*} = \frac{\partial^2 \theta}{\partial R^2} + \frac{1}{R}\frac{\partial \theta}{\partial R} + \frac{\partial^2 \theta}{\partial Z^{*2}} . \tag{5.2.16}$$

Boundary conditions

After non-dimensionalizing the variables the region in which we solve the equations is now $0 \leq R \leq 1$, $0 \leq Z^* \leq 1$. The boundaries are shown on Fig. 5.2.1.

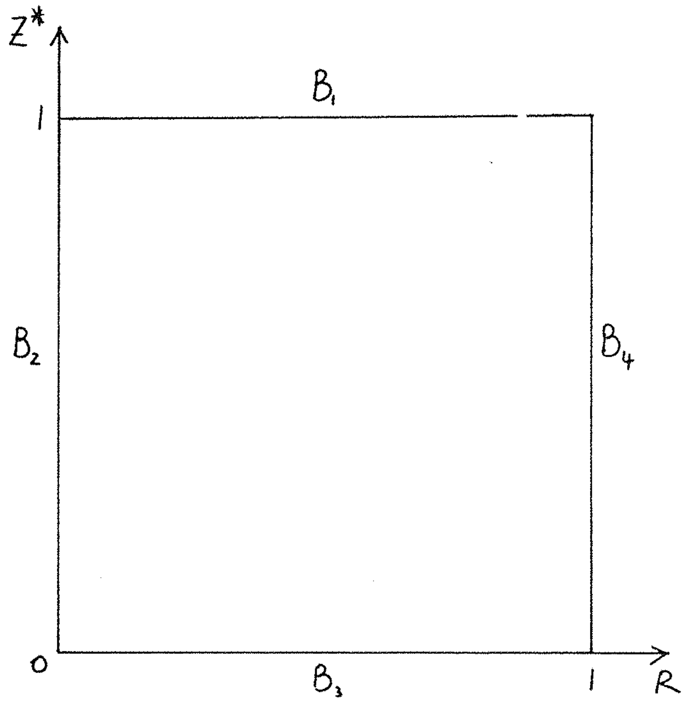

Fig. 5.2.1 Solution domain

1. On $B_1 = \{(R,1) \mid 0 \leq R \leq 1\}$, the temperature is ambient and so we require

$$\theta = 0 \quad . \tag{5.2.17}$$

The postulate of no evaporation on B_1 gives $V = 0$ which implies $V^* = 0$ and

$$\frac{\partial V^*}{\partial R} = 0 \quad . \tag{5.2.18}$$

The assumption that there is no shear stress on B_1 implies that the component

$$S_{RZ^*} = 0 \quad . \tag{5.2.19}$$

Now

$$S_{RZ^*} = \mu\left(\frac{\partial U^*}{\partial Z^*} + \frac{\partial V^*}{\partial R}\right) \qquad (5.2.20)$$

(Milne-Thomson, 1968)

and using (5.2.14), (5.2.18), (5.2.19) and (5.2.20) it then follows that

$$Q^* = 0 \quad . \qquad (5.2.21)$$

2. On the boundary $B_2 = \left\{ (0, Z^*) \,\middle|\, 0 < Z^* < 1 \right\}$, symmetry of flow implies

$$\frac{\partial T}{\partial r} = \frac{\partial V}{\partial r} = U = 0 \; . \qquad (5.2.22)$$

In non-dimensional form these requirements can be written

$$\frac{\partial \theta}{\partial R} = 0 \; , \quad \frac{\partial V^*}{\partial R} = 0 \; , \quad U^* = 0 \; . \qquad (5.2.23)$$

The last condition clearly yields

$$\frac{\partial U^*}{\partial Z^*} = 0 \quad \text{on} \quad B_2 \; . \qquad (5.2.24)$$

and equations (5.2.14), (5.2.24) and (5.2.25) then imply

$$Q^* = 0 \; . \qquad (5.2.25)$$

3. On the base B_3 , defined by $B_3 = \left\{ (R, 0) \,\middle|\, 0 \leq R \leq 1 \right\}$ the no-slip-condition implies that fluid is at rest, in which case we require

$$U^* = 0 \quad , \qquad (5.2.26)$$

$$V^* = 0 \quad . \qquad (5.2.27)$$

Using (5.2.7), (5.2.9), (5.2.10), (5.2.14) and (5.2.27) we find that the vorticity on B_3 is given by

$$Q^* = \frac{1}{R}\frac{\partial^2 \Psi^*}{\partial Z^{*2}} . \tag{5.2.28}$$

If Q_1 is the constant and uniform external heat flux at the base then, in physical variables, we have

$$\frac{\partial T}{\partial z} = -\frac{Q_1}{k} , \tag{5.2.29}$$

which in non-dimensional variables becomes

$$\frac{\partial \theta}{\partial Z^*} = -\frac{Q_1}{Q'} .$$

If we put $Q' = Q_1$, then the heat flux condition to be applied along the base is

$$\frac{\partial \theta}{\partial Z^*} = -1 . \tag{5.2.30}$$

4. Finally on the boundary $B_4 = \left\{ (1, Z^*) \mid 0 < Z^* < 1 \right\}$, the no-slip condition again implies

$$U^* = 0 , \tag{5.2.31}$$

$$V^* = 0 . \tag{5.2.32}$$

In a similar way to above we then deduce that the vorticity on B_4 satisfies

$$Q^* = \frac{\partial^2 \Psi^*}{\partial R^2} . \tag{5.2.33}$$

If Q_2 is the external heat flux then, in non-dimensional terms, we require

$$\frac{\partial \theta}{\partial R} = \frac{Q_2}{Q_1} . \tag{5.2.34}$$

The boundaries B_1 , B_2 , B_3 and B_4 are all streamlines that intersect, so on all boundaries we put

$$\Psi^* = 0 \quad . \tag{5.2.35}$$

In addition (5.2.26) and (5.2.32) imply that

$$\frac{\partial \Psi^*}{\partial Z^*} = 0 \quad \text{on} \quad B_3 \quad , \tag{5.2.36}$$

$$\frac{\partial \Psi^*}{\partial R} = 0 \quad \text{on} \quad B_4 \quad . \tag{5.2.37}$$

Finally, from (5.2.23),

$$\frac{\partial \Psi^*}{\partial Z^*} = 0 \tag{5.2.38}$$

and, with the aid of L'Hopital's Rule, it is clear that $U^* \to 0$ as $R \to 0$ only if

$$\frac{\partial^2 \Psi^*}{\partial R \partial Z^*} = 0 \quad \text{on} \quad B_2 \quad . \tag{5.2.39}$$

For convenience the stars on the non-dimensional quantities are now omitted and the governing system of equations plus the boundary and initial conditions can therefore be written:

$$\frac{\partial Q}{\partial \tau} + U\frac{\partial Q}{\partial R} + V\frac{\partial Q}{\partial Z} = P_r\left(\nabla^2 Q - \frac{Q}{R^2}\right) + \frac{UQ}{R} + G_r P_r^2 \frac{\partial \theta}{\partial R} \quad , \tag{5.2.40}$$

$$\frac{\partial \theta}{\partial \tau} + U\frac{\partial \theta}{\partial R} + V\frac{\partial \theta}{\partial Z} = \nabla^2 \theta \quad , \tag{5.2.41}$$

$$\frac{\partial^2 \Psi}{\partial R^2} - \frac{1}{R}\frac{\partial \Psi}{\partial R} + \frac{\partial^2 \Psi}{\partial Z^2} = QR \quad , \tag{5.2.42}$$

where

$$\nabla^2 = \frac{\partial^2}{\partial R^2} + \frac{1}{R}\frac{\partial}{\partial R} + \frac{\partial^2}{\partial Z^2} \quad . \tag{5.2.43}$$

Boundary conditions

1. On $\{(R,1) \mid 0 \le R \le 1\}$:

$$\Theta = 0, \ \Psi = 0, \ Q = 0 .$$

2. On $\{(0,Z) \mid 0 < Z < 1\}$:

$$\frac{\partial \Theta}{\partial R} = 0, \quad \Psi = 0, \quad \frac{\partial^2 \Psi}{\partial R \partial Z} = 0, \quad Q = 0 .$$

3. On $\{(R,0) \mid 0 \le R \le 1\}$:

$$\frac{\partial \Theta}{\partial Z} = -1, \quad \Psi = 0, \quad \frac{\partial \Psi}{\partial Z} = 0, \quad Q = \frac{1}{R}\frac{\partial^2 \Psi}{\partial Z^2} .$$

4. On $\{(1,Z) \mid 0 < Z < 1\}$:

$$\frac{\partial \Theta}{\partial R} = \frac{Q_2}{Q_1}, \quad \Psi = 0, \quad \frac{\partial \Psi}{\partial R} = 0, \quad Q = \frac{\partial^2 \Psi}{\partial R^2} .$$

For the initial conditions we use simply

$$\Psi = 0, \ Q = 0, \ \Theta = 0 \ \text{in} \ \{(R,Z) \mid 0 \le R \le 1, \ 0 \le Z \le 1\} .$$

§5.3 Numerical method

The numerical method is based on finite differences introduced in §3.2. The continuous region, over which the governing equations are defined, is discretized as follows:

$$\bar{\Omega} = \left\{ (R_i, Z_j) \;,\; R_i = (i-1)h \;,\; Z_j = (j-1)h \;\middle|\; i = 1,2,\dots,N \;;\; j = 1,2,\dots,N \right\}, \quad (5.3.1)$$

with Ω defined by

$$\Omega = \left\{ (R_i, Z_j) \;,\; R_i = (i-1)h \;,\; Z_j = (j-1)h \;\middle|\; i = 2,3,\dots,N-1 \;;\; j = 2,3,\dots,N-1 \right\}, \quad (5.3.2)$$

where $\quad h = 1/(N-1)$

Comparison of the system summarised at the end of §5.2 with the corresponding Cartesian system reveals close similarities and therefore the numerical procedure adopted here is basically the same as the one used for the Cartesian case described earlier. Thus the transport equations are solved by an ADI scheme and the Poisson equation is solved by the Block Cyclic Reduction method. The non-linear convection terms in the momentum equation are approximated by second upwind differencing scheme.

Due to the presence of the '$\frac{1}{R}$' and '$\frac{1}{R^2}$' terms in the governing equations, numerical methods are strongly prone to instabilities, especially near $R = 0$. In this section we confine attention to a regular grid which proves more stable, but the omission of scaling in the R direction does mean diminished accuracy in the solutions near $R = 0$ and $R = 1$.

1. Solution of transport equations

In view of the similarity of the numerical procedures, the algebra discussed in the derivation of the finite difference equations (FDE) in § 3.4 will not be repeated. We shall move directly to the final form of the FDE's, bearing in mind that here $A_x = 1,\ B_x = 0$. In updating the solution from time level n to time level $(n+\frac{1}{2})$, we have the following FDE

$$R^n_{i,j}\,\Gamma^{n+\frac{1}{2}}_{i-1,j} + S^n_{i,j}\,\Gamma^{n+\frac{1}{2}}_{i,j} + T^n_{i,j}\,\Gamma^{n+\frac{1}{2}}_{i+1,j} = U^n_{i,j}\ , \qquad (5.3.3)$$

where

$$R^n_{i,j} = -\left(U^n_L + |U^n_L|\right)\Big/4h - \alpha\left(\frac{1}{h^2} - \frac{1}{2hR_i}\right)\ , \qquad (5.3.4)$$

$$S^n_{i,j} = \frac{2}{\lambda\Delta\tau} + \frac{1}{4h}\left(U^n_R + |U^n_R| - U^n_L + |U^n_L|\right) + \frac{2\alpha}{h^2} + \delta^n_{i,j}\ , \qquad (5.3.5)$$

$$T^n_{i,j} = \frac{U^n_R - |U^n_R|}{4h} - \alpha\left(\frac{1}{h^2} + \frac{1}{2hR_i}\right) \qquad (5.3.6)$$

and

$$U^n_{i,j} = \Gamma^n_{i,j+1}\left(\frac{|V^n_R| - V^n_R}{4h} + \frac{\alpha}{h^2}\right) + \Gamma^n_{i,j}\left[\frac{2}{\lambda\Delta\tau} - \left(\frac{V^n_R + |V^n_R| - V^n_L + |V^n_L|}{4h}\right) - \frac{2\alpha}{h^2}\right] + \Gamma^n_{i,j-1}\left(\frac{V^n_L + |V^n_L|}{4h} + \frac{\alpha}{h^2}\right) + Gr\,P_r^2\big/2h\left(\theta^n_{i+1,j} - \theta^n_{i-1,j}\right), \qquad (5.3.7)$$

where α , λ and Γ are defined as in the Cartesian analysis.

In (5.3.5),

$$\delta_{i,j} = \frac{1}{R_i^2}\left(P_r + \frac{\Psi_{i,j+1} - \Psi_{i,j-1}}{2h}\right) \qquad (5.3.8)$$

for the momentum equation and $\delta_{i,j} = 0$ for the energy equation.

In proceeding to time level ($n+1$) from time ($n+\frac{1}{2}$) the FDE are

$$R_{i,j}^{n+\frac{1}{2}} \Gamma_{i,j-1}^{n+1} + S_{i,j}^{n+\frac{1}{2}} \Gamma_{i,j}^{n+1} + T_{i,j}^{n+\frac{1}{2}} \Gamma_{i,j+1}^{n+1} = U_{i,j}^{n+\frac{1}{2}}, \quad (5.3.9)$$

where

$$R_{i,j}^{n+\frac{1}{2}} = \frac{-\left(V_L^{n+\frac{1}{2}} + \left|V_L^{n+\frac{1}{2}}\right|\right)}{4h} - \frac{\alpha}{h^2} \quad , \quad (5.3.10)$$

$$S_{i,j}^{n+\frac{1}{2}} = \frac{\left(V_R^{n+\frac{1}{2}} + \left|V_R^{n+\frac{1}{2}}\right| - V_L^{n+\frac{1}{2}} + \left|V_L^{n+\frac{1}{2}}\right|\right)}{4h} + 2\left(\frac{1}{\Delta t} + \frac{\alpha}{h^2}\right) + \delta_{i,j}^{n+\frac{1}{2}} \quad , (5.3.11)$$

$$T_{i,j}^{n+\frac{1}{2}} = \frac{V_R^{n+\frac{1}{2}} - \left|V_R^{n+\frac{1}{2}}\right|}{4h} - \frac{\alpha}{h^2} \quad (5.3.12)$$

and

$$U_{i,j}^{n+\frac{1}{2}} = \Gamma_{i+1,j}^{n+\frac{1}{2}} \left[\frac{\left(\left|U_R^{n+\frac{1}{2}}\right| - U_R^{n+\frac{1}{2}}\right)}{4h} + \alpha\left(\frac{1}{h^2} + \frac{1}{2hR_i}\right)\right] +$$

$$+ \Gamma_{i,j}^{n+\frac{1}{2}} \left[- \frac{\left(U_R^{n+\frac{1}{2}} + \left|U_R^{n+\frac{1}{2}}\right| - U_L^{n+\frac{1}{2}} + \left|U_L^{n+\frac{1}{2}}\right|\right)}{4h} + 2\left(\frac{1}{\Delta t} - \frac{\alpha}{h^2}\right)\right] +$$

$$+ \Gamma_{i-1,j}^{n+\frac{1}{2}} \left[\frac{U_L^{n+\frac{1}{2}} + \left|U_L^{n+\frac{1}{2}}\right|}{4h} + \alpha\left(\frac{1}{h^2} - \frac{1}{2hR_i}\right)\right] + \frac{G_r P_r^2}{2h}\left(\theta_{i+1,j}^{n+\frac{1}{2}} - \theta_{i-1,j}^{n+\frac{1}{2}}\right) . \quad (5.3.13)$$

With the use of the non-dimensional analogue of expression (5.2.7), the formulae expressing U_L^n , U_R^n , V_L^n and V_R^n in terms of ψ^n are determined by approximating the derivatives by central differences.

2. Boundary conditions in finite difference form.

(i) At the node points $\left\{ (R_i, 1) , R_i = (i-1)h \,\middle|\, i = 1, 2, \ldots, N \right\}$, we impose the conditions

$$\theta_{i,N}^{n+\frac{1}{2}} = 0 \quad (5.3.14)$$

$$\Psi_{i,N}^{n+\frac{1}{2}} = 0 \ , \tag{5.3.15}$$

$$Q_{i,N}^{n+\frac{1}{2}} = 0 \ . \tag{5.3.16}$$

(ii) At the nodes $\left\{ (0, z_j),\ z_j = (j-1)h \,\middle|\, j = 2,3,\ldots,N-1 \right\}$, the boundary conditions take the form

$$\Psi_{1,j}^{n} = Q_{1,j}^{n} = 0 \ . \tag{5.3.17}$$

As in the Cartesian case, an expression for the temperature condition is obtained by parabolic approximation, yielding

$$\theta_{1,j}^{n} = \frac{4}{3}\,\theta_{2,j}^{n} - \frac{1}{3}\,\theta_{3,j}^{n} \ . \tag{5.3.18}$$

(iii) At the nodes $\left\{ (R_i, 0),\ R_i = (i-1)h \,\middle|\, i = 1,2\ldots, N \right\}$, we can immediately apply

$$\Psi_{i,1}^{n} = 0 \ . \tag{5.3.19}$$

Using a Taylor's series expansion for Ψ we can obtain the expression for the vorticity:

$$Q_{i,1}^{n+\frac{1}{2}} = \frac{2\,\Psi_{i,2}^{n}}{R_i\, h^2} + o(h) \ . \tag{5.3.20}$$

The temperature condition, again obtained by parabolic interpolation, is found to be

$$\theta_{i,1}^{n} = \frac{4}{3}\,\theta_{i,2}^{n} - \frac{1}{3}\,\theta_{i,3}^{n} + \frac{2}{3}h \ . \tag{5.3.21}$$

(iv) At the nodes $\left\{ (1, z_j),\ z_j = (j-1)h \,\middle|\, j = 2,3,\ldots,N-1 \right\}$, we have

$$\Psi_{N,j}^{n} = 0 \ . \tag{5.3.22}$$

As in (iii), an expression for the wall vorticity is obtained through

$$Q_{N,j}^{n+\frac{1}{2}} = \frac{2\,\Psi_{N-1,j}^{n}}{h^2} + o(h) \qquad (5.3.23)$$

and the temperature condition leads to the formula

$$\theta_{N,j}^{n} = \theta_{N-1,j}^{n}\,C_1 + \theta_{N-2,j}^{n}\,C_2 + C_3\,, \qquad (5.3.4)$$

where

$$C_1 = 4/3\,, \qquad (5.3.25)$$

$$C_2 = -1/3 \qquad (5.3.26)$$

and

$$C_3 = \frac{2h}{3}\,\frac{Q_2}{Q_1}\,. \qquad (5.3.27)$$

3. Construction of tridiagonal matrices

The construction of the solution matrices is dealt with along the same lines as in § 3.6 .

Calculating quantities at time level ($n+\frac{1}{2}$) the system of equations (5.3.3) can be written as the matrix equation

$$A\,\underline{\Gamma} = \underline{B}\,. \qquad (5.3.28)$$

In particular, the momentum equations yield

$$A_Q\,\underline{Q} = \underline{B_Q}\,, \qquad (5.3.29)$$

where

$$A_Q = \begin{pmatrix} S^n_{2,j} & T^n_{2,j} & 0 & \cdots & 0 \\ R^n_{3,j} & & & \ddots & \vdots \\ & & \ddots & & 0 \\ 0 & & \ddots & & T^n_{N-2,j} \\ \vdots & \ddots & & & \\ 0 & \cdots & 0 & R^n_{N-1,j} & S^n_{N-1,j} \end{pmatrix}, \tag{5.3.30}$$

$$B_Q = \begin{pmatrix} U^n_{2,j} \\ U^n_{3,j} \\ \vdots \\ U^n_{N-1,j} - T^n_{N-1,j} \dfrac{2\Psi^n_{N-1,j}}{h^2} \end{pmatrix} \tag{5.3.31}$$

and the energy equations lead to

$$A_\theta \underline{\theta} = \underline{B_\theta} \quad , \tag{5.3.32}$$

where

$$A_\theta = \begin{bmatrix} \left(S^n_{2,j} + \frac{4}{3} R^n_{2,j}\right) & \left(T^n_{2,j} - \frac{1}{3} R^n_{2,j}\right) & 0 & \cdots & 0 \\ R^n_{3,j} & & & \ddots & \vdots \\ 0 & & \ddots & \ddots & 0 \\ \vdots & \ddots & \ddots & & T^n_{N-2,j} \\ 0 & \cdots & 0 & \left(R^n_{N-1,j} + T^n_{N-1,j} C_2\right) & \left(S^n_{N-1,j} + T^n_{N-1,j} C_1\right) \end{bmatrix}, \tag{5.3.33}$$

C_1 and C_2 being defined through (5.3.25) and (5.3.36) respectively and

$$\underline{B_\theta} = \begin{pmatrix} U^n_{2,j} \\ U^n_{3,j} \\ \vdots \\ U^n_{N-1,j} - T^n_{N-1,j} C_3 \end{pmatrix}, \tag{5.3.34}$$

C_3 being defined through (5.3.27).

In proceeding to the next half time level equations (5.3.9) again yield system (5.3.28),

where now

$$A_Q = \begin{pmatrix} S^{n+\frac{1}{2}}_{i,2} & T^{n+\frac{1}{2}}_{i,2} & 0 & \cdots & 0 \\ R^{n+\frac{1}{2}}_{i,3} & & & \ddots & \vdots \\ 0 & & \ddots & & 0 \\ \vdots & \ddots & & & T^{n+\frac{1}{2}}_{i,N-1} \\ 0 & \cdots & 0 & R^{n+\frac{1}{2}}_{i,N-1} & S^{n+\frac{1}{2}}_{i,N-1} \end{pmatrix}, \tag{5.3.35}$$

$$B_Q = \begin{pmatrix} U^{n+\frac{1}{2}}_{i,2} - R^{n+\frac{1}{2}}_{i,2}\, Q^{n+\frac{1}{2}}_{i,1} \\ U^{n+\frac{1}{2}}_{i,3} \\ \vdots \\ U^{n+\frac{1}{2}}_{i,N-1} \end{pmatrix} \tag{5.3.36}$$

and

$$A_\theta = \begin{bmatrix} \left(S^{n+\frac{1}{2}}_{i,2} + \frac{4}{3} R^{n+\frac{1}{2}}_{i,2}\right) & \left(T^{n+\frac{1}{2}}_{i,2} - \frac{1}{3} R^{n+\frac{1}{2}}_{i,2}\right) & 0 & \cdots & 0 \\ R^{n+\frac{1}{2}}_{i,3} & & & \ddots & \vdots \\ 0 & & \ddots & & 0 \\ \vdots & \ddots & & & T^{n+\frac{1}{2}}_{i,N-2} \\ 0 & \cdots & 0 & R^{n+\frac{1}{2}}_{i,N-1} & S^{n+\frac{1}{2}}_{i,N-1} \end{bmatrix}, \tag{5.3.37}$$

$$B_\theta = \begin{pmatrix} U_{i,2}^{n+\frac{1}{2}} - R_{i,2}^{n+\frac{1}{2}} \frac{2h}{3} \\ U_{i,3}^{n+\frac{1}{2}} \\ \vdots \\ U_{i,N-1}^{n+\frac{1}{2}} \end{pmatrix} . \qquad (5.3.38)$$

The solutions of the matrix equation (5.3.28) for all the various cases is obtained by applying the Crout Decomposition method given in §3.6.

4. Solution of Poisson Equation

This subsection deals with the solution of equation (5.2.43) by the Block Cyclic Reduction Method which was elaborated in §3.7. By approximating the derivatives in (5.2.42) by finite difference formulae we obtain the following finite difference equation

$$a_i \Psi_{i-1,j} - 4\Psi_{i,j} + c_i \Psi_{i+1,j} + \Psi_{i,j-1} + \Psi_{i,j+1} = QH_{i,j}, \qquad (5.3.39)$$

$$i,j = 2, 3, \ldots, N-1$$

where

$$a_i = 1 + \frac{1}{2(i-1)} , \qquad (5.3.40)$$

$$c_i = 1 - \frac{1}{2(i-1)} , \qquad (5.3.41)$$

$$QH_{i,j} = Q_{i,j}(i-1)h^3 .$$

Following the same discussion given in §3.7, we find that equation (5.3.39) is equivalent to the block matrix equation

$$M\underline{X} = \underline{Y} , \qquad (5.3.42)$$

where

$$\underline{X} = \begin{pmatrix} \Psi_2 \\ \Psi_3 \\ \vdots \\ \Psi_{N-1} \end{pmatrix} , \quad \underline{Y} = \begin{pmatrix} QH_2 \\ QH_3 \\ \vdots \\ QH_{N-1} \end{pmatrix} ,$$

with
$$\Psi_j = \begin{pmatrix} \Psi_{2,j} \\ \Psi_{3,j} \\ \vdots \\ \Psi_{N-1,j} \end{pmatrix}, \quad QH_j = \begin{pmatrix} QH_{2,j} \\ QH_{3,j} \\ \vdots \\ QH_{N-1,j} \end{pmatrix}, \; j = 2,3,\ldots,N-1$$

and
$$M = \begin{pmatrix} A & I & 0 & \cdots & 0 \\ I & A & I & \ddots & 0 \\ 0 & \ddots & \ddots & \ddots & I \\ \vdots & \ddots & & & \\ 0 & \cdots & 0 & I & A \end{pmatrix}. \tag{5.3.43}$$

In (5.3.43)
$$A = \begin{pmatrix} -4 & c_2 & 0 & \cdots & 0 \\ a_3 & -4 & & \ddots & \vdots \\ 0 & & \ddots & \ddots & 0 \\ \vdots & \ddots & \ddots & & c_{N-2} \\ 0 & \cdots & 0 & a_{N-1} & -4 \end{pmatrix}. \tag{5.3.44}$$

The solution of system (5.3.42) is obtained by exactly the same method as was described in § 3.7.

§ 5.4 Numerical results

The program for the axisymmetric case was run on a (17 x 17) mesh with a Prandtl number equal to unity. A constant time step satisfying the Courant-Fredericks-Lewy condition (see § 4.1) was used. Thus, the computational procedure was identical to the one described in § 4.2 except for the calculation of the time step at each half time level.

Tests for both the heat and mass balances were used to check whether steady state was reached, but since we are now in a different geometry the formulae used vary somewhat from those given in § 4.4. For a global balance of heat we now have

$$\overline{Q}_1 \text{ x Area of base} + \overline{Q}_2 \text{ x Surface area of cylinder} =$$

$$= -\int_0^1 2\pi R \left(\frac{\partial\theta}{\partial Z}\right)_{Z=1} dR \ ,$$

yielding

$$\overline{Q}_1/2 + \overline{Q}_2 = -\int_0^1 \frac{\partial\theta}{\partial Z}\bigg|_{Z=1} R\, dR \ , \qquad (5.4.1)$$

where (referring to the non dimensional cavity)

$\overline{Q}_1$ is the heat flux at the base,

$\overline{Q}_2$ is the heat flux through the side of the cylindrical cavity.

Using a parabolic distribution for θ close to the top surface, and with the aid of the boundary condition there the right hand side of (5.4.1) was then evaluated using the trapezoidal rule. Unlike the Cartesian problem, the mass balance analysis involving the axial velocity V is now evaluated on an arbitrary disc D parallel to the base,
where

$$D = \left\{ (R, Z) \middle| \ 0 \le R \le 1, \ Z = h_1 \right\} \ . \qquad (5.4.2)$$

In the steady state the total mass flow through D must be zero, which yields

$$\int_0^1 \rho\left(V(R)\,2\pi R\right) dR = 0 \; . \qquad (5.4.3)$$

A corresponding expression for mass balance in terms of the radial velocity can also be found.

The integral on the left hand side of (5.4.3) was calculated for several values of h_1 , and in all cases was close to zero. Much the same accuracy was achieved for the mass balance in the radial direction. Calculation of both sides of equation (5.4.1), however, revealed errors of up to 5% (see § 4.5 for percentage meaning), higher than the corresponding comparisons for the Cartesian case. This decrease in accuracy is perhaps to be expected since the axisymmetric program proved much less stable than the corresponding Cartesian one. In fact, due to instabilities it was not possible to obtain a solution for the axisymmetric problem for Gr $> 10^4$.

Numerical results in the axisymmetric case are presented here for Gr = 10^4, with both the aspect ratio γ and the ratio of the lateral heat flux to the one from bottom (Q_2/Q_1) equal to unity. The streamline pattern in Fig. 5.4.1 reveals a single plane vortex, almost identical to the corresponding pattern in Cartesian geometry (see Fig. 4.4.1). The vortex in Fig. 5.4.1 is generated by a negative temperature gradient relative to $-R$, thus producing an anti-clockwise flow as indicated.

The axial velocity profile plotted in Fig. 5.4.2 is the one occurring at midheight of the cylinder. At first sight this profile seems to violate conservation of mass, but if one recalls that in this geometry the same velocity profile is valid for all values of φ ($0 \leq \varphi < 2\pi$) then rotation of the region about the axis of the cylinder results in the appearance of a scaling factor R (see equation (5.4.3)).

In this chapter no coordinate transformation is made and, therefore, the boundary layers in Fig.'s 5.4.2 and 5.4.3 are likely to be less accurate. However, for Gr = 10^4 these boundary layers are comparatively thick and the loss in accuracy is not significant. Apart from the changes introduced in the axial velocity due to difference in geometry, the results are qualitatively similar to the corresponding Cartesian ones. The dominant features of the flow remain the downward jet near the axis of symmetry, the linearity of the axial velocity in the core region and the thermal boundary layer at the top surface. The low Grashof number implies minimal convective effects, as confirmed by the relatively low velocities in Fig. 5.4.2, and the θ -plot in Fig. 5.4.3 also indicates that most heat transfer is by conduction and not convection.

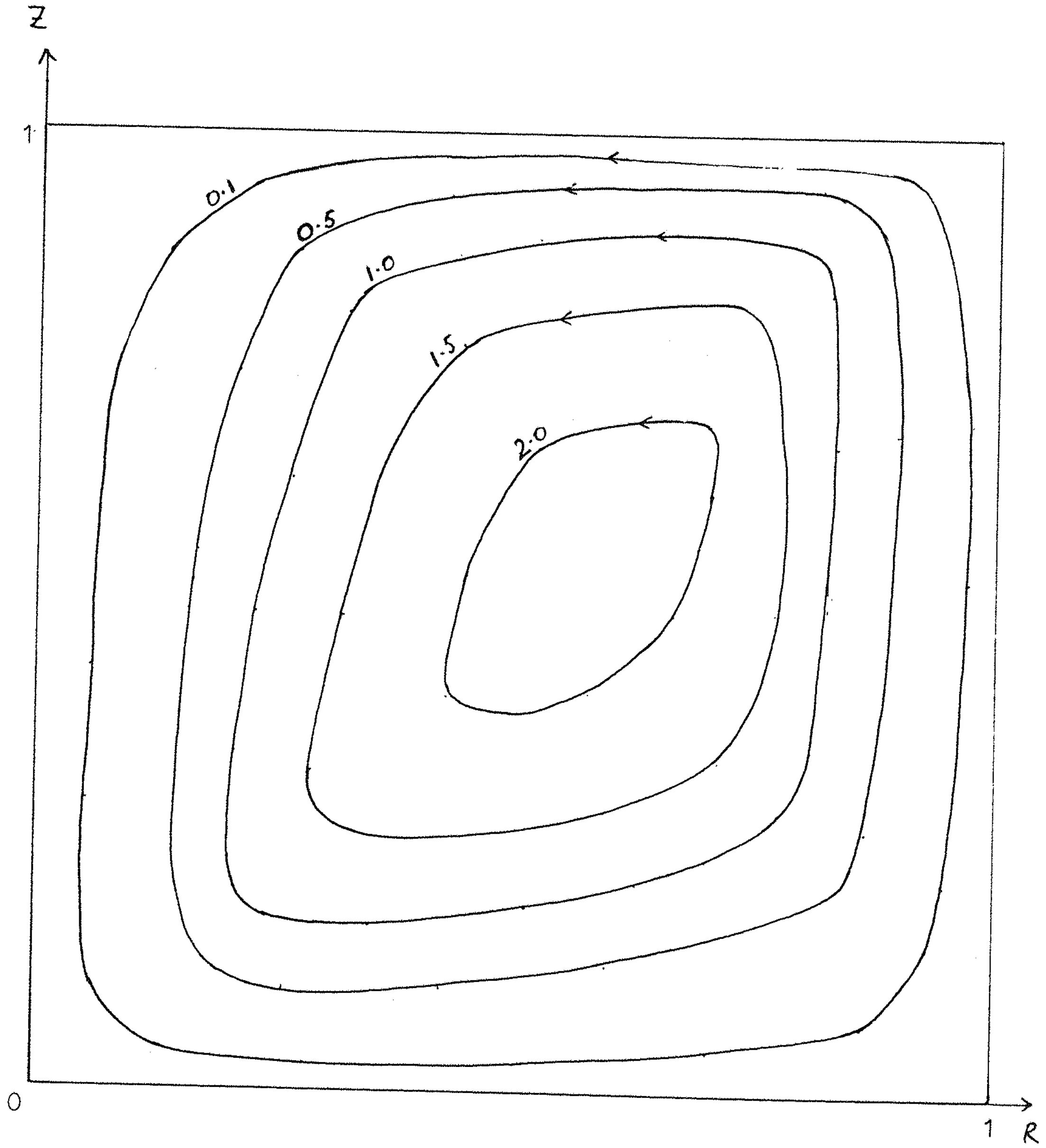

Fig. 5.4.1 Streamline pattern, Gr = 10^4

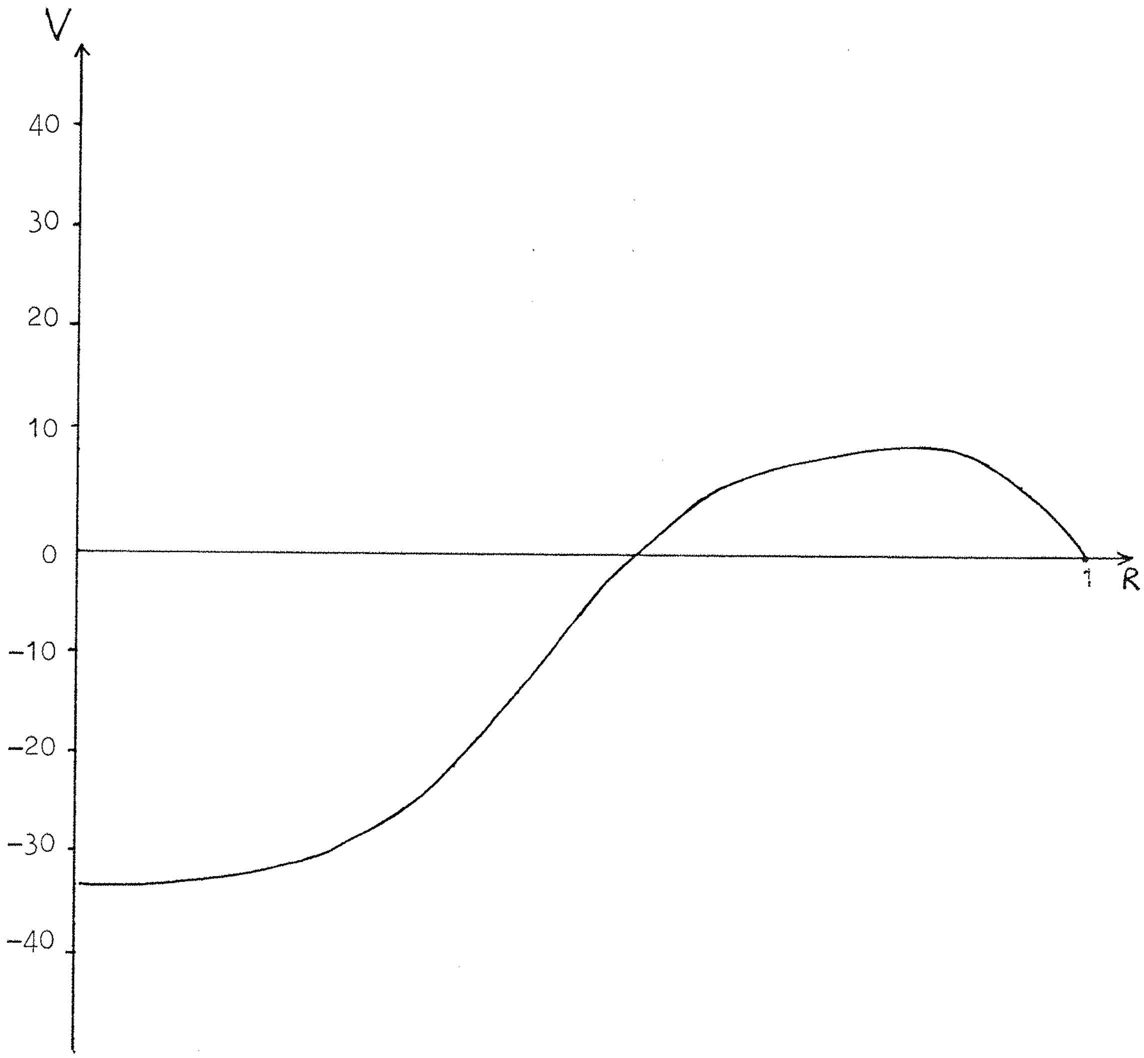

Fig. 5.4.2 Axial velocity profile, Gr = 10^4

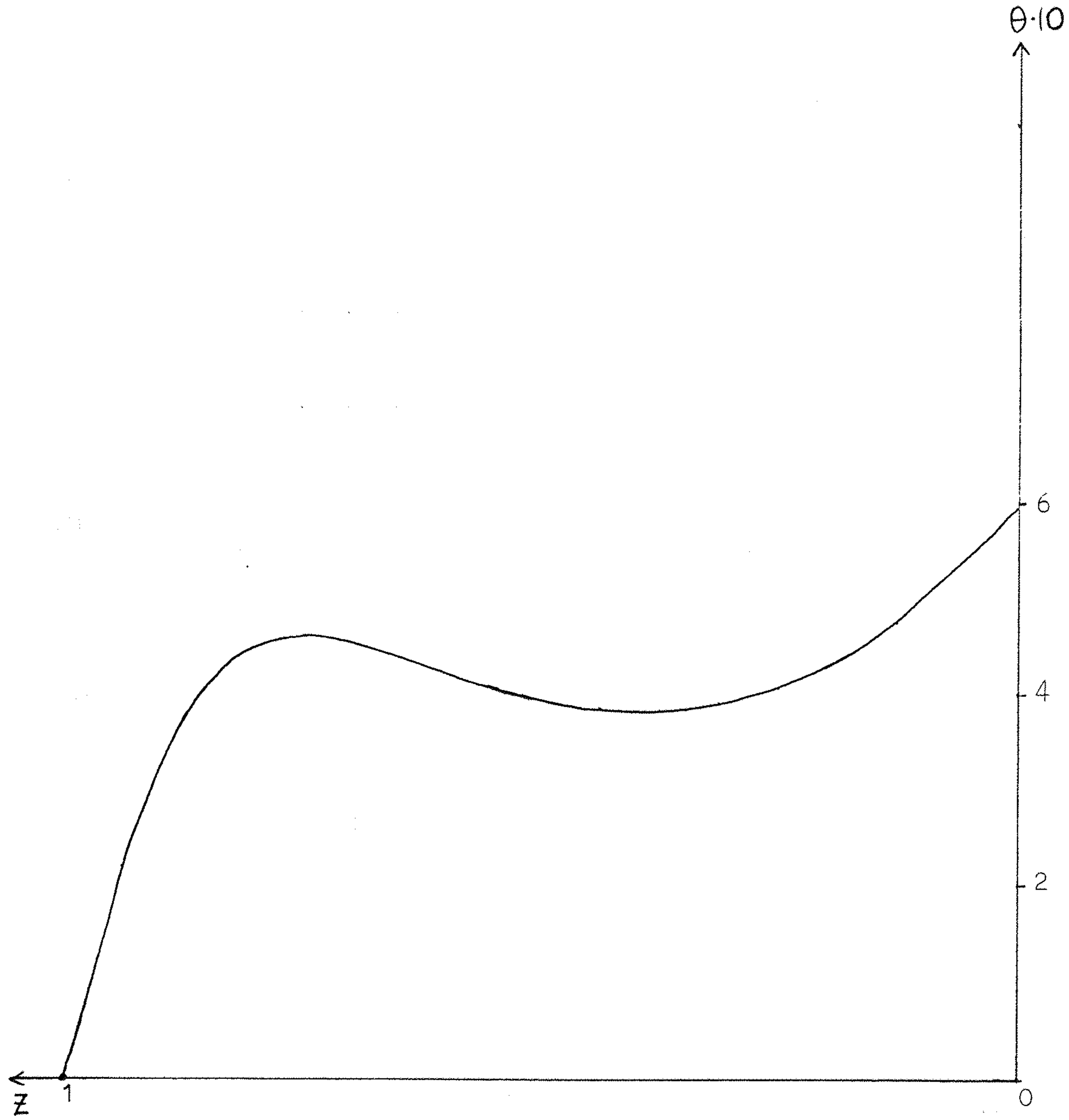

Fig. 5.4.3 Temperature profile along inner cylinder
$(R = \frac{1}{2})$ $Gr = 10^4$

CONCLUDING REMARKS AND FURTHER RECOMMENDATIONS

In this thesis we have shown how a combination of the ADI and cyclic reduction methods can be implemented to solve the problem of natural convection in cavities containing cryogenic fluids. After eliminating the pressure from the governing fluid flow equations, which avoids the need for a pressure boundary condition, the resulting vorticity equation together with the energy equation were converted into parabolic form, thus enabling us to march forward in time to the steady state solution through an adaptation of the ADI method. The method of cyclic reduction, was used to solve the Poisson equation at every half time step. The use of second upwind differencing scheme has allowed us to obtain numerical results for Gr up to 10^{12}. Boundary layers have been resolved efficiently using a non-uniform grid. The rate of convergence to steady state has been enhanced by using a variable time step and by incorporating accurate expressions for the temperature derivatives at the boundaries. The problem was also investigated in cylindrical geometry using the same numerical procedure, thus showing the latter's flexibility, although stability problems were encountered for Gr $> 10^4$. Numerical results were presented in graphical form for different boundary conditions and different aspect ratios. These results indicate, in particular, the existence of a recirculating flow, incorporating velocity boundary layers at the walls, a thermal shear layer at the free surface and a downward jet in the middle of the cavity. As the external heat flux is increased the boundary layers become thinner and are more clearly defined and buoyancy effects become predominant: the liquid moves much faster and the downward jet is thinner and stronger. From the numerical results we find that if a narrower cavity (a Dewar flask, for instance) containing a cryofluid is subjected to a heat flux only at the side walls, the liquid flow is mostly confined to the boundaries. Our model predicts that, in this case, side wall heating produces the greatest amount of vertical thermal stratification thereby inhibiting vertical motion in the core region. Results, however, show that vertical heat paths can be generated if some heat leaks into the system from the bottom. This result may find useful application in the design of cryogenic storage vessels. One simple way of increasing the amount of heat from the bottom into the system (but not to such an extent as to cause superheating of the liquid) would be to design the base with material of thermal conductivity slightly higher than that of the walls. Numerical results also reveal that, as the total amount of external heat is increased, plume-like flows start developing from the bottom corners of the cavity.

A few simplifying assumptions were made in the setting up of our model. However, as far as research in this area is concerned, these assumptions are quite commonly introduced and most of them are quite acceptable when one considers real storage situations. The usefulness of the model was tested by comparing the numerical solution with available experimental data and good qualitative agreement was achieved. Nonetheless, as is customary in these situations, some refinements of our model can be suggested. Possible improvements are:- the transformation of both coordinates x and y, the inclusion of evaporation and allowing the external heat fluxes to be functions of space. Much more work is necessary on the axisymmetric model to enable results to be found for higher Grashof numbers and further theoretical investigation in plume-convection in cryogenic liquids is also recommended. These are all lines of research that can be pursued.

Mention should be made of the general usefulness of our numerical method. By simply changing some of the boundary conditions and varying the Prandtl number, the method could be used to investigate a wide variety of practical problems including, for instance, double glazing, a fire alarm in a closed room and the numerical modelling of convection in the atmosphere, the last two relating to enclosed flows driven by localized heating from below.

Finally, much more experimental data on natural convection in cryogenic liquids is required in order to assess fully the quantitative implications of our mathematical model.

REFERENCES

Beresford, G. (1984), "Laser Doppler Velocimetry on cryogenic fluids", Ph.D. Thesis, Department of Physics, University of Southampton.

Buzbee, B. L., Golub, G. H., Nielson, C. W. (1970), "On direct methods for solving Poisson's equations", S.I.A.M. Journal on numerical analysis, Vol. 7, pp. 627-656.

Carlslaw, H. S. (1959), "Heat Conduction in Solids", Oxford Press, London.

Catton, I. (1978), "Natural Convection in Enclosures", Heat Transfer 1978, National Research Council of Canada, Vol. 6, pp. 13-30.

De Vahl Davis, G. (1968), "Laminar natural convection in an enclosed rectangular cavity", International Journal of Heat and Mass Transfer, Vol. 11, pp. 1675-1693.

De Vahl Davis, G. (1983), "Natural convection of air in a square cavity: a benchmark numerical solution," International journal of Numerical Methods in Fluids, Vol. 3, pp. 249-264.

EcKert, E. R. G., and Carlson, W. O. (1961), "Natural convection in an air layer enclosed between two vertical plates with different temperatures", International Journal of Heat and Mass Transfer, Vol. 2, pp. 106-120.

Elder, J. W. (1966), "Numerical experiments with free convection in a vertical slot", Journal of Fluid Mechanics, Vol. 24, pp. 823-843.

Fan, S. C. and Chu, J. C. (1968), "Thermal stratification in closed, cryogenic containers" in Advances in Cryogenic Engineering, Vol. 14, pp. 249-257.

Hellums, J. D. and Churchill, S. W. (1961), "Computation of natural convection by Finite Difference Methods", International development in Heat Transfer, Part V, A.S.M.E., New York, pp. 984-994.

Huntley, S. C. (1960), "Temperature-pressure-time relations in a closed cryogenic container" in Advances in Cryogenic Engineering, Vol. 3, pp. 342-352.

Jaluria, Y. (1980), "Natural Convection Heat and Mass Transfer", H.M.T., Vol. 5, Pergamon Press.

Kublbeck, K., Merker, G. P., Straub, J. (1980), "Advanced numerical computation of two-dimensional time-dependent free convection in cavities", International Journal of Heat and Mass Transfer, Vol. 23, No. 2, pp. 203-217.

Li, W. and Lam, S. (1966), "Principles of Fluid Mechanics", Addison-Wesley Publishing Company Inc., U.S.A.

Markatos, N. C., Pericleous, K. A. (1984), "Laminar and turbulent natural convection in an enclosed cavity", International Journal of Heat and Mass Transfer, Vol. 27, No. 5, pp. 755-772.

Milne-Thomson, L. M. (1968), "Theoretical Hydrodynamics", 5th edition, Macmillan, London.

Neff, B. D. and Chiang, C. W. (1966), "Free convection in a container of cryogenic fluid" in Advances in Cryogenic Engineering, Vol. 12, pp. 112-124.

Newell, M. E. and Schmidt, F. W. (1970), "Heat Transfer by laminar convection within rectangular enclosures", Journal of Heat Transfer, Vol. 92, pp. 159-168.

Ostrach, S. (1972), "Natural convection in enclosures" in Advances in Heat Transfer (edited by J. P. Harnett and T. F. Irvine Jr.), Vol. 8, Academic Press, New York, pp. 161-227.

Ostrach, S. (1982), "Natural convection heat transfer in cavities and cells", Proceedings of International Heat Transfer Conference, pp. 365-379, Hemisphere, Washington D.C.

Patankar, S. V. (1980), "Numerical Heat Transfer and Fluid Flow", McGraw-Hill Book Company, New York.

Peaceman, D. V. and Rachford, H. H. (1955), "The numerical solution of parabolic and elliptic differential equations", Journal of Society of Industrial applied Mathematicians, Vol. 3, No. 1, pp. 28-41.

Phillips, T. N. (1984), "Natural convection in an enclosed cavity", Journal of Computational Physics, Vol. 54, pp. 365-381.

Roache, P. J. (1976), "Computational Fluid Dynamics", Hermosa Publishers, Albuquerque, New Mexico.

Schumann, U. and Sweet, R. A. (1976), "A direct method for the solution of Poisson's equation with Neumann boundary conditions on a staggered grid of arbitrary size", Journal of Computational Physics, Vol. 20, pp. 171-182.

Scurlock, R. G., Beduz, C., Rebiai, R., Atkinson, M. C. M. (1984), "Heat and evaporative mass transfer correlation at the Liquid-vapour interface of cryogenic liquids". Proceedings of I.C.E.C10, pp. 95-99.

Torrance, K. E. (1968), "Comparison of finite difference computations of natural convection", Journal of Research of National Bureau Standard, Vol. 72B, pp. 281-300.

Wilkes, J. O. and Churchill, S. W. (1966), "The finite difference computation of natural convection in a rectangular enclosure", A.I.Ch.E. Journal, Vol. 12, pp. 161-166.